Cosmic Microwave Background Observations from Tenerife

implications on angular power spectrum at high multipoles and new foregrounds

Rafael Rebolo

Instituto de Astrofísica de Canarias

Consejo Superior de Investigaciones Científicas, Spain

and

J. Alberto Rubiño-Martin

Instituto de Astrofisica de Canarias

"Modern Cosmology"

Benasque 31 Julio 2006

Outline

- Interferometry. Very Small Array (VSA)
  - Angular power spectrum
  - Sunyaev-Zeldovich observations
    - Clusters of galaxies
    - Superclusters
- Circular scan mapping experiment COSMOSOMAS
  - Evidence for a new Galactic foreground: spinning dust?

Tenerife Experiment

1984-2000

Jodrell Obs.-Cambridge Univ.
IAC

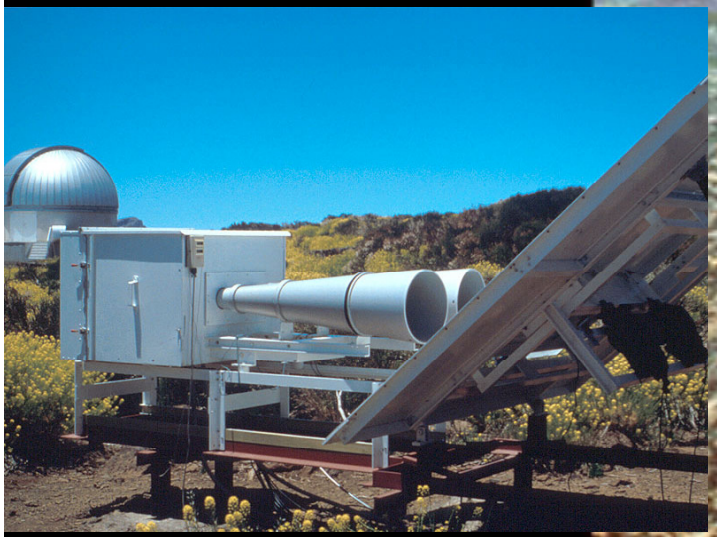

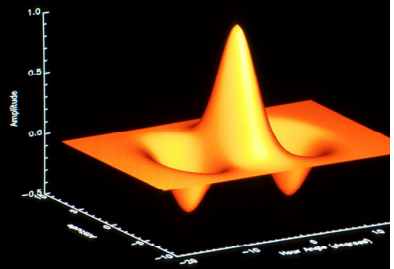

Three double switch Radiometers
FWHM=5 degrees

Frequencies:
10,15, 33 GHz

Davies et al. 1987
Gutiérrez et al. 2000

CMB experiments at Tenerife

The Very Small Array

Cavendish Astrophysics Group
Jodrell Bank Observatory
Instituto de Astrofisica de Canarias

COSMOSOMAS

Instituto de Astrofísica
de
Canarias

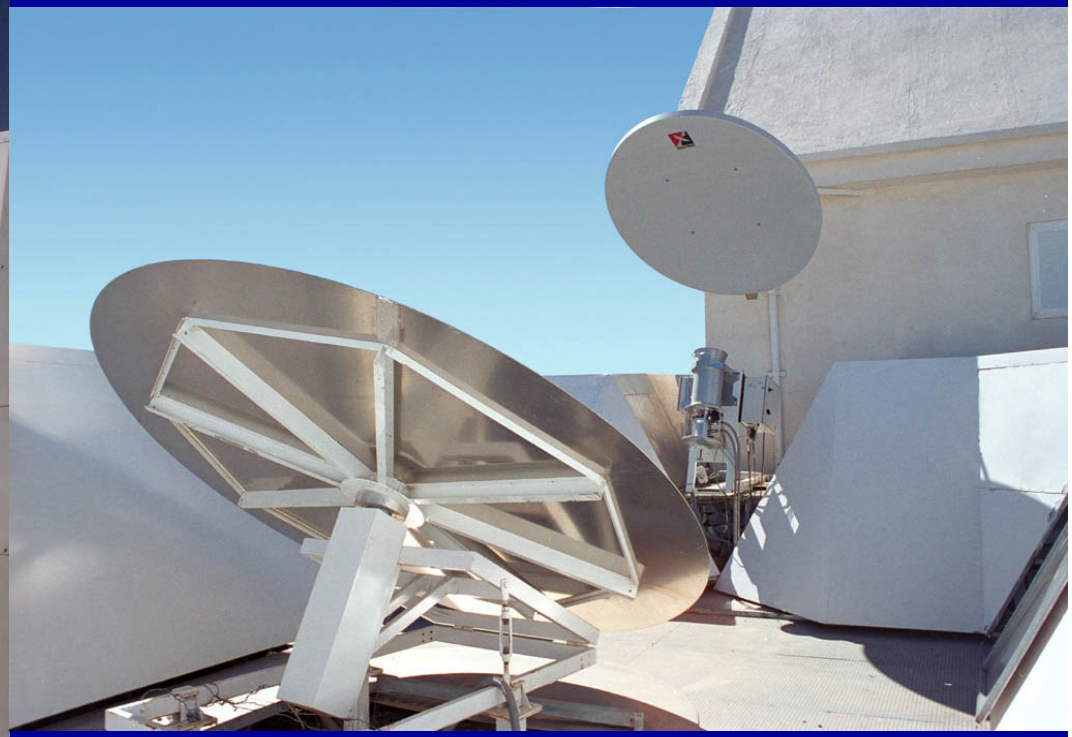

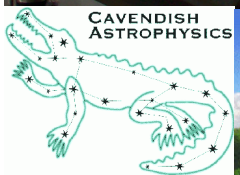

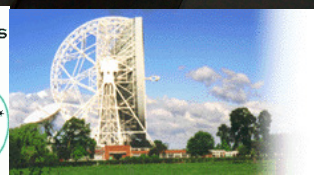

Jodrell Bank
Observatory

The Very Small Array

Extended configuration

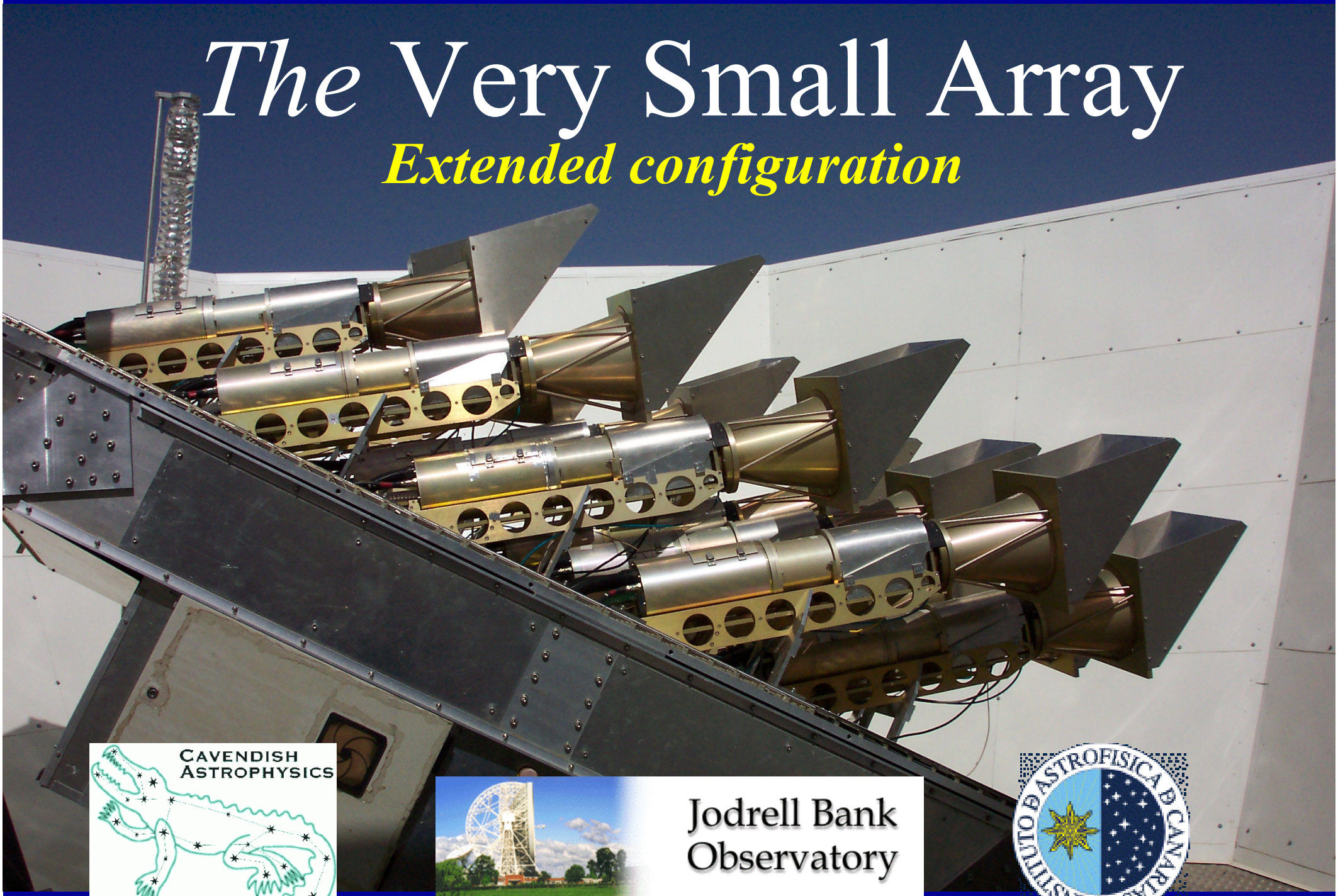

CAVENDISH ASTROPHYSICS

Jodrell Bank Observatory

INSTITUTO DE ASTROFISICA DE CANARIAS · IAC

Very Small Array (VSA)

- Array of 14 conical horn antennas located at Tenerife
- HEMT based receivers working in the range 26 - 36 GHz
- Single-channel analogue phase-switched correlator 1.5 GHz bandwidth.
- Horn reflectors mounted on a tip table. Close packing
- Compact configuration

  FoV 4.5 degrees. Resolution element : approx. 30 arcmin.

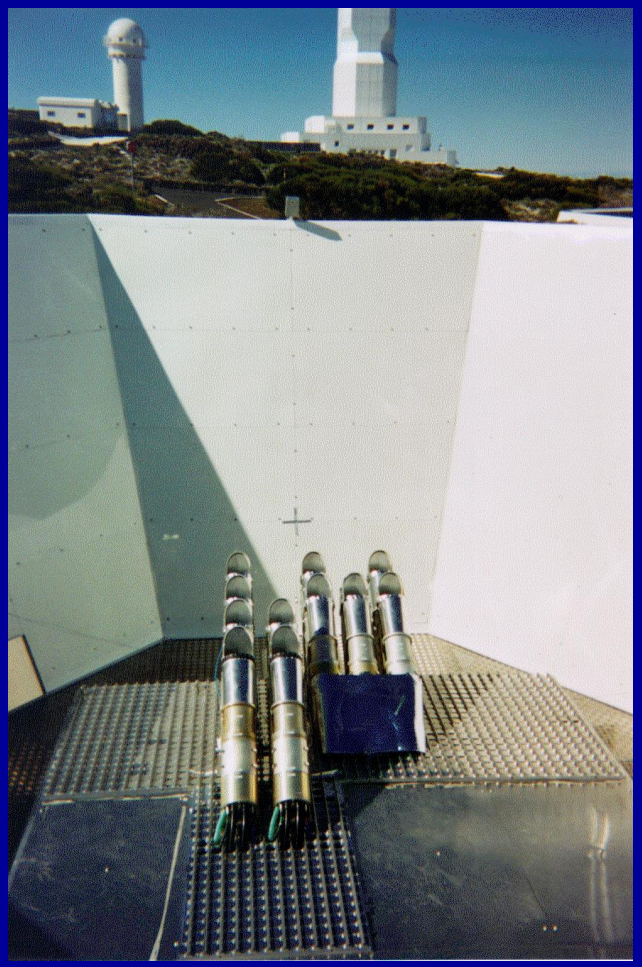

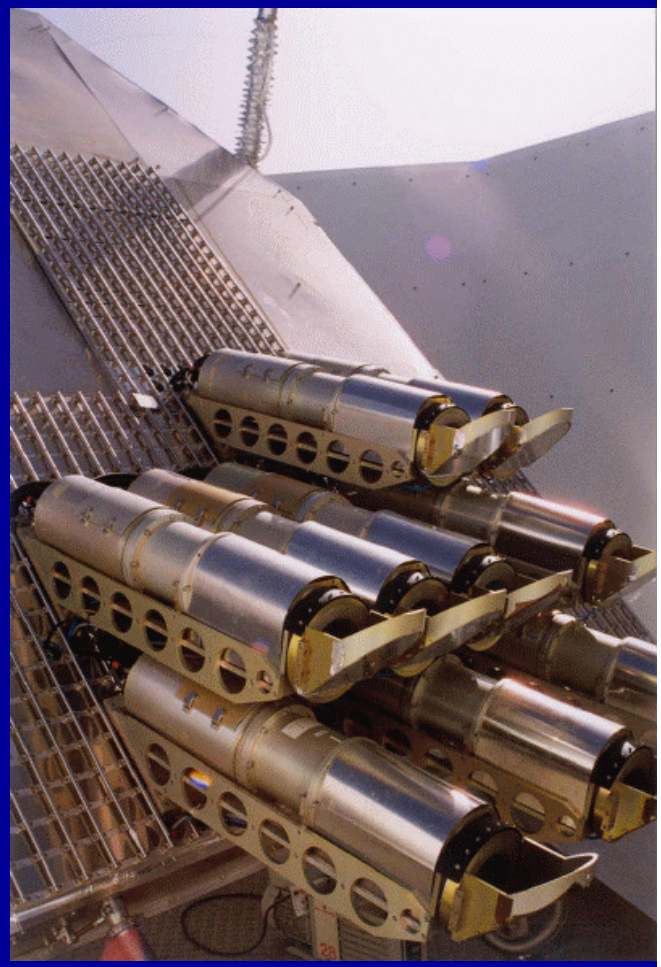

-compact configuration-

The Antennas

(extended configuration)

- Efficient, unblocked with a clean aperture
- Compact for close packing (small aperture)
- Low cross-coupling
- Can track independently (fringe rate tracking)

These conditions are met by conical horn reflector antennas (CHRA).

The 90º reflector gives the antennas a periscope-like property so they can be close packed like organ pipes.

This can be rotated to give one dimension of independent tracking.

Side blinders are required to block cross Coupling

Primary beam 2 degrees FWHM ,
Synthetized beam approx. 11 arcmin

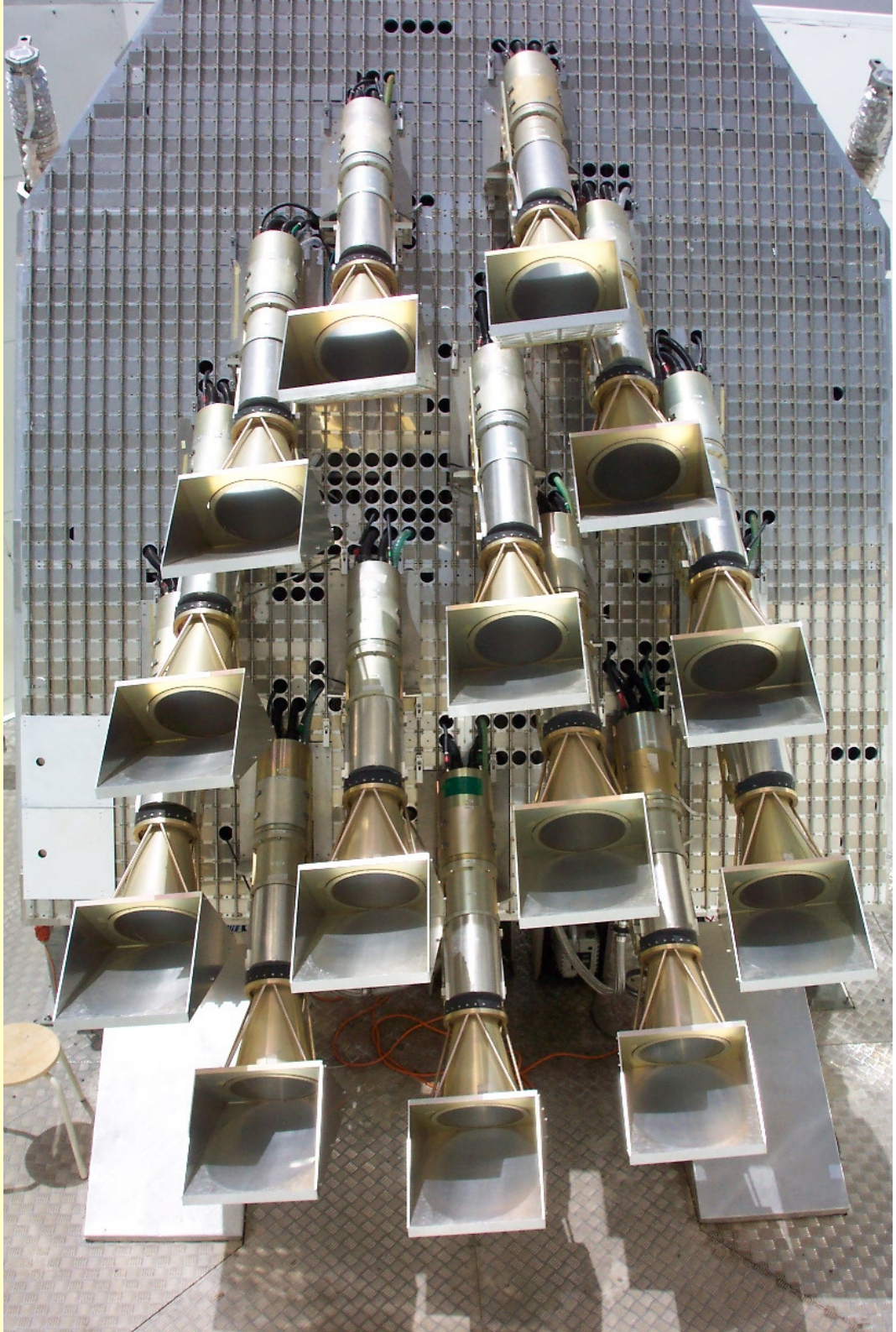

The Receivers

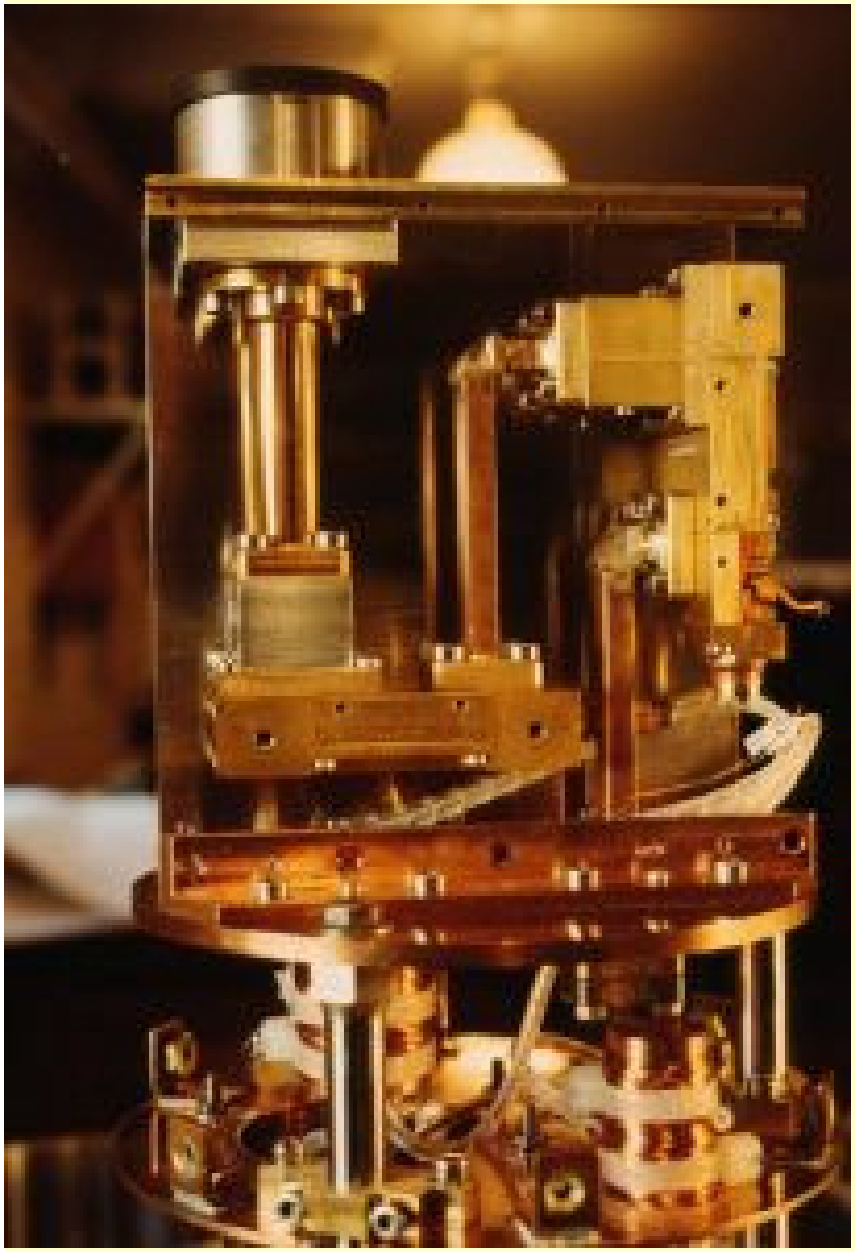

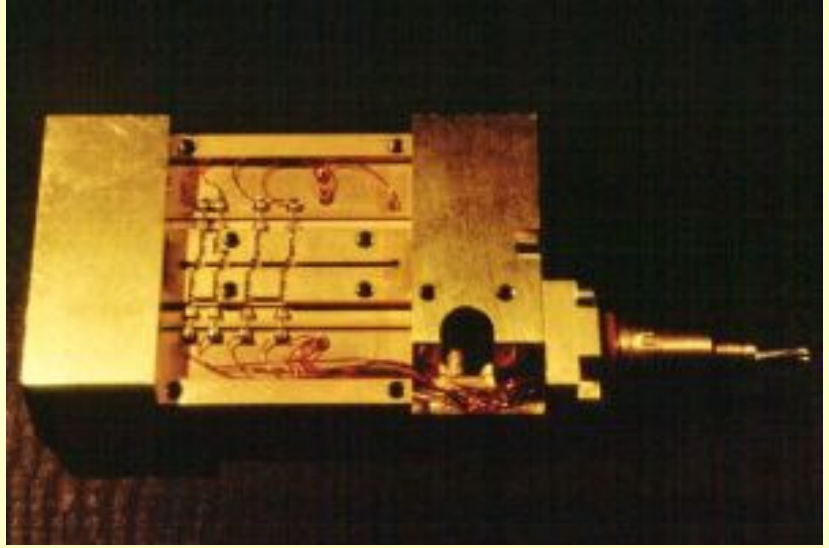

The amplifiers are based on the 26-36 GHz Pospieszalski NRAO design. Built and modified by Eddie Blackhurst at the Jodrell Bank Observatory, using unpassivated InP HEMTs from Hughes and Fujitsu.

The bias supplies are fed from a battery pack to give a low noise protected voltage free from switch transients which can cause damage to the HEMTs.

Each antenna has a 4-stage (Hughes) and a 2-stage (Fijitsu) amps. Bias conditions can be set individually for each transistor to optimize sensitivity.

Noise temperatures of 25 K (including horn) are achieved across the band which is flat to 1dB.

CMB interferometry

- ✓ CMB anisotropies in small fields

$$\frac{\Delta T}{T_0}(\vec{x}) = \sum_{\ell m} a_{\ell m} Y_{\ell m} \approx \int a(\vec{u}) e^{i 2\pi \vec{u}\cdot\vec{x}} d^2\vec{u}$$

$u \approx \ell/(2\pi)$

- ✓ Statistics:

$$< a(\vec{u}) >= 0$$

$$< a^*(\vec{u}) a(\vec{u}') >= S(u)\delta^{(2)}(\vec{u} - \vec{u}'),$$

$$a(-\vec{u}) = a^*(\vec{u})$$

- ✓ Power sp

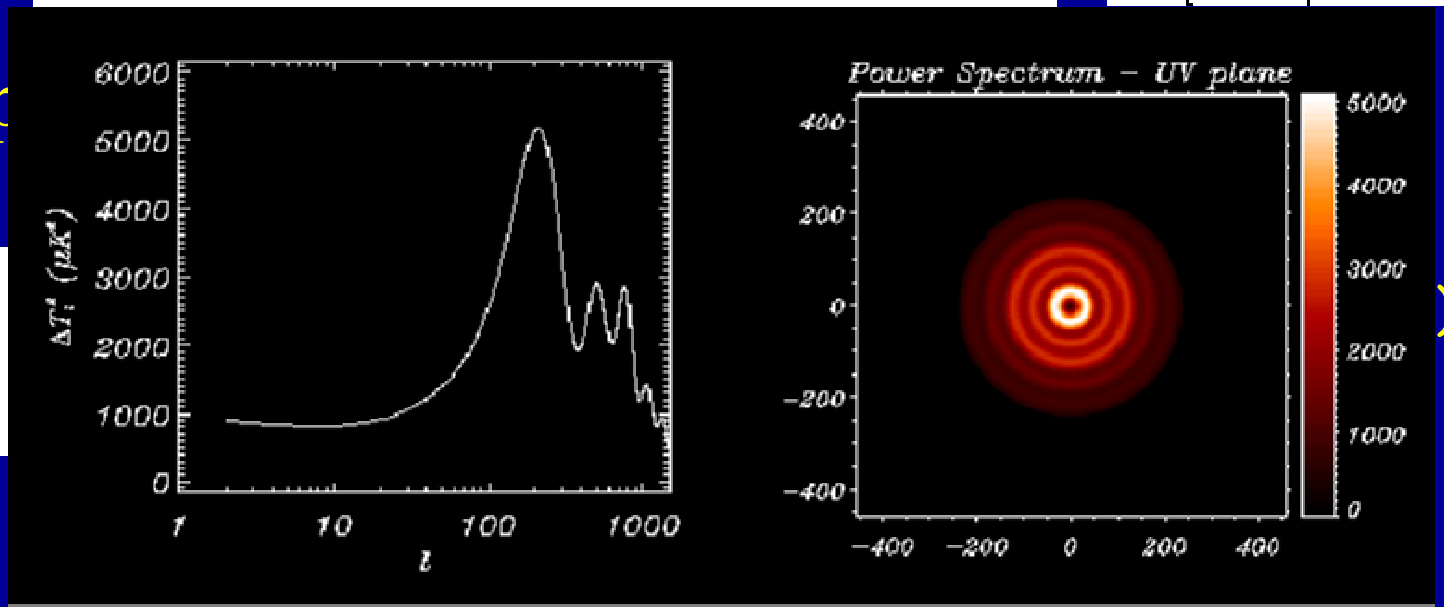

What a CMB interferometer measures

- We

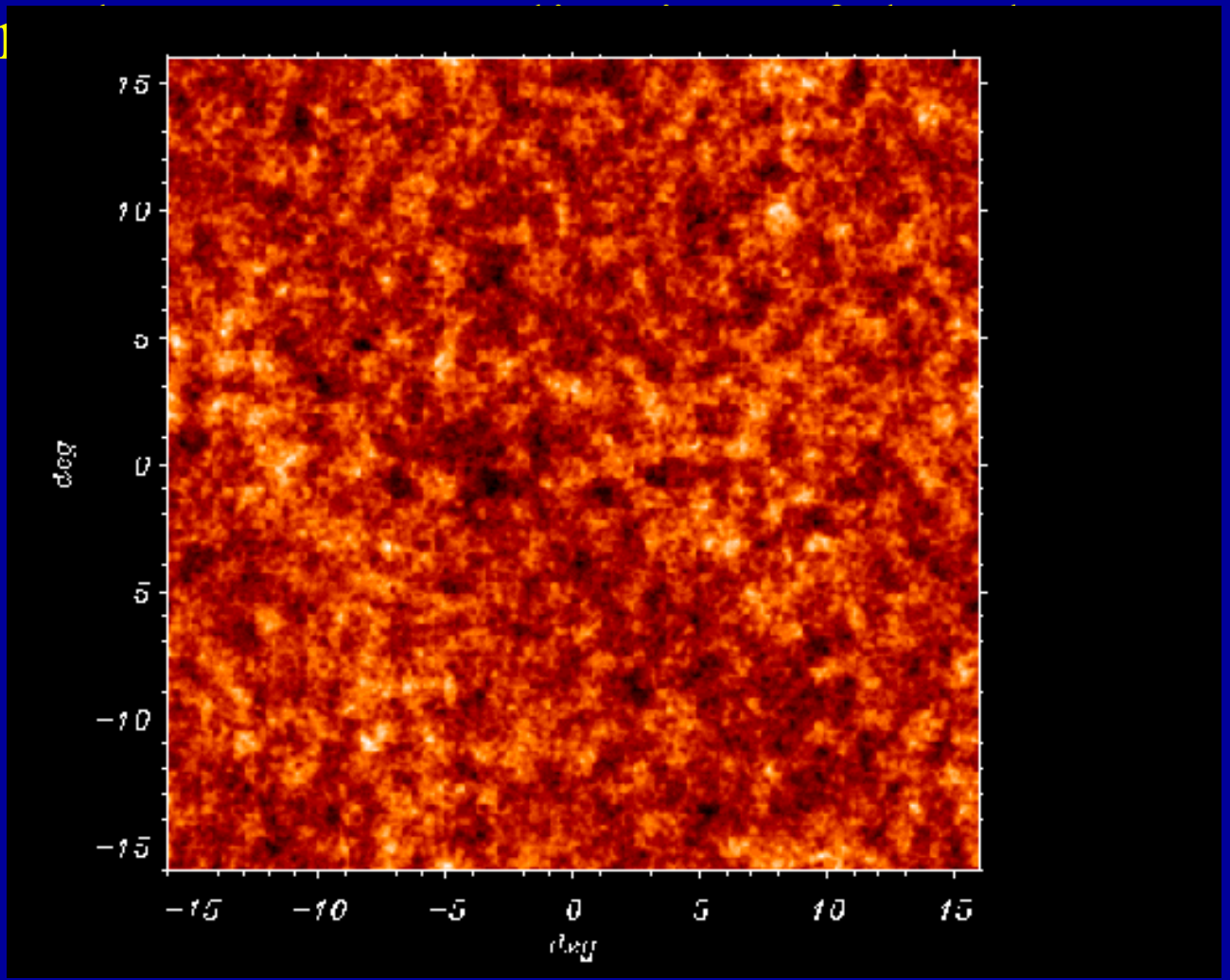

What a CMB interferometer measures

- the p

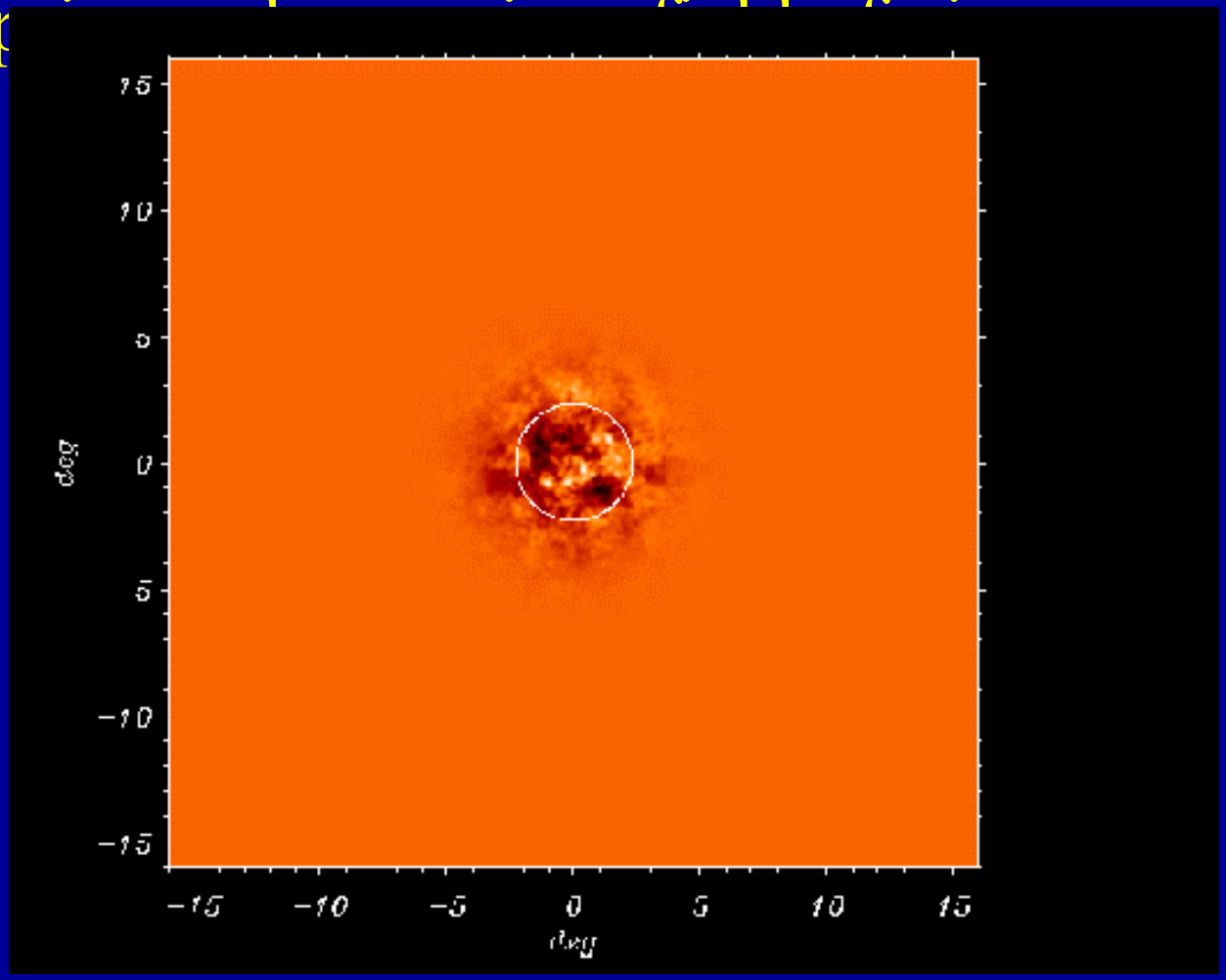

FWHM=4.6°

What a CMB interferometer measures

- and w

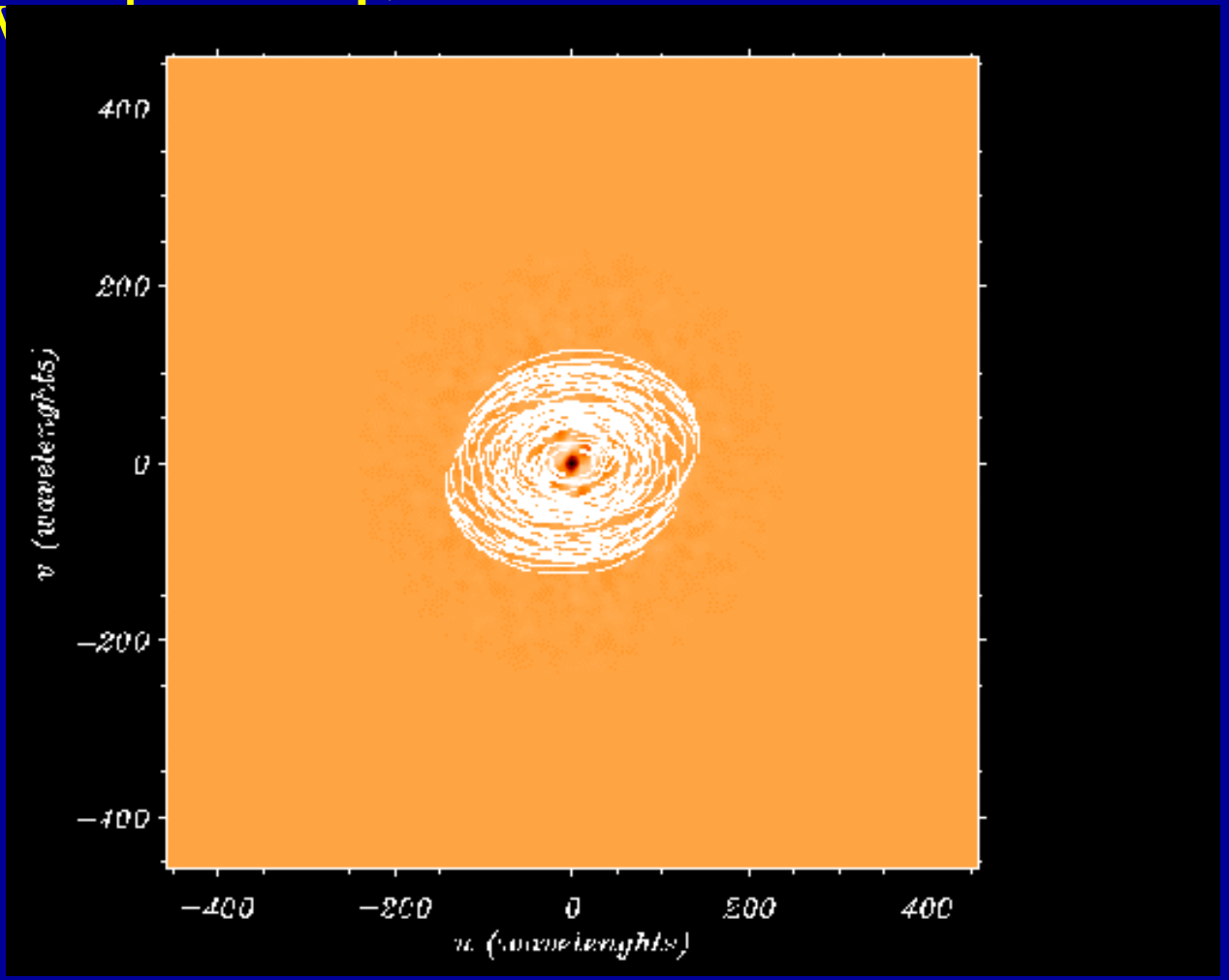

What a CMB interferometer measures

- … s
  is

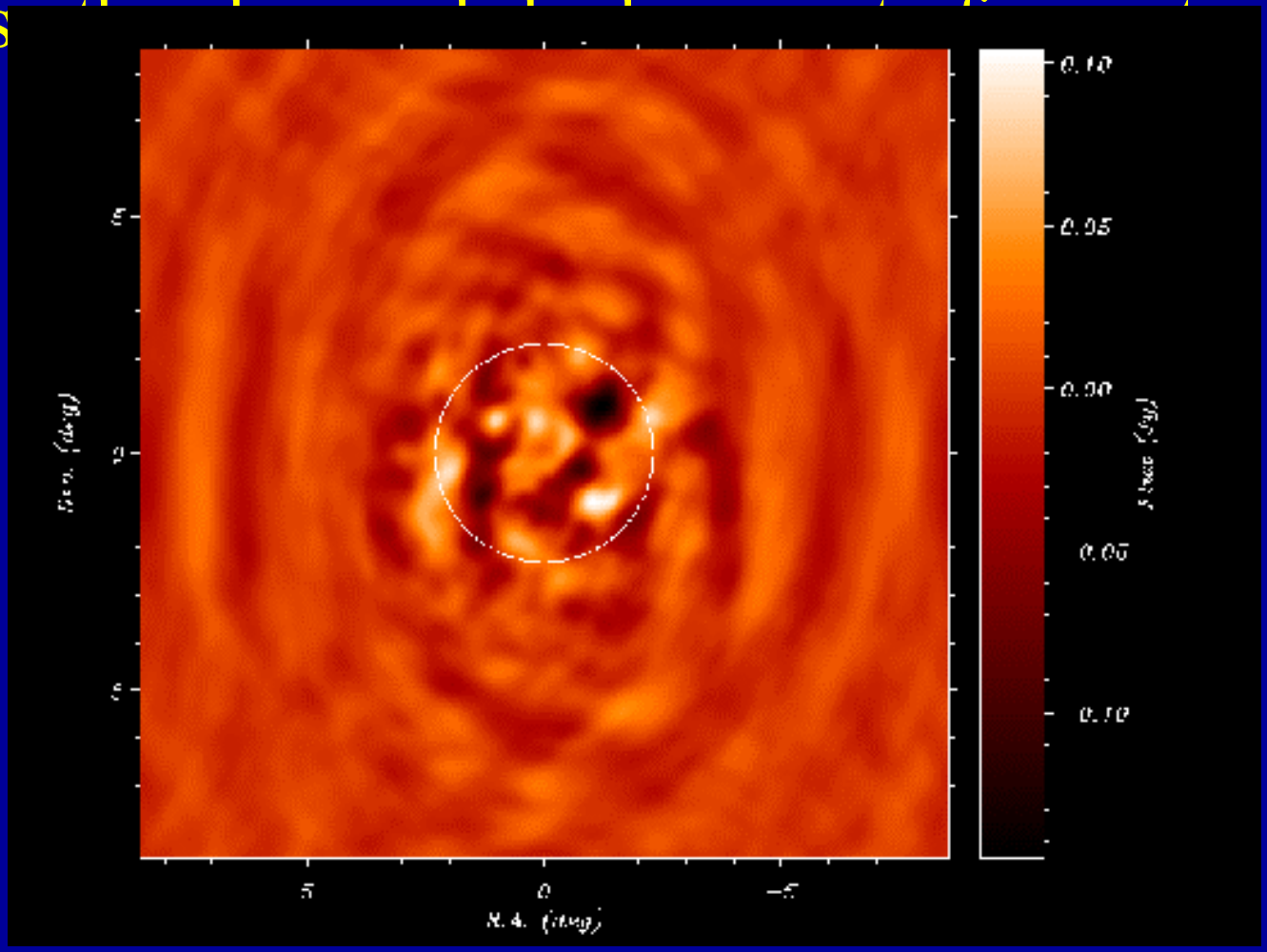

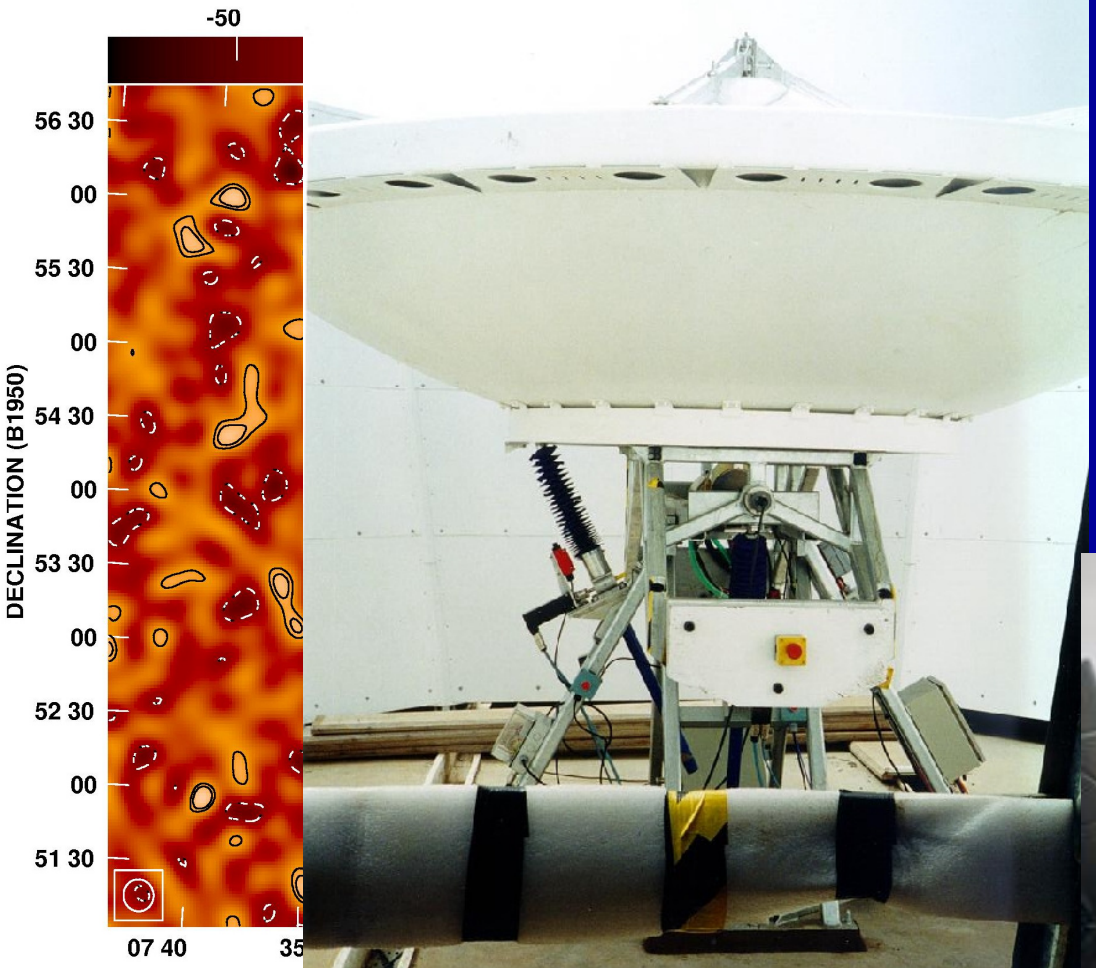

VSA
source subtractor
Tenerife.

3.7 m dishes

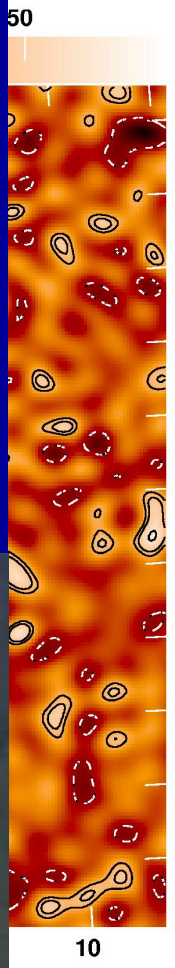

Before after
subtraction of radiosources

First VSA angular power spectrum (compact configuration)

Scott et al. astro-ph/0205380
MNRAS 341, 1076 (2003)

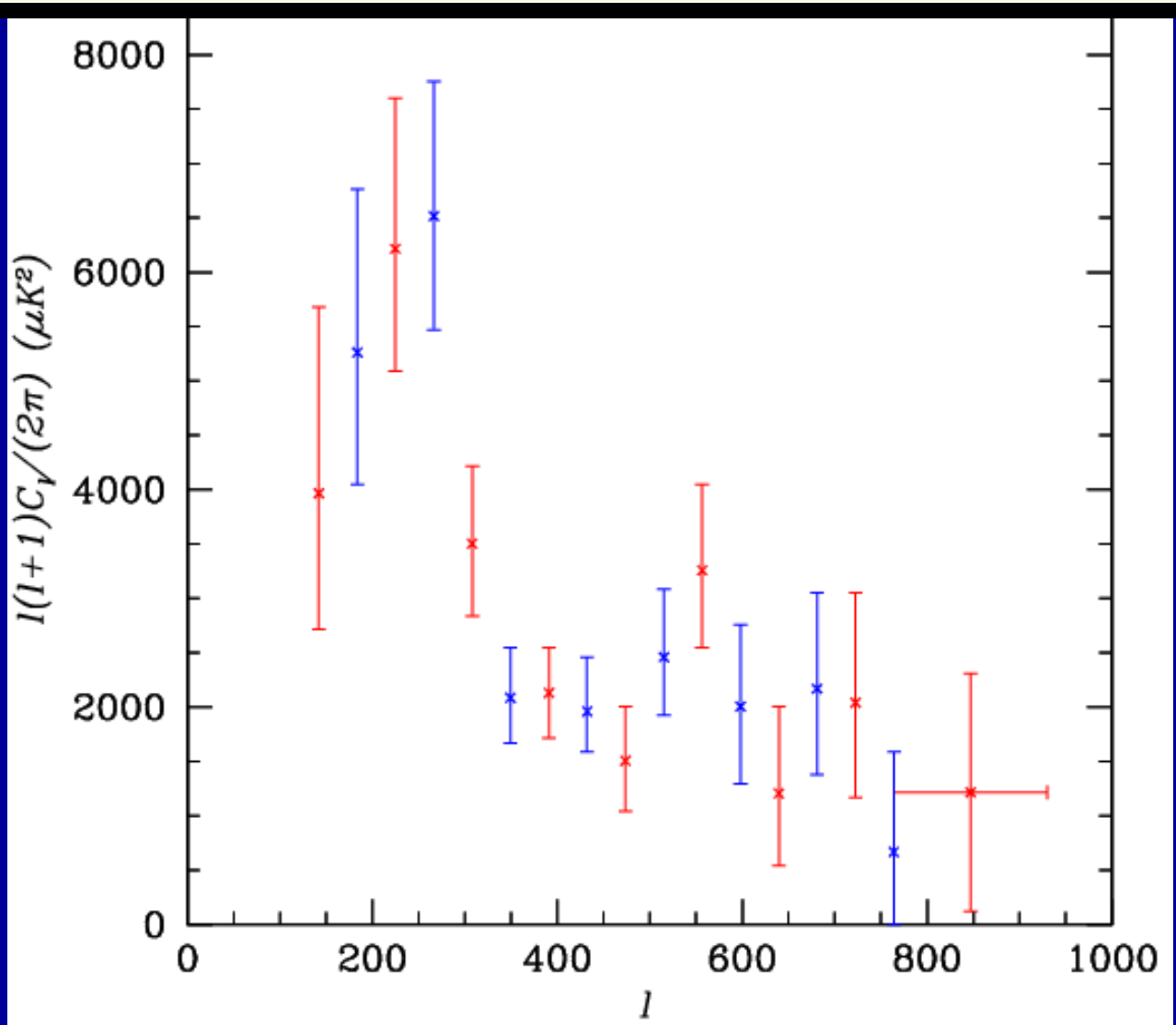

$\Omega_b\ h^2$

Ωtot

n_s

$\Omega_{cdm}\ h^2$

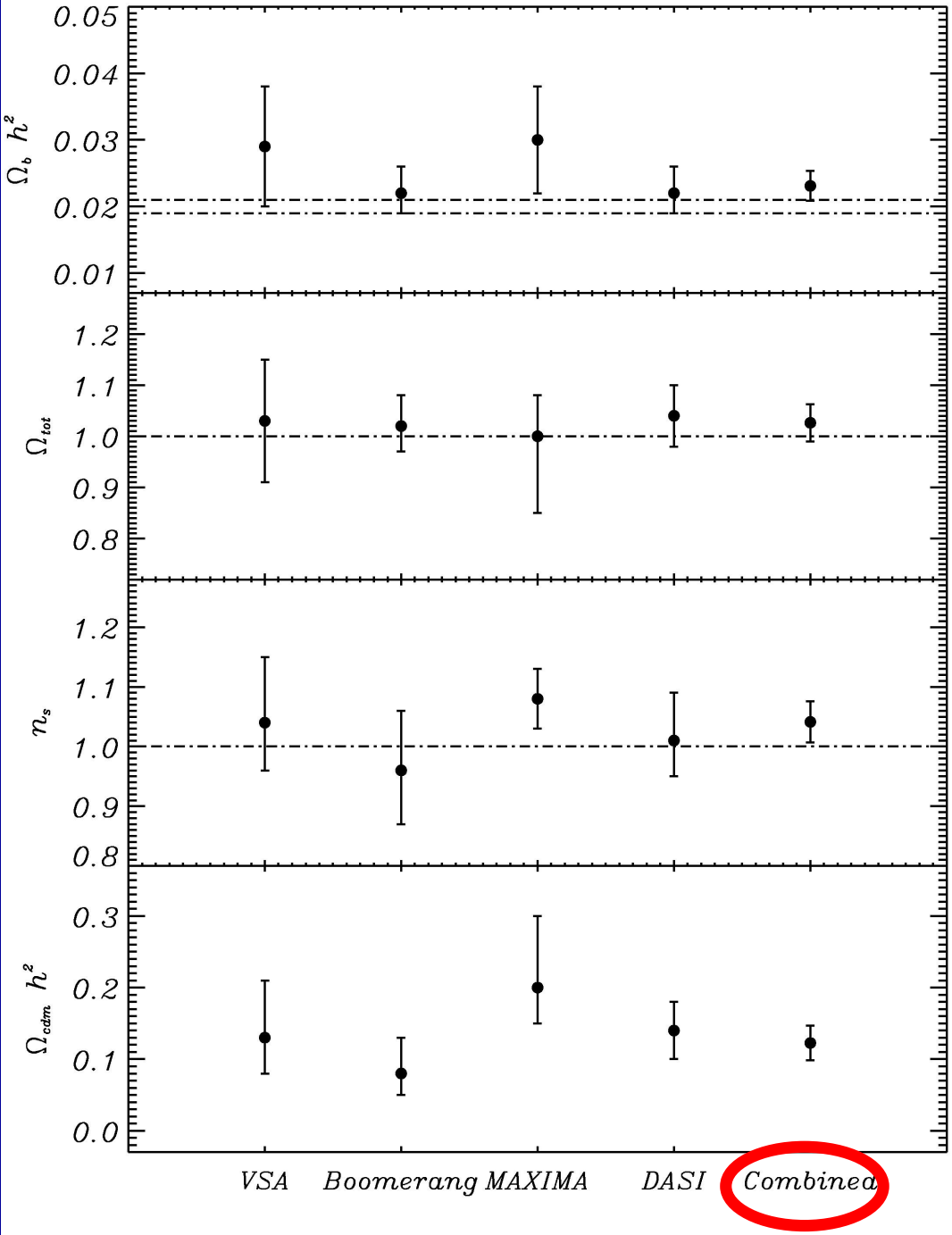

CMB constraints on cosmological parameters

(pre-WMAP Data)

Rubiño-Martín, Rebolo et al. 2003

Ω_m

Ω_{lambda}

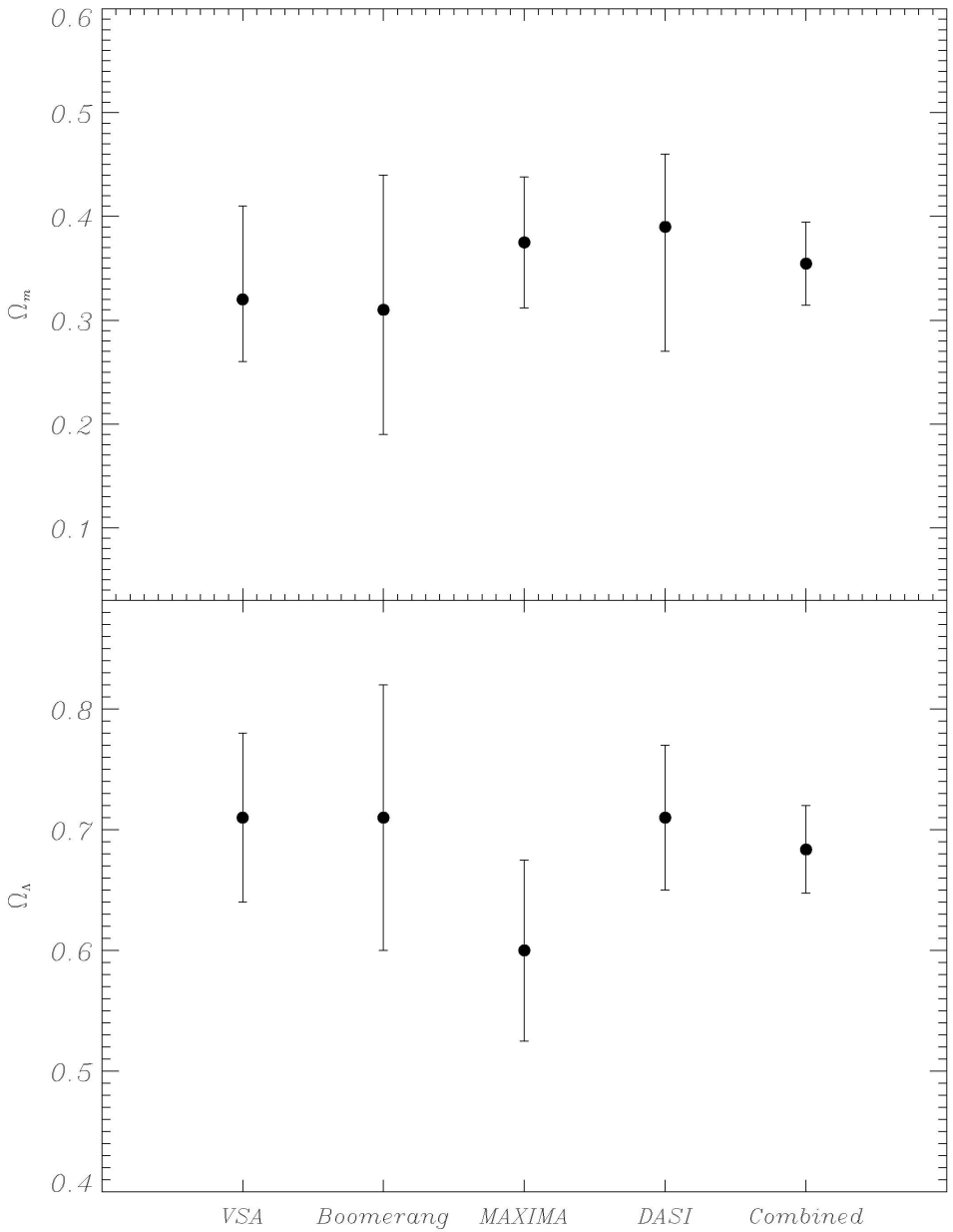

CMB constraints on cosmological parameters

Rubiño-Martín et al. 2003, MNRAS 341, 1084

Extended configuration VSA

(December 2002)

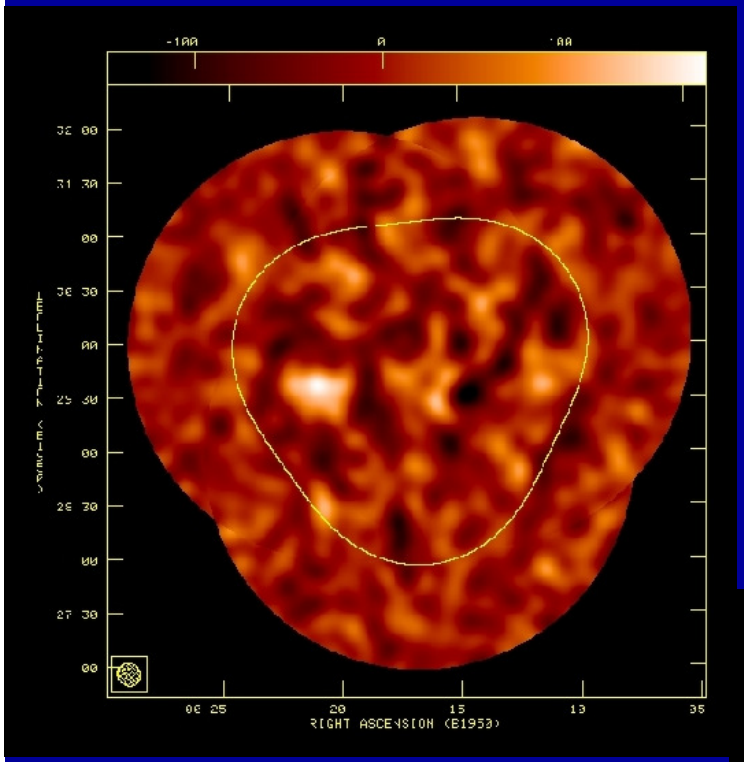

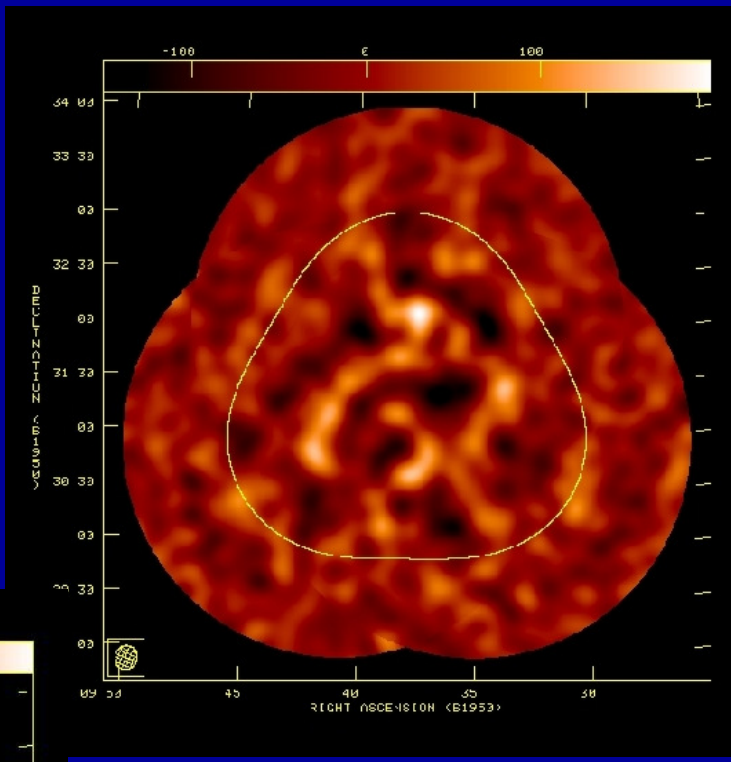

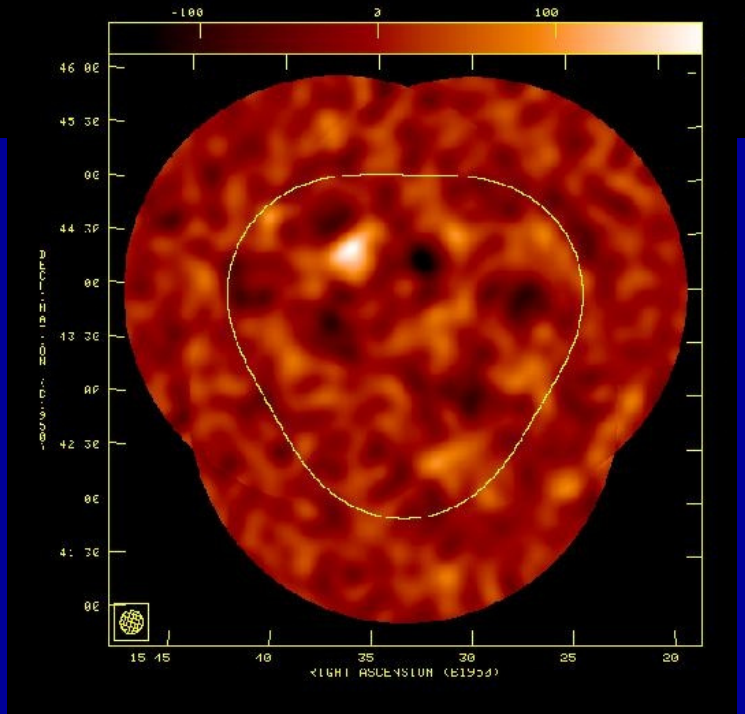

(Grainge et al.2003)

MNRAS 341, L23

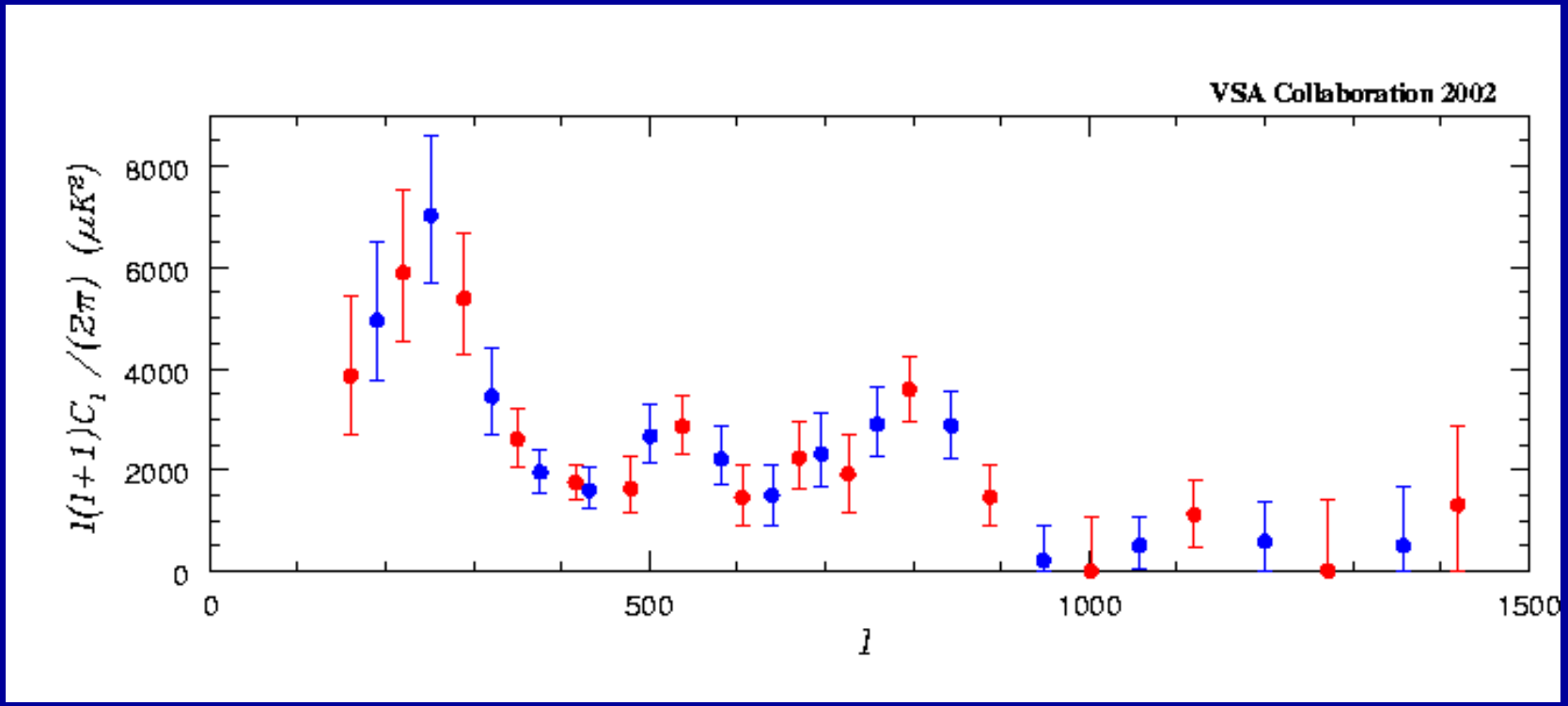

Bayesian analysis using Monte-Carlo Markov Chains.

Priors: Hubble constant, 2dF and SNIa

$\Omega_b h^2$	0.0219 ±0.0014
Ωtot	0.99± 0.03
n	1.01± 0.05
$\Omega_{cdm} h^2$	0.128± 0.02
h	0.68 ± 0.05
Ω_m	0.32 ± 0.06
Ω_{lambda}	0.66± 0.05
Age	13.6± 0.9 Gyr

(Grainge et al.2003)

Slosar et al.2003

MNRAS 341, L29

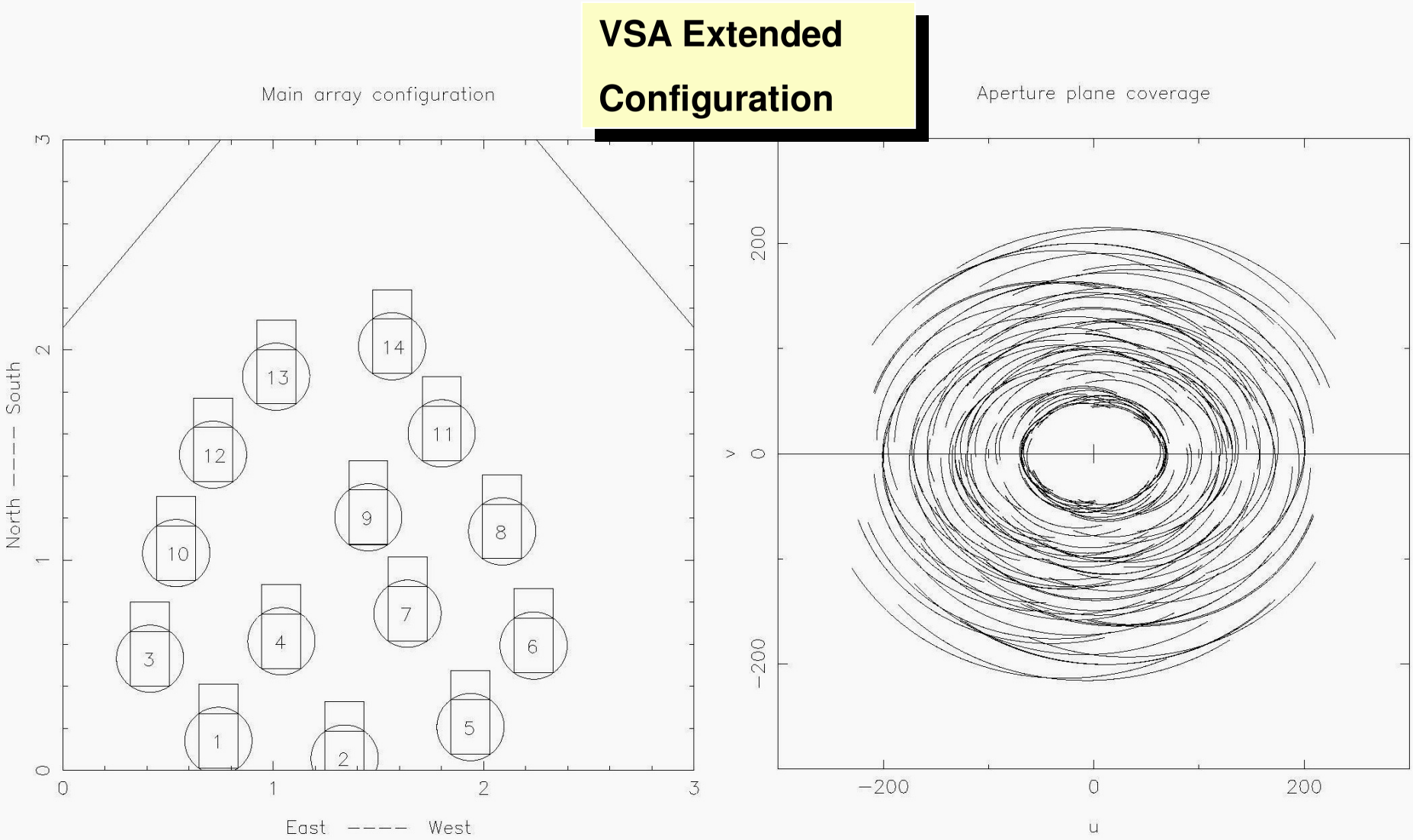

Figure 1. *Left*: Extended array configuration of the 14 antennas on the tip-tilt table. *Right*: The corresponding u,v coverage calculated for a 5 hour observation of a source at declination of $+40°$.

Window function

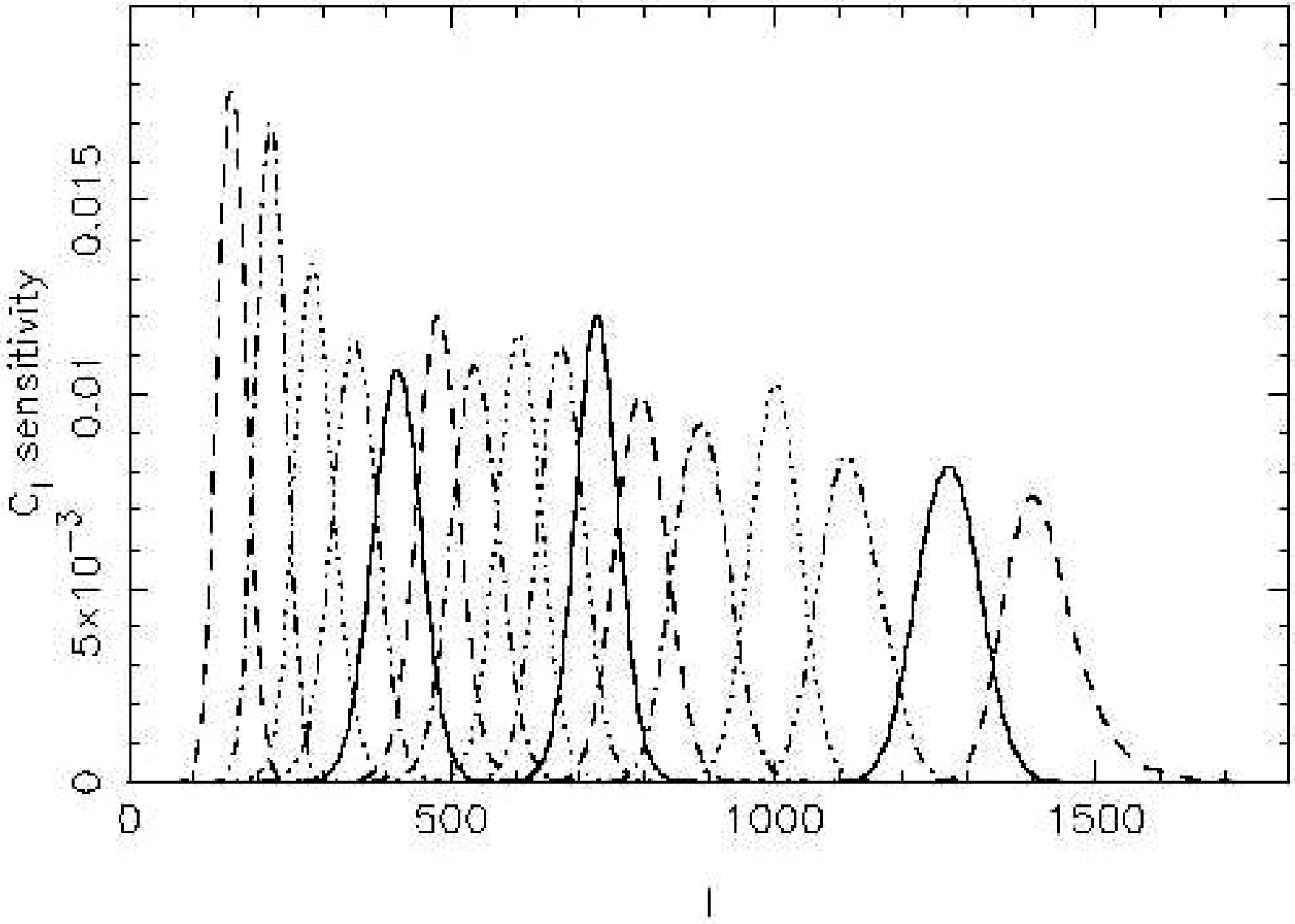

Selection of Fields

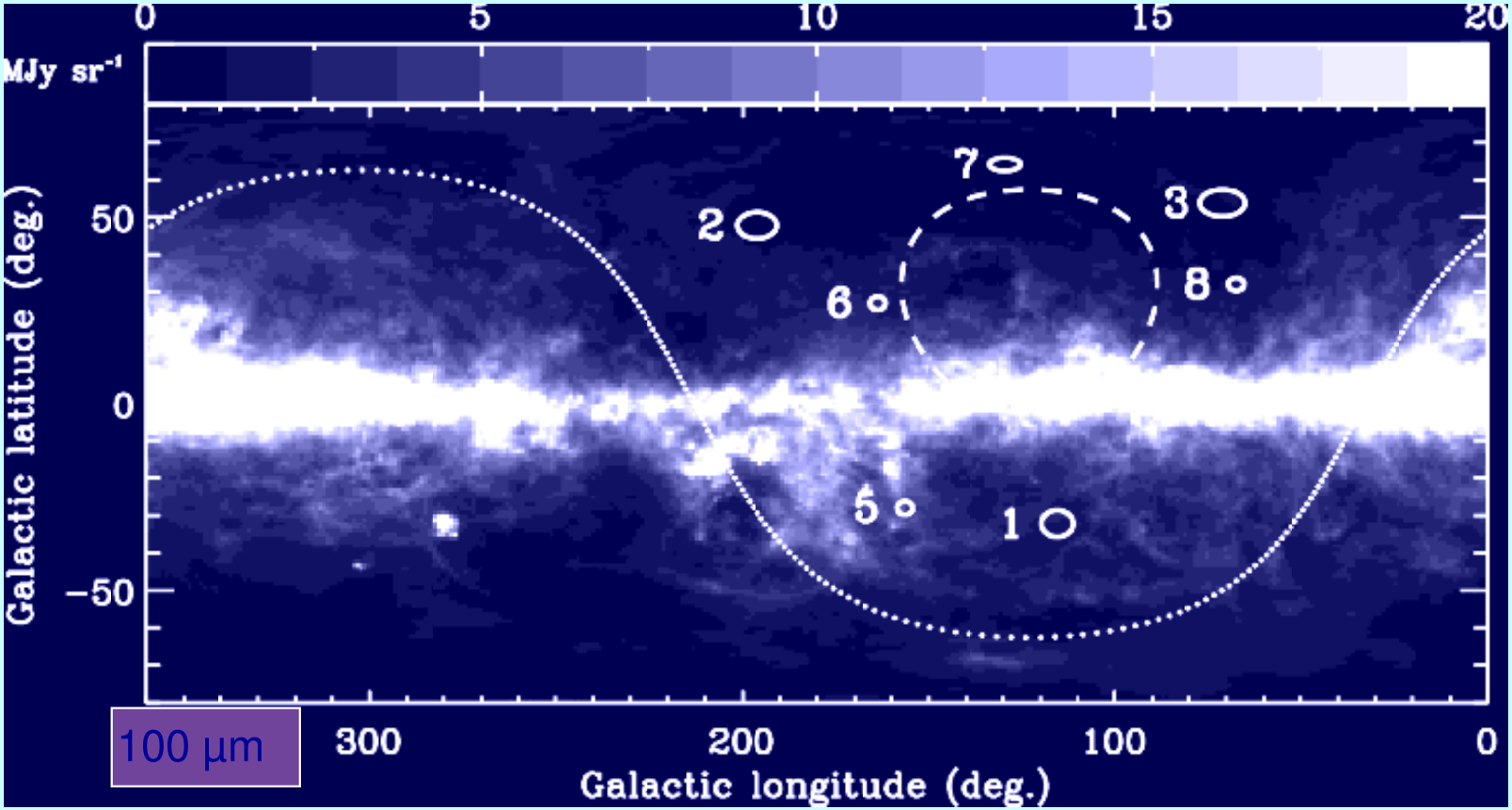

The 7 VSA Regions

VSA1: 7 fields
α $00^h19^m22^s$ δ +29º16'39"

VSA2: 7 fields
09 40 53 +31 46 21

VSA3: 7 fields
15 35 13 +42 45 05

VSA5: 3 fields
03 05 45 +27 16 35

VSA6: 3 fields
07 24 48 +55 05 00

VSA7: 3 fields
12 28 14 +53 48 25

VSA8: 7 fields
17 34 58 +40 53 07

Fields chosen to limit Galactic and extragalactic emission by avoiding:

- Bright radio sources (>500 mJy) via NVSS and GB6
- Bright galaxy clusters via Ebeling et al. and Abell catalogues
- Diffuse galactic emission: Synchrotron (408 MHz Halslam et al 1981),
  Free-free (Hα WHAM Haffner et al 2003),
  Dust (100 μm Schlegel et al 1998)

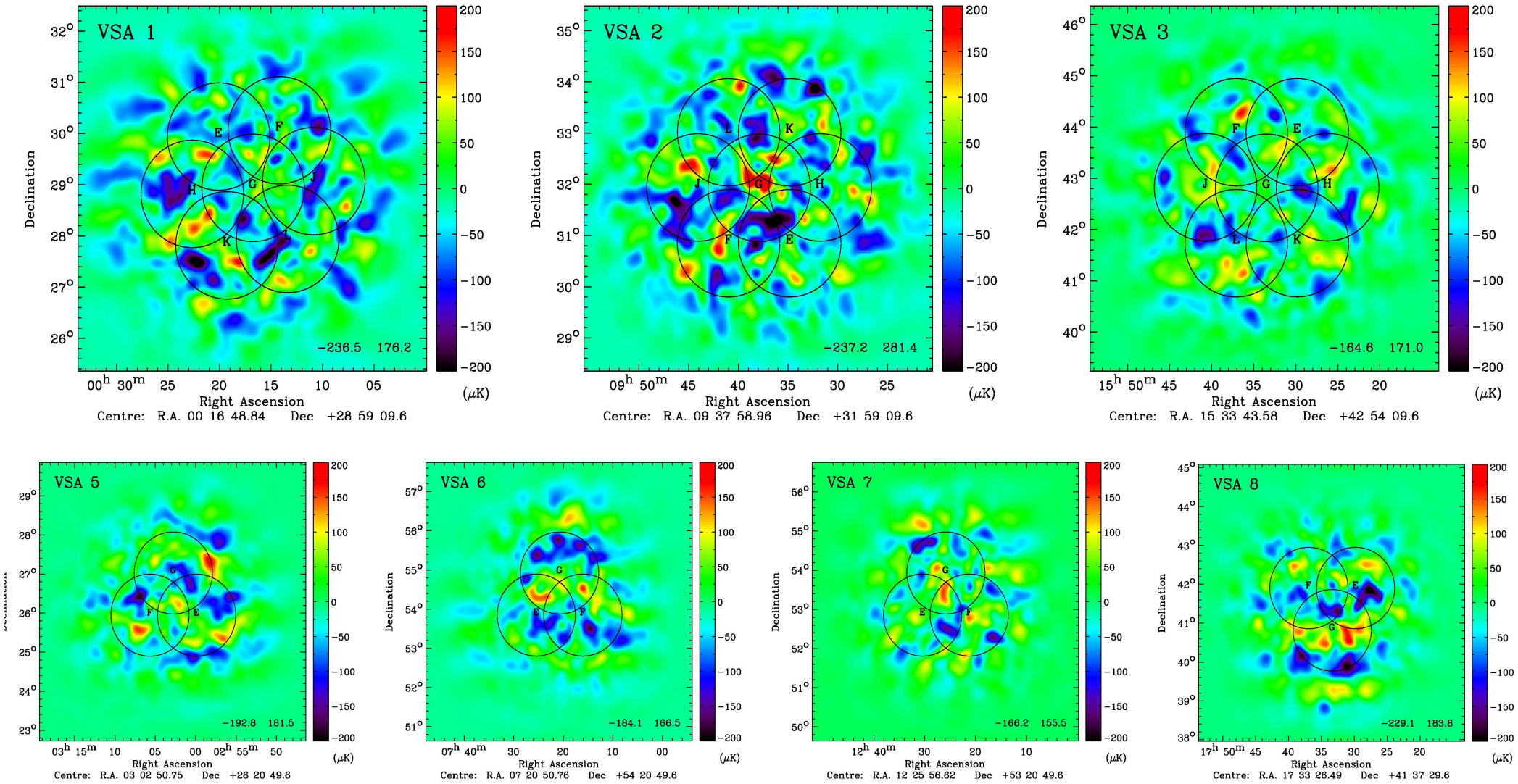

Dickinson et al. 2004 (MNRAS)

Typical rms values of 5-25 microK beam^{-1}

VSA CMB angular power spectrum (compact + extended configuration)

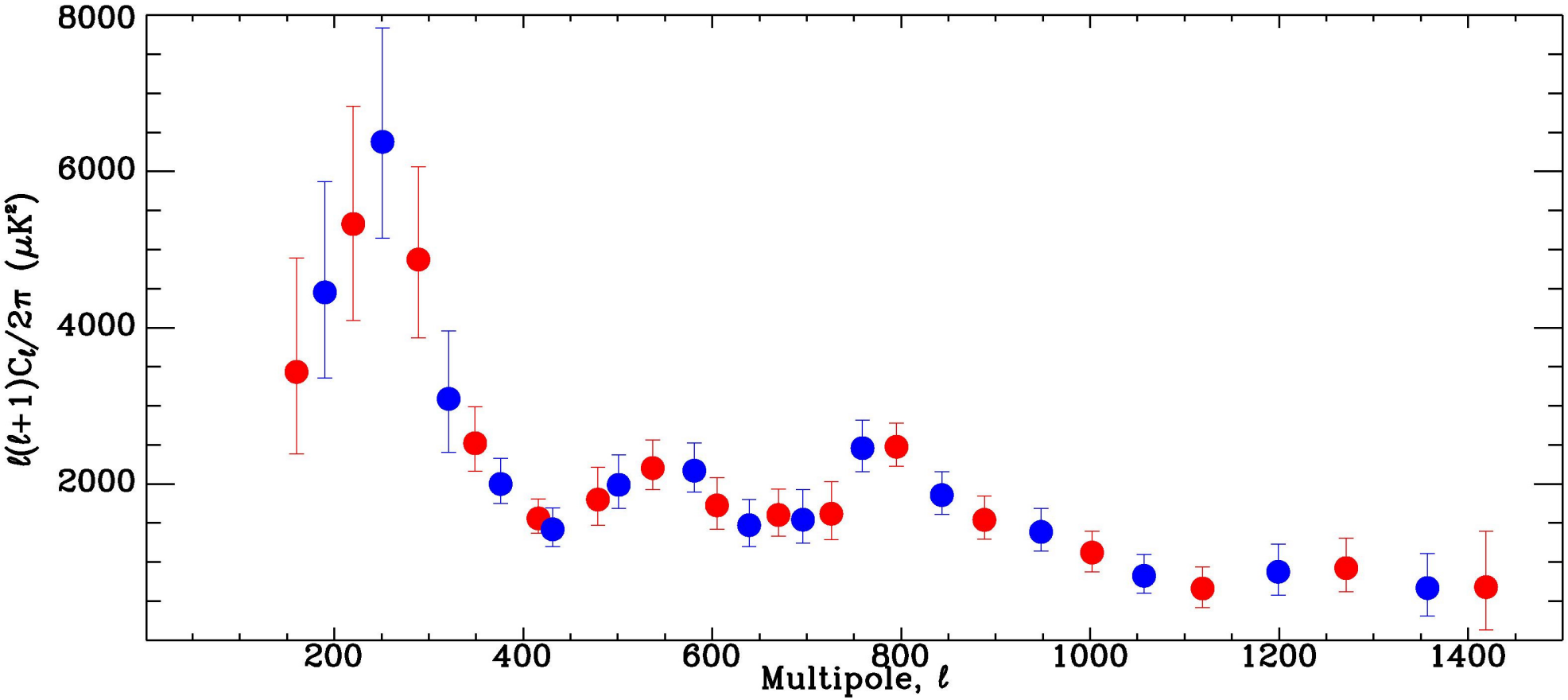

(Dickinson et al. 2004 two alternate binnings)

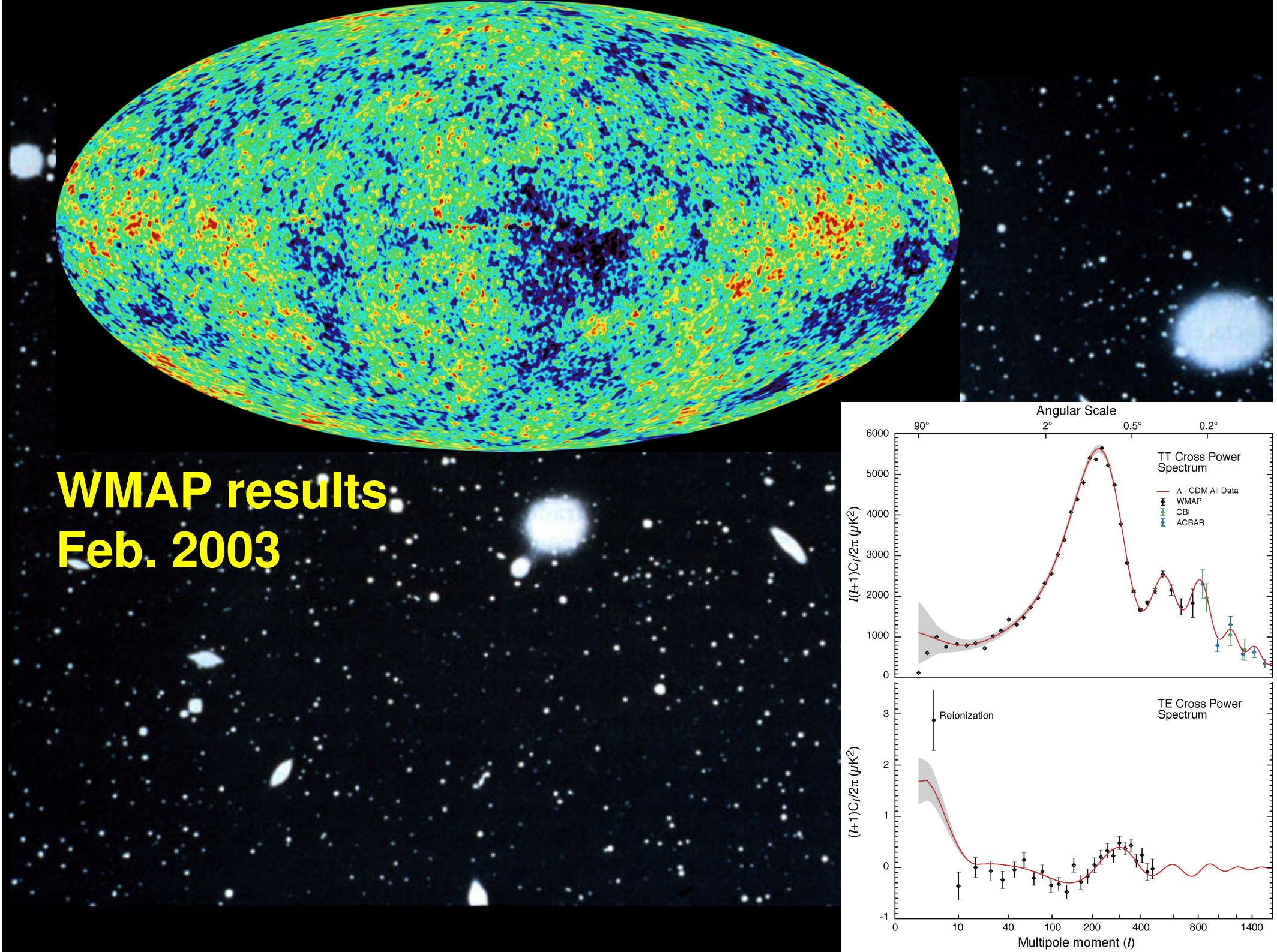
WMAP results
Feb. 2003
Angular Scale
90°
2°
0.5°
0.2°
TT Cross Power Spectrum
Λ - CDM All Data
WMAP
CBI
ACBAR
$l(l+1)C_l/2\pi$ (μK^2)
6000
5000
4000
3000
2000
1000
0
TE Cross Power Spectrum
Reionization
$(l+1)C_l/2\pi$ (μK^2)
3
2
1
0
-1
0
10
40
100
200
400
800
1400
Multipole moment (l)

Table 2. Parameter estimates and 68% confidence limits for the standard six-parameter flat ΛCDM model.

1st year

Parameter	COBE+VSA	WMAP	WMAP+VSA
$\omega_{\rm b}$	$0.0328^{+0.0073}_{-0.0071}$	$0.0240^{+0.0027}_{-0.0016}$	$0.0234^{+0.0019}_{-0.0014}$
$\omega_{\rm dm}$	$0.125^{+0.031}_{-0.027}$	$0.117^{+0.018}_{-0.018}$	$0.111^{+0.014}_{-0.016}$
h	$0.77^{+0.15}_{-0.17}$	$0.73^{+0.10}_{-0.06}$	$0.73^{+0.09}_{-0.05}$
$n_{\rm S}$	$1.05^{+0.12}_{-0.08}$	$1.00^{+0.09}_{-0.04}$	$0.97^{+0.06}_{-0.03}$
$10^{10}A_{\rm S}$	25^{+11}_{-6}	27^{+9}_{-5}	23^{+7}_{-3}
τ	Unconstrained	$0.18^{+0.16}_{-0.08}$	$0.14^{+0.14}_{-0.07}$

$$z_{reion} \approx 92\,(0.03\ h\ \tau\ /\ \Omega_b\ h^2)^{2/3}\ \Omega_m{}^{1/3}$$

General Lambda CDM analysis

Cosmological parameters (68 %C.L.)

For neutrinos and R (95% C.L.)

Rebolo et al. 2004 (MNRAS)

	WMAP	WMAP+VSA	AllCMB
$\Omega_{\rm b}h^2$	$0.025^{+0.003}_{-0.003}$	$0.024^{+0.003}_{-0.002}$	$0.023^{+0.002}_{-0.002}$
$\Omega_{\rm dm}h^2$	$0.108^{+0.022}_{-0.021}$	$0.111^{+0.021}_{-0.019}$	$0.113^{+0.017}_{-0.017}$
h	$0.66^{+0.07}_{-0.06}$	$0.66^{+0.06}_{-0.06}$	$0.65^{+0.07}_{-0.07}$
$z_{\rm re}$	18^{+7}_{-7}	19^{+7}_{-7}	17^{+7}_{-8}
$\Omega_{\rm k}$	$-0.02^{+0.03}_{-0.03}$	$-0.01^{+0.03}_{-0.03}$	$-0.02^{+0.03}_{-0.03}$
f_ν	< 0.093	< 0.083	< 0.083
w	$-1.00^{+0.24}_{-0.27}$	$-0.99^{+0.24}_{-0.27}$	$-1.06^{+0.24}_{-0.25}$
$n_{\rm S}$	$1.04^{+0.12}_{-0.11}$	$0.99^{+0.09}_{-0.09}$	$0.96^{+0.07}_{-0.07}$
$n_{\rm T}$	$0.26^{+0.53}_{-0.60}$	$0.13^{+0.49}_{-0.51}$	$0.12^{+0.48}_{-0.51}$
$n_{\rm run}$	$-0.02^{+0.07}_{-0.05}$	$-0.04^{+0.05}_{-0.04}$	$-0.04^{+0.04}_{-0.05}$
$10^{10}A_{\rm S}$	27^{+8}_{-5}	26^{+9}_{-5}	25^{+6}_{-5}
R	< 0.78	< 0.77	< 0.68
Ω_Λ	$0.71^{+0.07}_{-0.09}$	$0.70^{+0.06}_{-0.08}$	$0.69^{+0.07}_{-0.09}$
t_0	$14.1^{+1.4}_{-1.1}$	$14.1^{+1.3}_{-1.2}$	$14.4^{+1.4}_{-1.3}$
$\Omega_{\rm m}$	$0.31^{+0.09}_{-0.07}$	$0.31^{+0.08}_{-0.06}$	$0.33^{+0.10}_{-0.07}$
σ_8	$0.76^{+0.14}_{-0.14}$	$0.77^{+0.13}_{-0.13}$	$0.76^{+0.11}_{-0.12}$
τ	$0.20^{+0.13}_{-0.11}$	$0.20^{+0.15}_{-0.10}$	$0.17^{+0.12}_{-0.10}$

Current CMB data

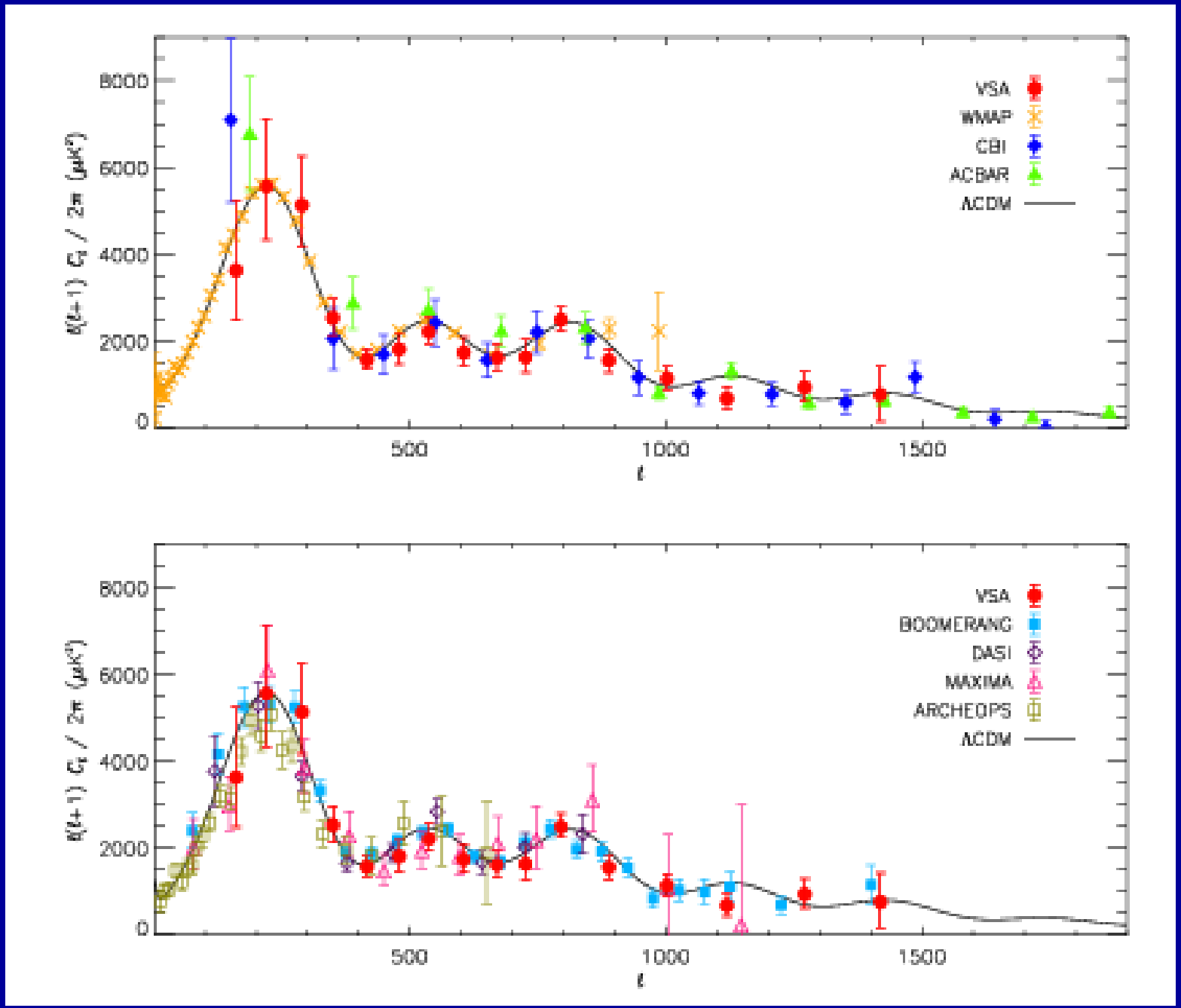

WMAP
3rd year

WMAP Cosmological Parameters Model: lcdm Data: wmap		WMAP Cosmological Parameters Model: lcdm Data: wmap+cbi+vsa	
$10^2\Omega_b h^2$	$2.230^{+0.075}_{-0.073}$	$10^2\Omega_b h^2$	2.208 ± 0.071
$\Delta^2_{\mathcal{R}}(k = 0.002/\mathrm{Mpc})$	$(23.7 \pm 1.4) \times 10^{-10}$	$\Delta^2_{\mathcal{R}}(k = 0.002/\mathrm{Mpc})$	$(23.5^{+1.3}_{-1.4}) \times 10^{-10}$
h	0.735 ± 0.032	h	0.742 ± 0.031
H_0	73.5 ± 3.2 km/s/Mpc	H_0	74.2 ± 3.1 km/s/Mpc
$n_s(0.002)$	0.951 ± 0.016	$n_s(0.002)$	0.947 ± 0.015
$\Omega_b h^2$	$0.02230^{+0.00075}_{-0.00073}$	$\Omega_b h^2$	0.02208 ± 0.00071
Ω_Λ	0.763 ± 0.034	Ω_Λ	0.774 ± 0.031
Ω_m	0.237 ± 0.034	Ω_m	0.226 ± 0.031
$\Omega_m h^2$	$0.1265^{+0.0081}_{-0.0080}$	$\Omega_m h^2$	$0.1233^{+0.0075}_{-0.0074}$
σ_8	0.742 ± 0.051	σ_8	$0.721^{+0.047}_{-0.046}$
A_{SZ}	1.00 ± 0.64	A_{SZ}	$0.85^{+0.62}_{-0.58}$
t_0	$13.73^{+0.16}_{-0.15}$ Gyr	t_0	13.76 ± 0.15 Gyr
τ	$0.088^{+0.029}_{-0.030}$	τ	0.087 ± 0.029
θ_A	$0.5948^{+0.0021}_{-0.0022}$ °	θ_A	0.5942 ± 0.0020 °
z_r	10.9 ± 2.5	z_r	10.8 ± 2.4

VSA Super-Extended Configuration

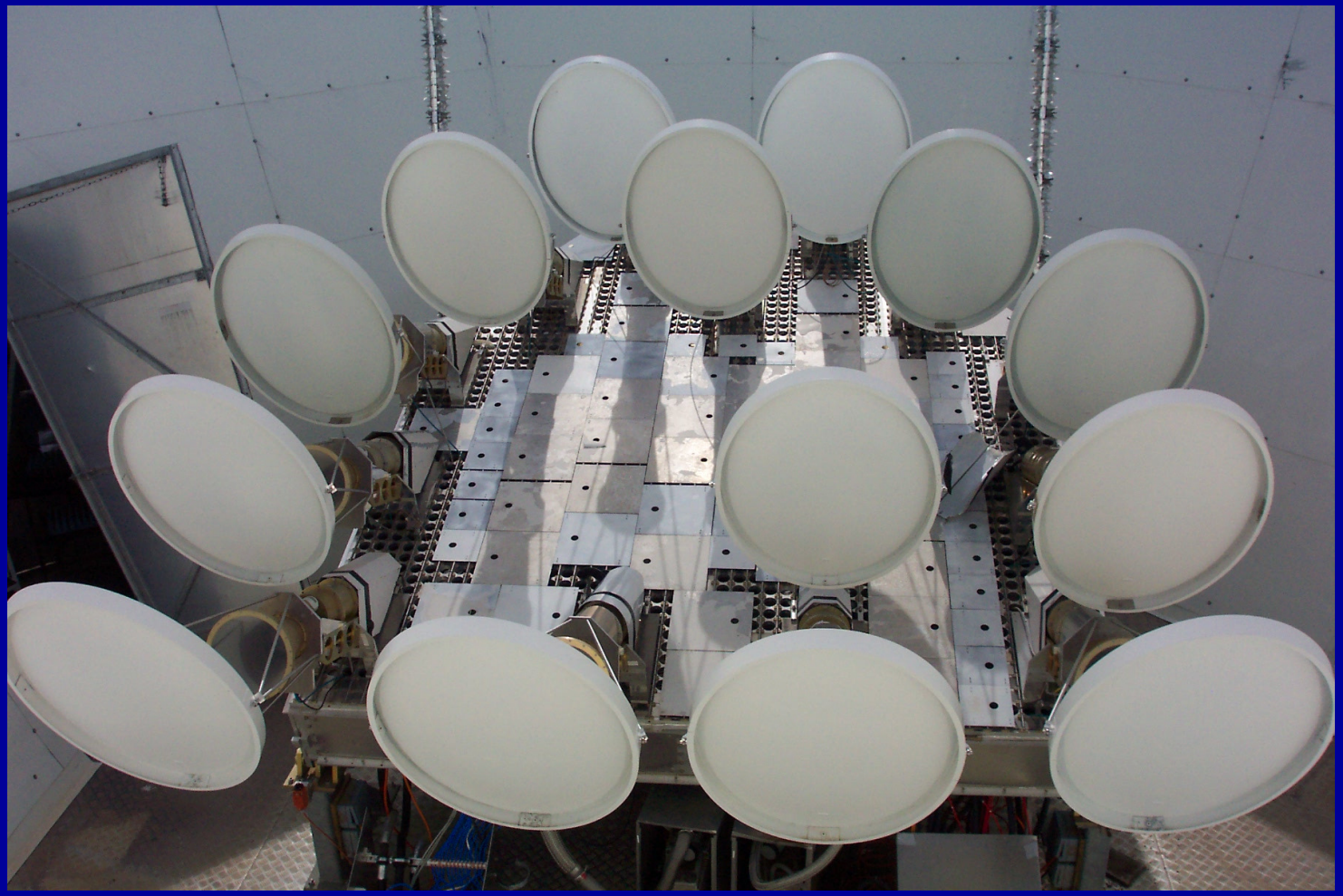

o We have increased the ℓ-range further up to 2500 by using bigger carbon fibre reflectors (55 cm diameter) and scattering the antennas to the edges of the table.

o Primary beam: 1°. Synthesized beam: **6 arcmin.**

oA limited deep survey can probe the high l tail of the power spectrum.

- **Parameters to constrain:**
  - **Constraints on inflationary physics: spectral index, running?**
  - **Better bounds on neutrino mass**
  - **Normalisation of the spectrum (σ_8) or total number of clusters.**

SuperExtended VSA Configuration

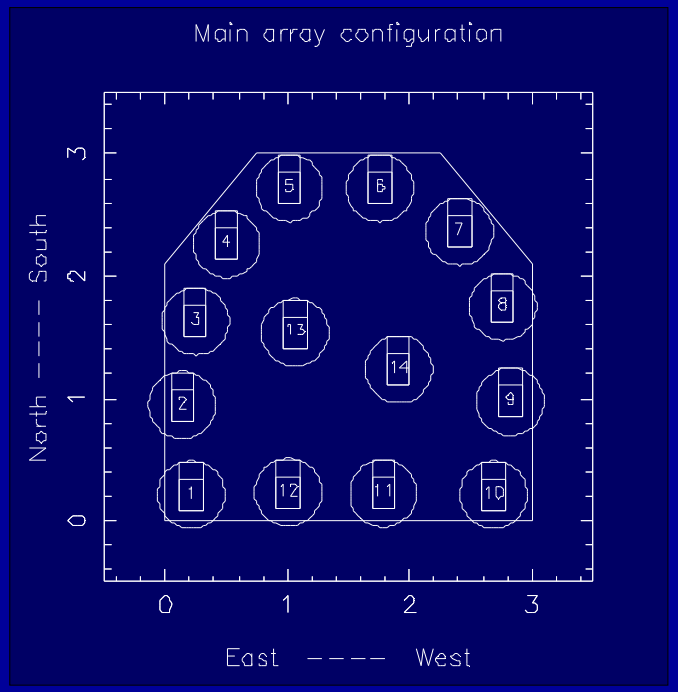

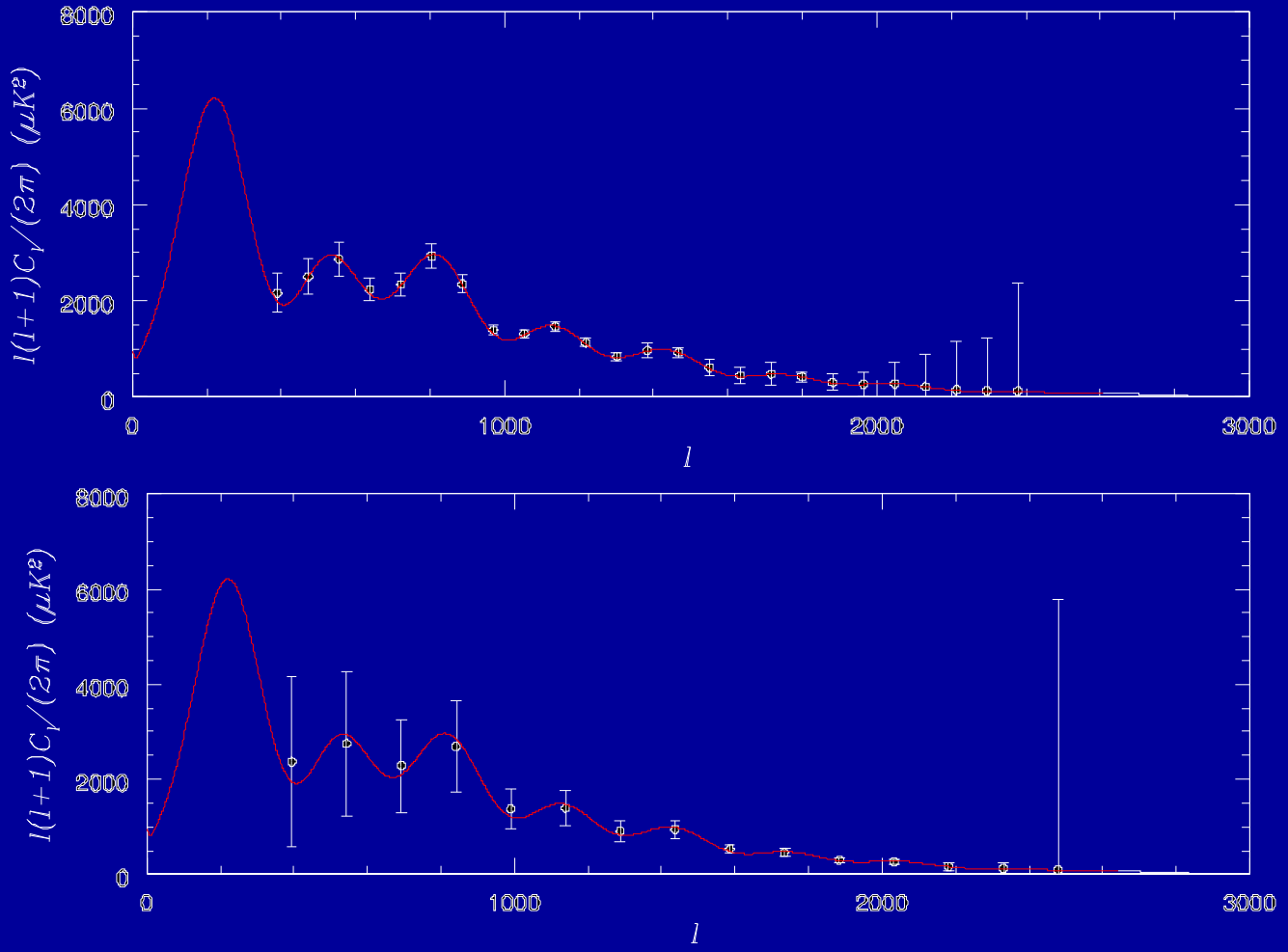

Synth. Beam ~ 6´

With a shallow survey with big mosaics the 4th and 5th the peaks can be investigated.

A limited deep survey can probe the high l tail (CBI excess of power at ℓ>2000).

VSA observations of the Sunyaev-Zeldovich (SZ) effect

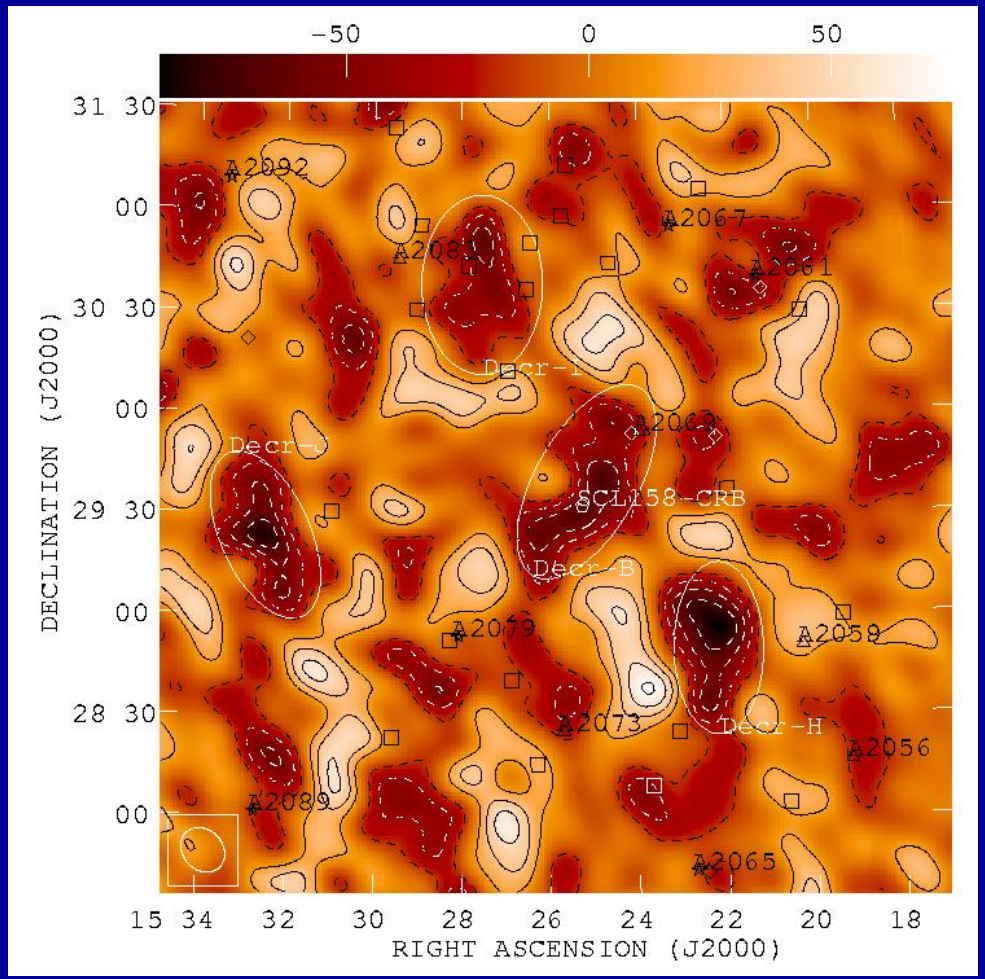

Thermal Sunyaev-Zel´dovich Effect

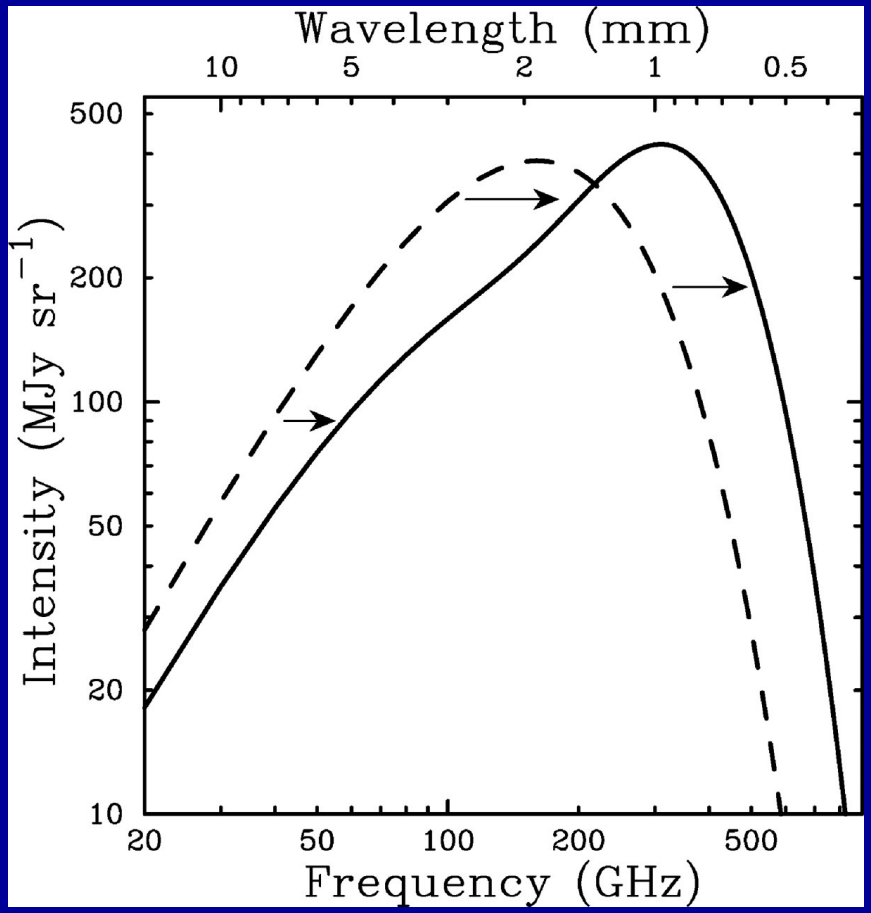

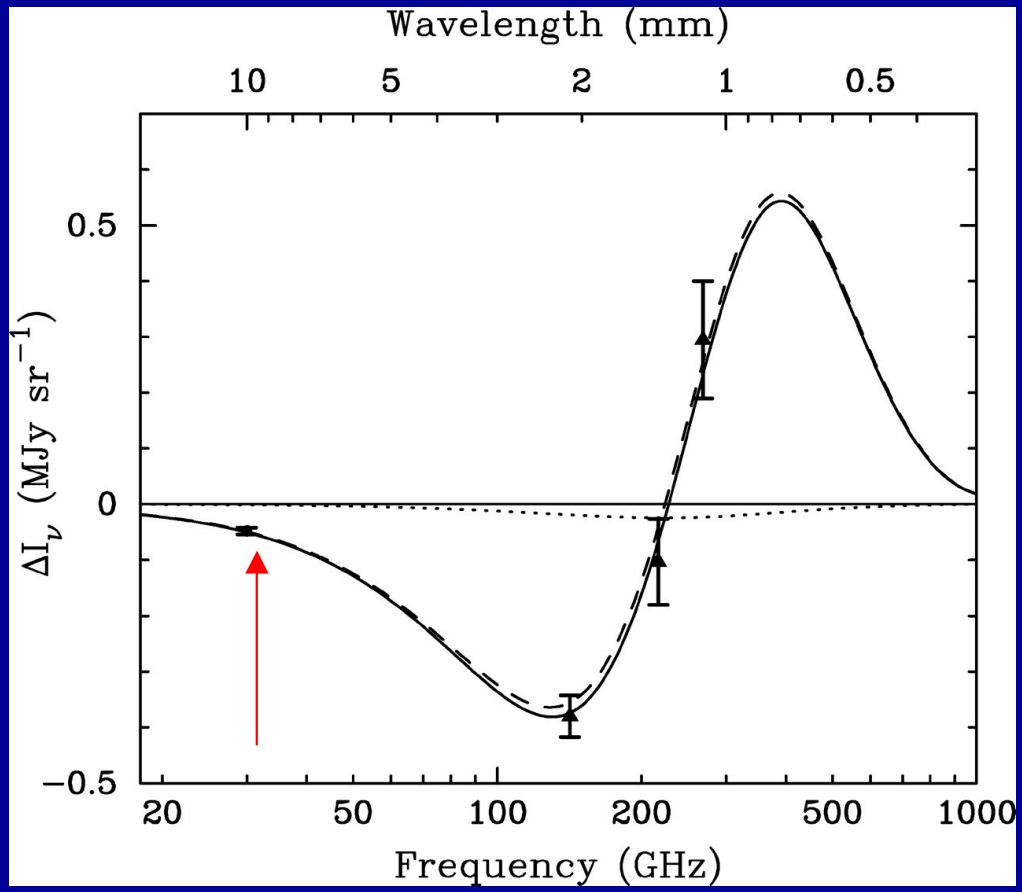

$$\frac{\delta T_{tSZ}}{T_0} = g(\nu) \int d\mathbf{r}\, \sigma_T n_e(\mathbf{r}) \frac{k_B T_e(\mathbf{r})}{m_e c^2} = g(\nu) \frac{\sigma_T}{m_e c^2} \int d\mathbf{r}\, p_e(\mathbf{r})$$

Comptonization parameter: $y \equiv \int d\mathbf{r}\, \sigma_T n_e(\mathbf{r}) \frac{k_B T_e(\mathbf{r})}{m_e c^2}$

Cluster sample

Cúmulo	A.R. [a] (B1950)	Dec. [a] (B1950)	z [b]	L_X(0.1-2.4 keV) [a] ($10^{44} h_{50}^{-2}$ erg s^{-1})	T_e [c] (keV)	N_H [d] (10^{-20}cm^{-2})
A399	02 55 05.33	12 50 57.6	0.0715	6.78	7.0 ± 0.4	10.24
A401	02 56 12.55	13 22 50.1	0.0748	11.76	8.0 ± 0.4	9.70
A478	04 10 40.89	10 20 26.0	0.0881	13.31	$8.4^{+0.5}_{-1.4}$	14.69
A1795	13 46 34.43	26 50 37.5	0.0622	9.93	7.8 ± 1.0	1.00
A2142	15 56 16.45	27 22 08.0	0.0899	20.52	$9.7^{+1.5}_{-1.1}$	3.91
A2244	17 00 52.86	34 07 54.5	0.0968	7.39	$7.1^{+5.0}_{-2.2}$ [f]	1.97
Coma	12 57 30.00"	28 11 00.0"	0.0232	7.01	9.1 ± 0.7 [g]	0.78

Abell 1795

Abell 2142

Radiosource
Corrected

Cleaned
Maps

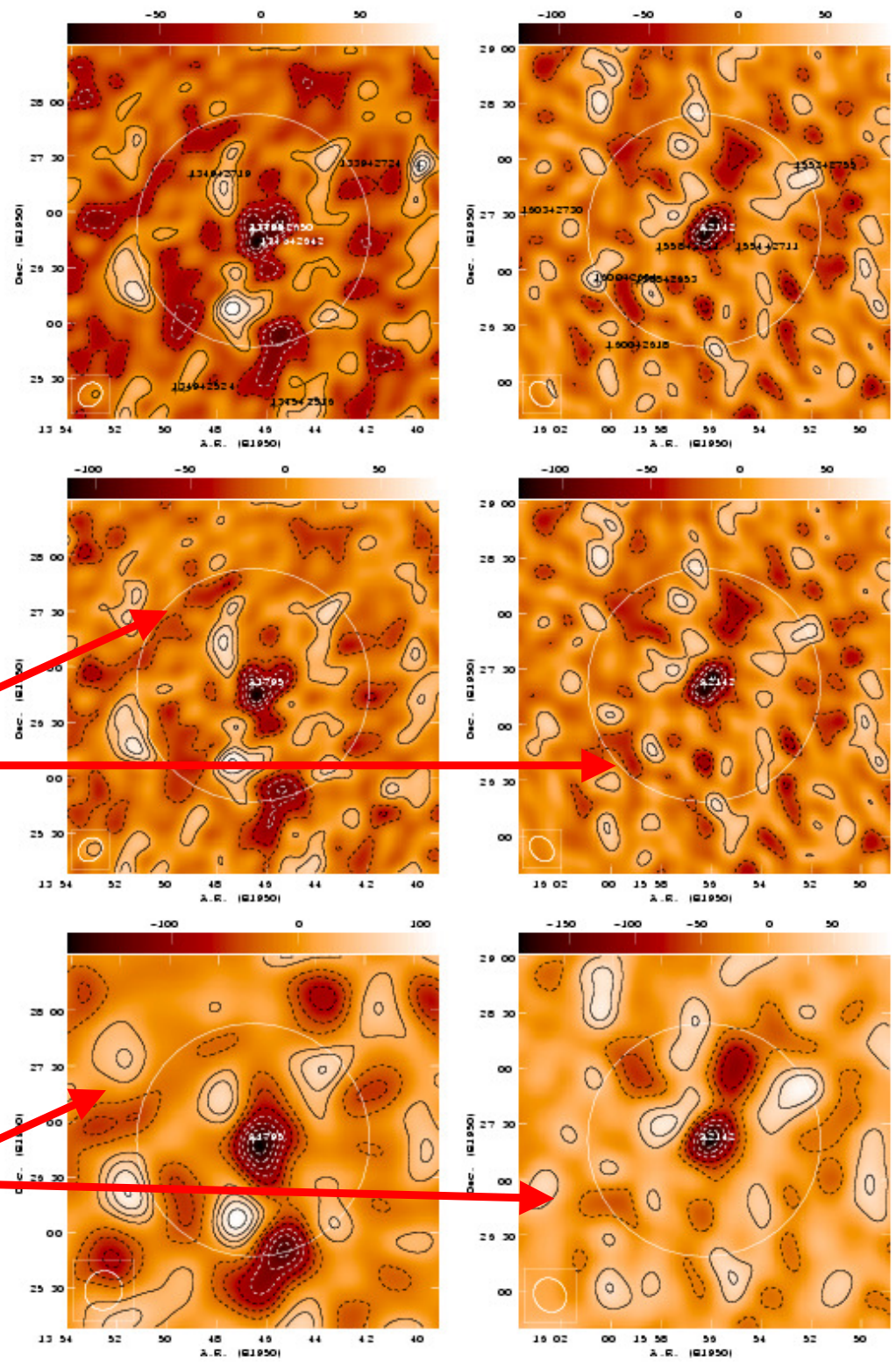

SZ prediction from X-ray imaging

Cluster	ΔT_0 (μK)	$y_{r=0}$ ($\times 10^{-5}$)	χ^2_ν	$\Delta T_0^{\rm pred}$ [a] ($h^{-1/2}$ μK)
A399	-161 ± 83	3.03 ± 1.56	2.92	-347 ± 58
A401	-474 ± 134	8.95 ± 2.35	2.66	-680 ± 106
A478	-1439 ± 305	27.16 ± 3.89	2.83	-1156^{+223}_{-294}
A1795	-762 ± 135	14.39 ± 2.56	2.90	-646 ± 138
A2142	-956 ± 163	18.05 ± 3.09	3.33	-1170^{+252}_{-241}
A2244	$+157 \pm 301$	-	1.95	-695^{+812}_{-278}
Coma	-499 ± 82	9.42 ± 1.55	1.83	-544 ± 91

Lancaster, Génova-Santos et al. 2005

Results

$\Omega_m = 0.27 \pm 0.1$

Cúmulo	r_{cz} $(h^{-1}\mathrm{Mpc})$	r_{500} $(h^{-1}\mathrm{Mpc})$	M_T $(10^{14}h^{-1}\mathrm{M}_\odot)$	n_{e0}^{SZ} $(10^{-3}h\ \mathrm{cm}^{-3})$	M_{gas}^{SZ} $(10^{14}\ h^{-2}\ \mathrm{M}_\odot)$	f_{gas}^{SZ} (h^{-1})	Ω_M
A399	$0.2313^{+0.0021}_{-0.0020}$	1.037 ± 0.093	5.33 ± 0.69	1.54 ± 0.86	0.20 ± 0.11	0.038 ± 0.026	0.55 ± 0.60
A401*	$0.1227^{+0.0009}_{-0.0008}$	1.109 ± 0.097	5.90 ± 0.71	6.22 ± 1.86	0.43 ± 0.13	0.073 ± 0.031	0.31 ± 0.25
A478*	0.0617 ± 0.0003	$1.136^{+0.118}_{-0.140}$	$6.66^{+1.07}_{-1.80}$	$37.81^{+7.76}_{-9.39}$	$0.72^{+0.15}_{-0.18}$	$0.109^{+0.040}_{-0.052}$	$0.21^{+0.16}_{-0.16}$
A1795*	0.0977 ± 0.0002	1.095 ± 0.122	6.58 ± 1.25	15.67 ± 4.02	0.46 ± 0.12	0.069 ± 0.031	0.33 ± 0.27
A2142*	0.0983 ± 0.0004	$1.221^{+0.146}_{-0.131}$	$7.87^{+1.69}_{-1.40}$	$12.78^{+3.43}_{-3.11}$	$0.71^{+0.19}_{-0.15}$	$0.090^{+0.044}_{-0.036}$	$0.25^{+0.22}_{-0.21}$
A2244	0.0572 ± 0.0010	$1.045^{+0.299}_{-0.174}$	$4.70^{+3.37}_{-1.69}$	$<7.12^{+9.00}_{-7.30}$	$<0.16^{+0.20}_{-0.16}$	$<0.033^{+0.067}_{-0.047}$	$>0.62^{+1.47}_{-1.10}$
Coma*	$0.1855^{+0.0002}_{-0.0001}$	1.183 ± 0.113	7.88 ± 1.12	4.43 ± 0.94	0.50 ± 0.11	0.064 ± 0.023	0.35 ± 0.26
Prom.						0.074 ± 0.014	0.27 ± 0.10

$$f_{gas}^{SZ} = \frac{M_{gas}^{SZ}}{M_T} \approx 0.0630\ h^{-1}\ \beta^{-1} \left[\frac{-\Delta T_0}{100\mu\mathrm{K}}\right] \left[\frac{T_e}{\mathrm{keV}}\right]^{-5/2} \left[\frac{r_{cz}}{10^{-1}h^{-1}\mathrm{Mpc}}\right]^2 \frac{I_{gas}(\beta, r_{500}/r_{cz})}{I_{SZ}(\beta)}$$

SZ effect in superclusters

BBN and CMB fluctuations agree on baryon density $\Omega_b h^2 = 0.0223 \pm 0.0007$

Local baryon budget is a factor 2 lower.

Component	Ω(baryons)
• Stars in spheroids	0.0026
• Stars in disks	0.00086
• Stars in irregulars	0.000069
• Neutral atomic gas	0.00033
• Molecular gas	0.00030
• Plasma in clusters	0.0026
• Plasma in groups	0.0076-0.014

Where are the rest of the baryons in the local Universe?

Possible explanations:

- Low mass objects (Brown dwarfs, planets...)?
  - **but** mass function for low mass objects does not provides enough mass $dN/dm \sim m^{-1}$ (Béjar et al. 2001)
- High mass MACHOs...?
  - **but** there are microlensing constraints

Hydrodynamical simulations suggest these baryons could be found as Warm-hot 10^5- 10^7 K gas in the intrasupercluster medium

(Cen & Ostriker 1999, 2006)

A Survey with the VSA in the Corona Borealis Supercluster

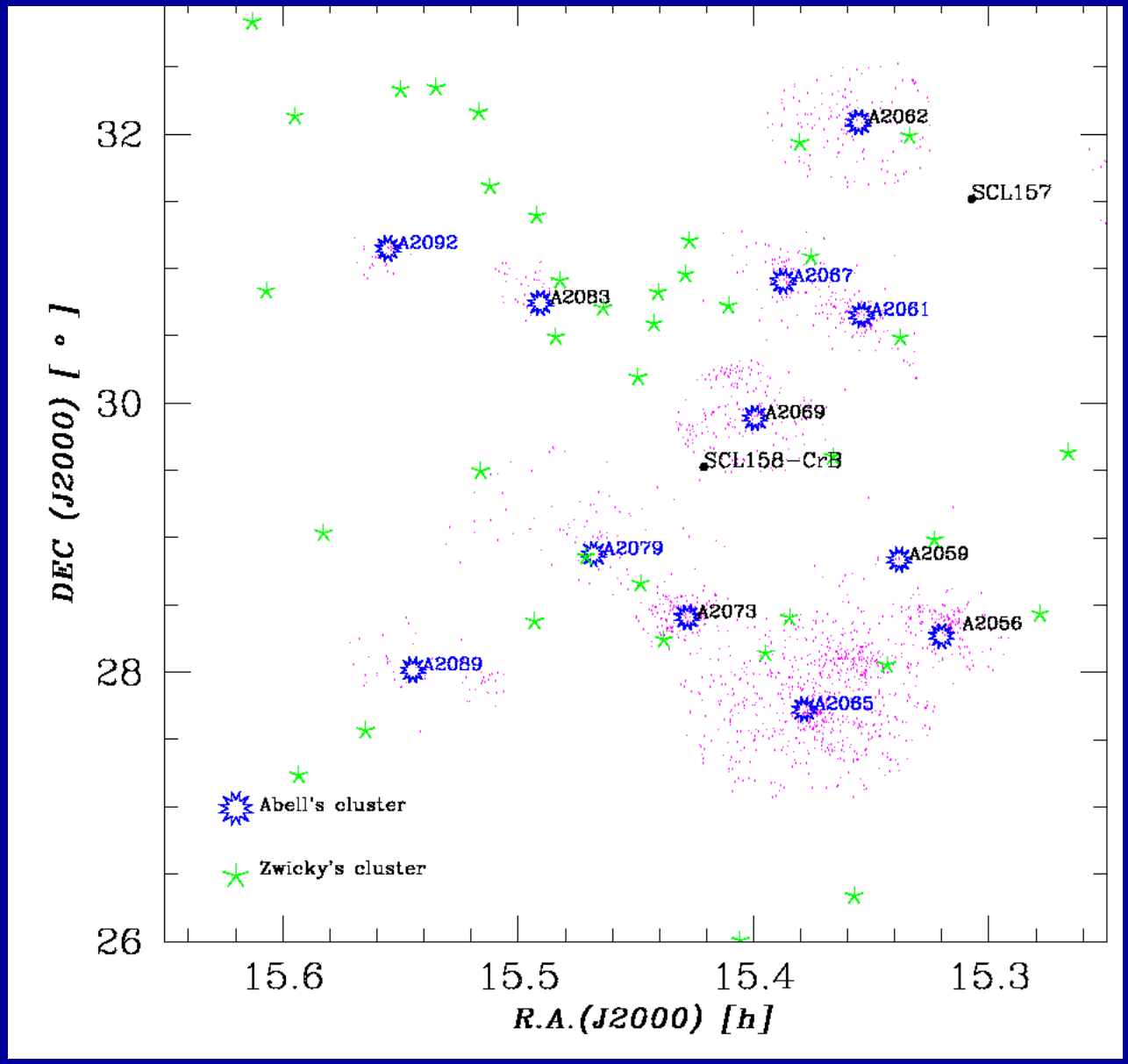

The "missing baryons" problem: are half of the baryons in the local Universe in a Warm-Hot phase?

A total area of 24 deg^2 was imaged using a mosaic of 9 pointings, with 11′ resolution.

The total integration time was approx. 300 hrs.

(Génova-Santos, Rubiño-Martín et al. 2005)

VSA mosaic of the Corona Borealis Supercluster

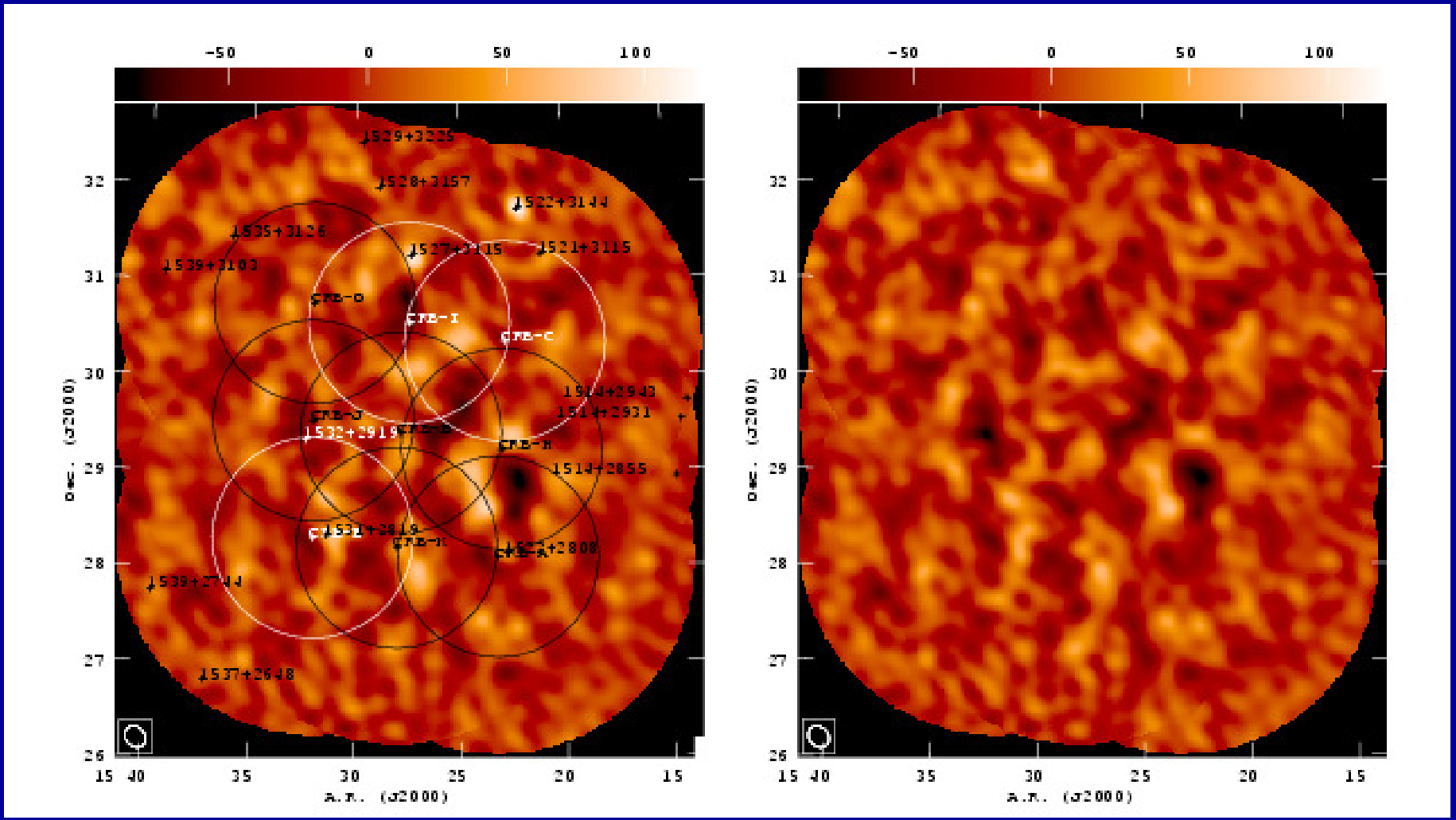

CrB SC seen by VSA

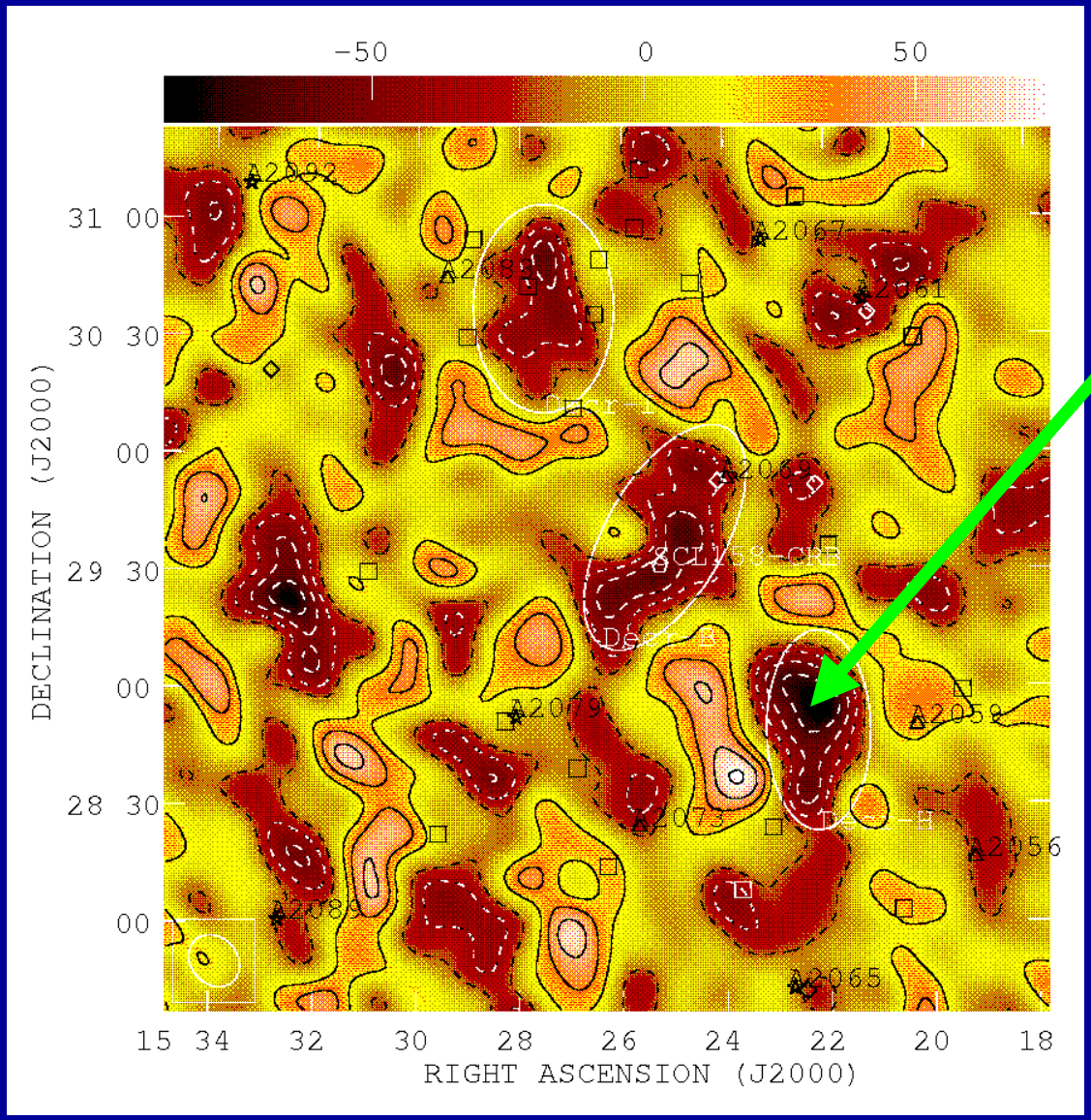

	ΔS_ν (mJy/beam)	ΔT_{RJ} (μK)
Decrement H	-103 ± 10	-231 ± 23

The H spot is detected with a significance greater than 10-sigma (4-sigma with respect to the CMB+noise).

No known cluster of galaxies is associated to this spot

(Génova-Santos et al. 2005)

Origin of the spot (I): primordial CMB?

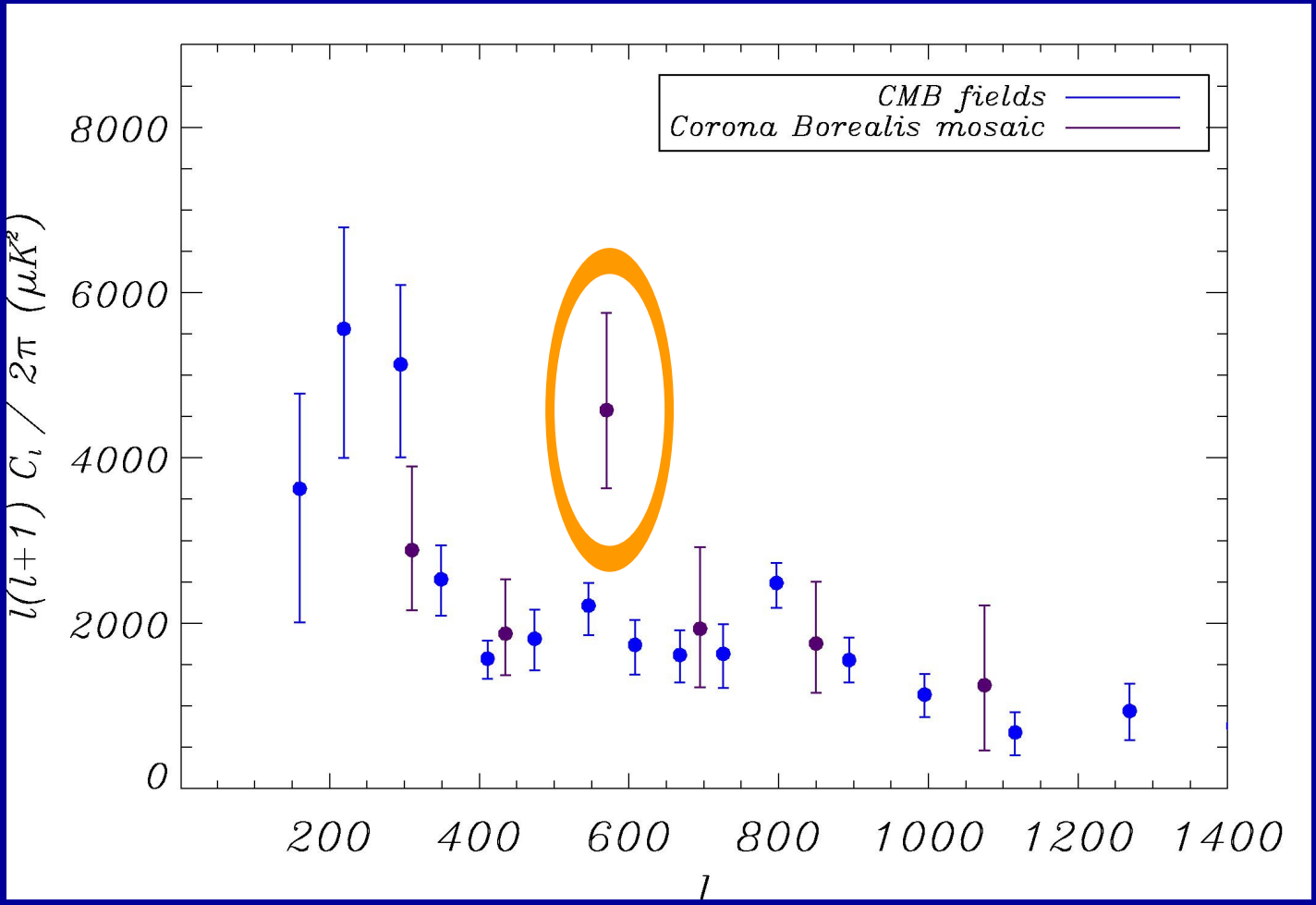

The deviation in the power spectrum at l=550 is due to the presence of decrement H. Using MC simulations (CMB+noise), we find that the probability for H spot is 0.16%.

Origin of the spot (I): primordial CMB?

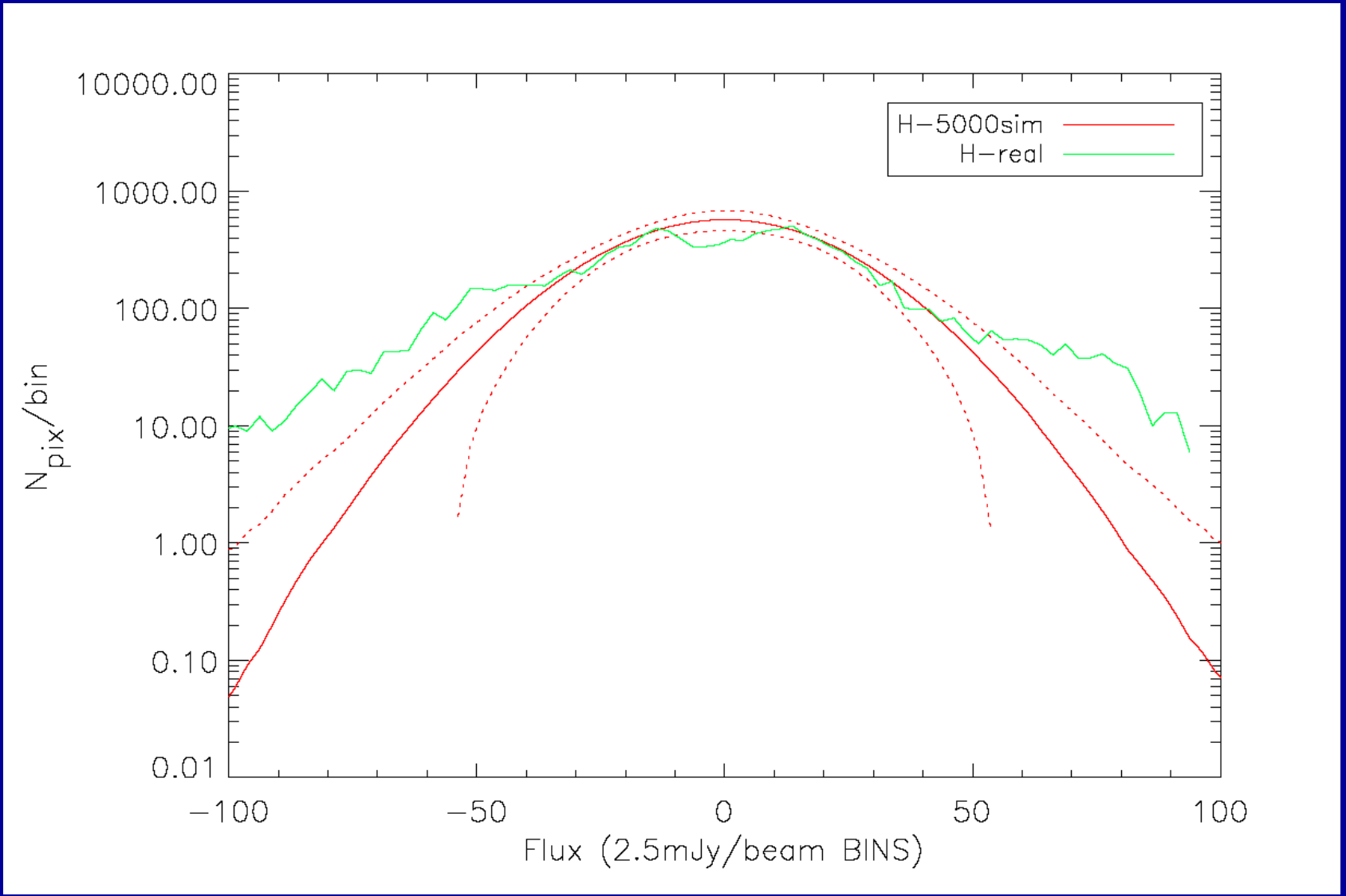

A fluctuation analysis shows the deviation from Gaussianity as well.

Primordial CMB origin? Gaussianity analysis

- We carried out a complete Gaussianity analysis of all the VSA fields, using a new statistical technique called the "**Smooth Tests of Goodness of Fit**", developed by Rayner & Best (1989).

- The technique has been adapted to deal with data from interferometers (see details in Aliaga et al. 2005). We follow to steps:

  - First, data are transformed into signal-to-noise eigenmodes (Bond 1995), and then normalised.

  - The following statistics test smooth deviations of the actual distribution from a Gaussian one:

$$S_k = \sum_{i=1}^{k} U_i^2$$

with

$$\begin{aligned} U_1^2 &= n(\hat{\mu}_1)^2 \\ U_2^2 &= n(\hat{\mu}_2 - 1)^2/2 \\ U_3^2 &= n(\hat{\mu}_3 - 3\hat{\mu}_1)^2/6 \\ U_4^2 &= n[(\hat{\mu}_4 - 3) - 6(\hat{\mu}_2 - 1)]^2/24 \end{aligned}$$

Results of the STGOF analysis

(Rubiño-Martín et al. 2006)

- We analyse the Corona Borealis region, and all the 41 pointings dedicated to primordial observations.
- We find a strong **non-Gaussianity deviation (99.8% C.L.)** in the Corona Borealis mosaic analysis, for the statistic U_2^2.
- This is **the strongest non-Gaussian deviation found in any of the fields observed with the VSA.**
- This deviation from Gaussianity **can NOT be explained as drawn from a Gaussian field with the local power spectrum** (i.e. when the data are decorrelated with the local power spectrum, the NG signal remains).

Origin of the spot (II): unknown cluster?

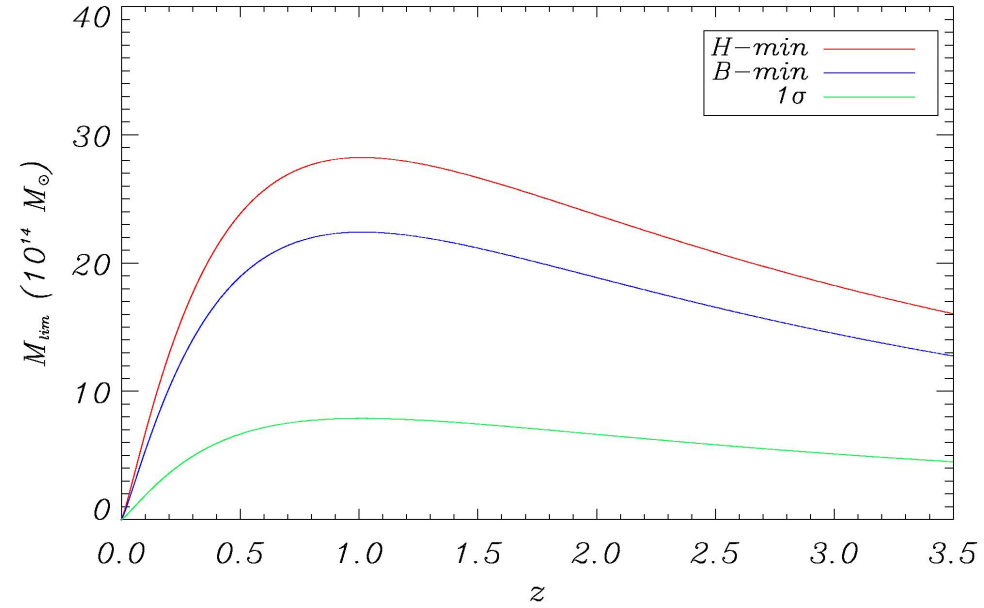

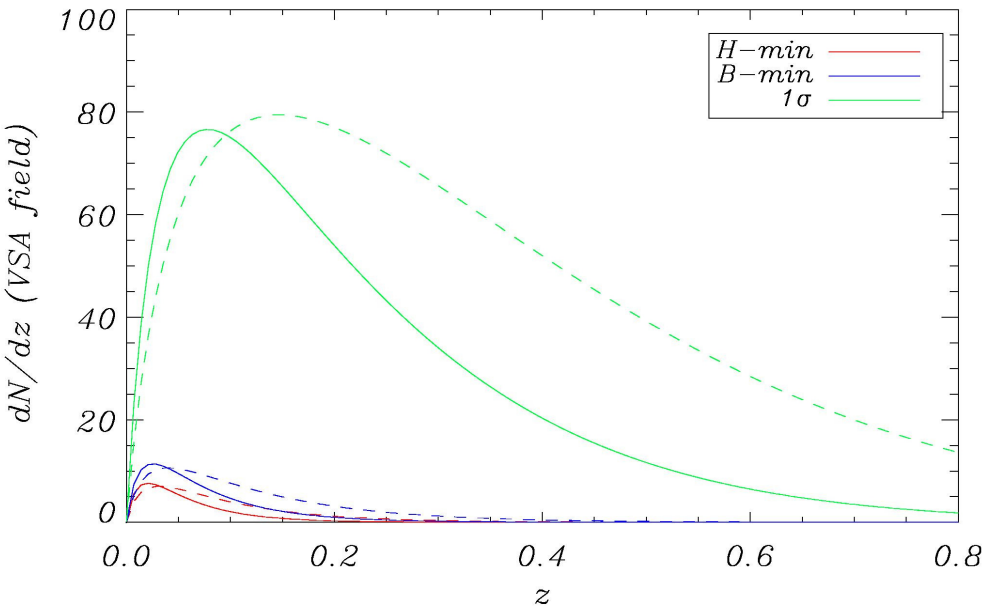

SZ effect from (unknown) clusters of galaxies.

We can estimate the number of expected clusters in the region following Holder et al. (2000).

We used two different prescriptions for mass function, PS (solid) and ST (dashed).

On average, we expect 0.38 clusters of galaxies in the region which are able to produce such a decrement.

Origin of the spot (III): WHIM?

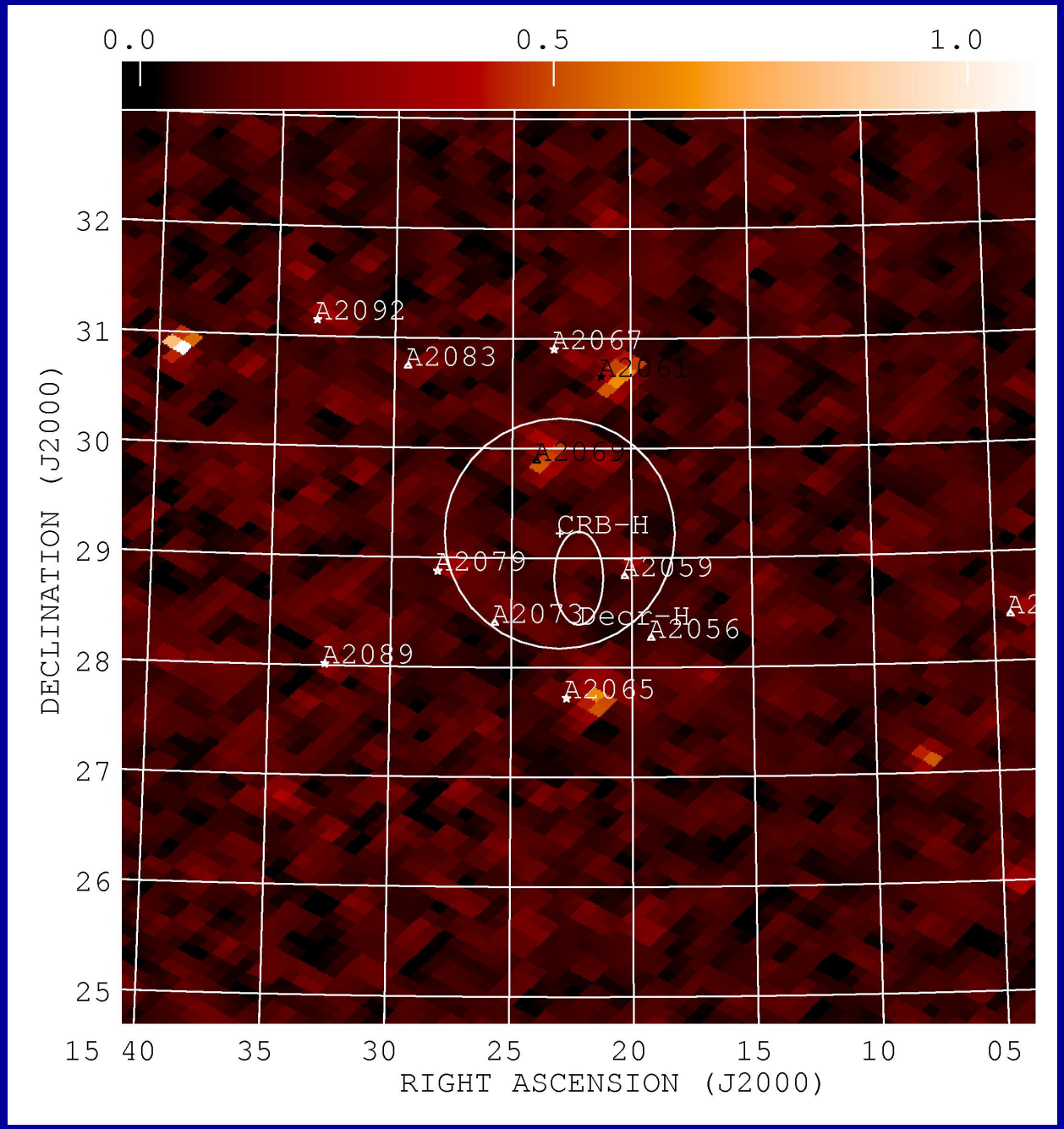

No clear excess in the ROSAT-R6 band (0.73-1.56 keV). A correlation analysis yields:

$\alpha = -0.28 \pm 0.74\ \mu K/X$

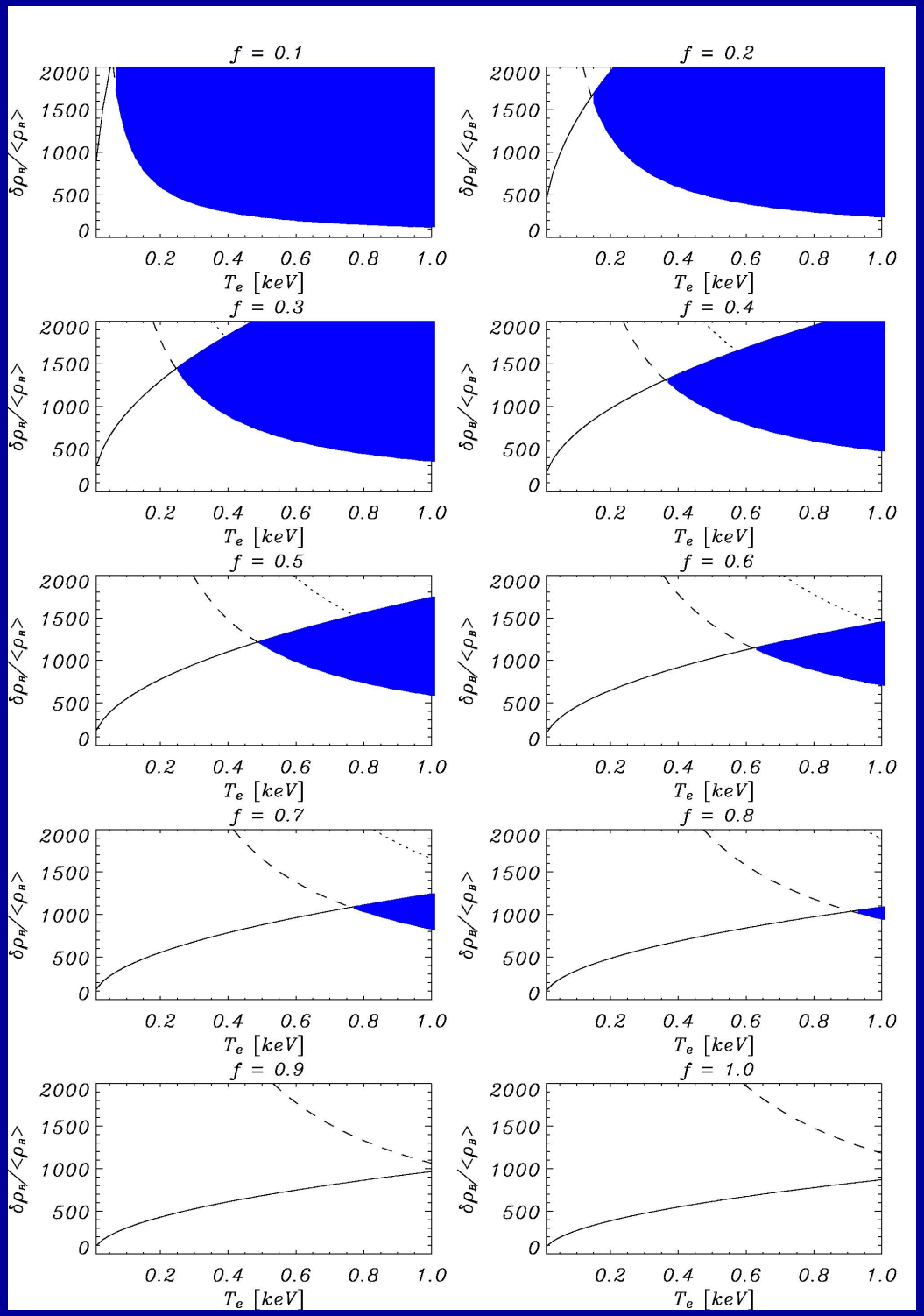

Origin of the spot (III)

We can infer the parameters allowed by the observations if the signal is produced by diffuse gas.

If the case of **a filament is pointing towards us**:

$\delta\rho_B/\rho_B = 450$, and

2 x 2 x 40 Mpc, then

$M_{gas} \approx 5 \times 10^{14} M_o$

This is 10% of the total baryonic mass of the SC!

Multifrequency Observations in CrB

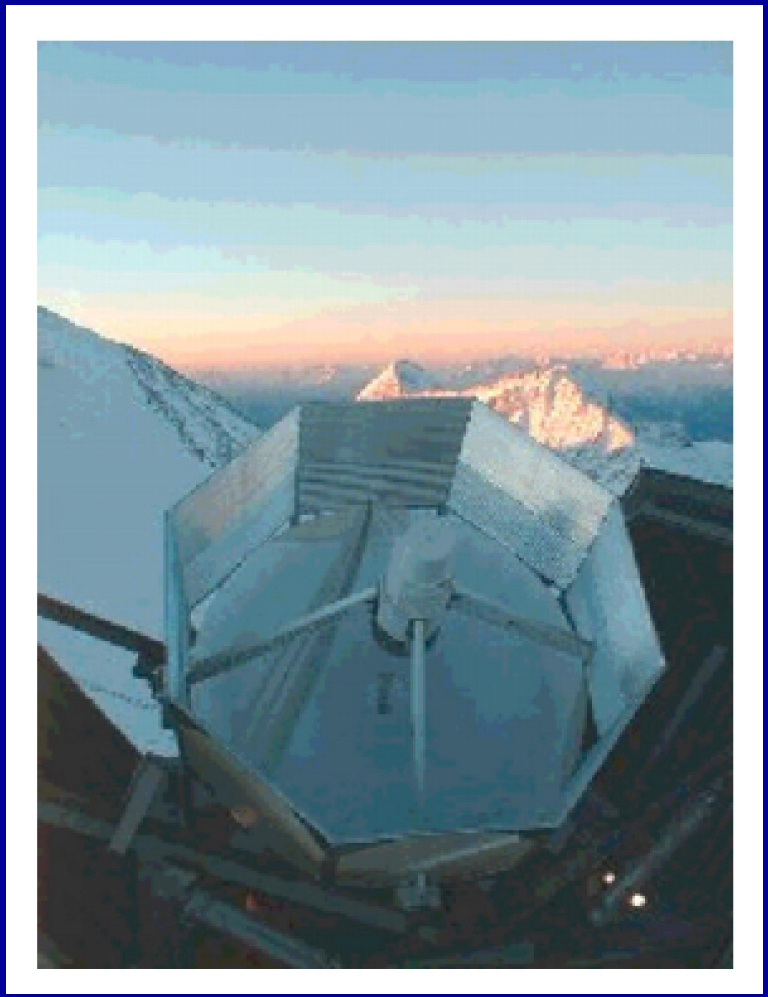

MITO (Millimeter and Infrared Testa Grigia Observatory)

- Collaboration between IAC and Univ. Roma (F. Melchiorri, M. De Petris).
- Observations during one campaign in the Cr-B H spot at **143, 214, 272** and **353** GHz, with angular resolution of 16'.

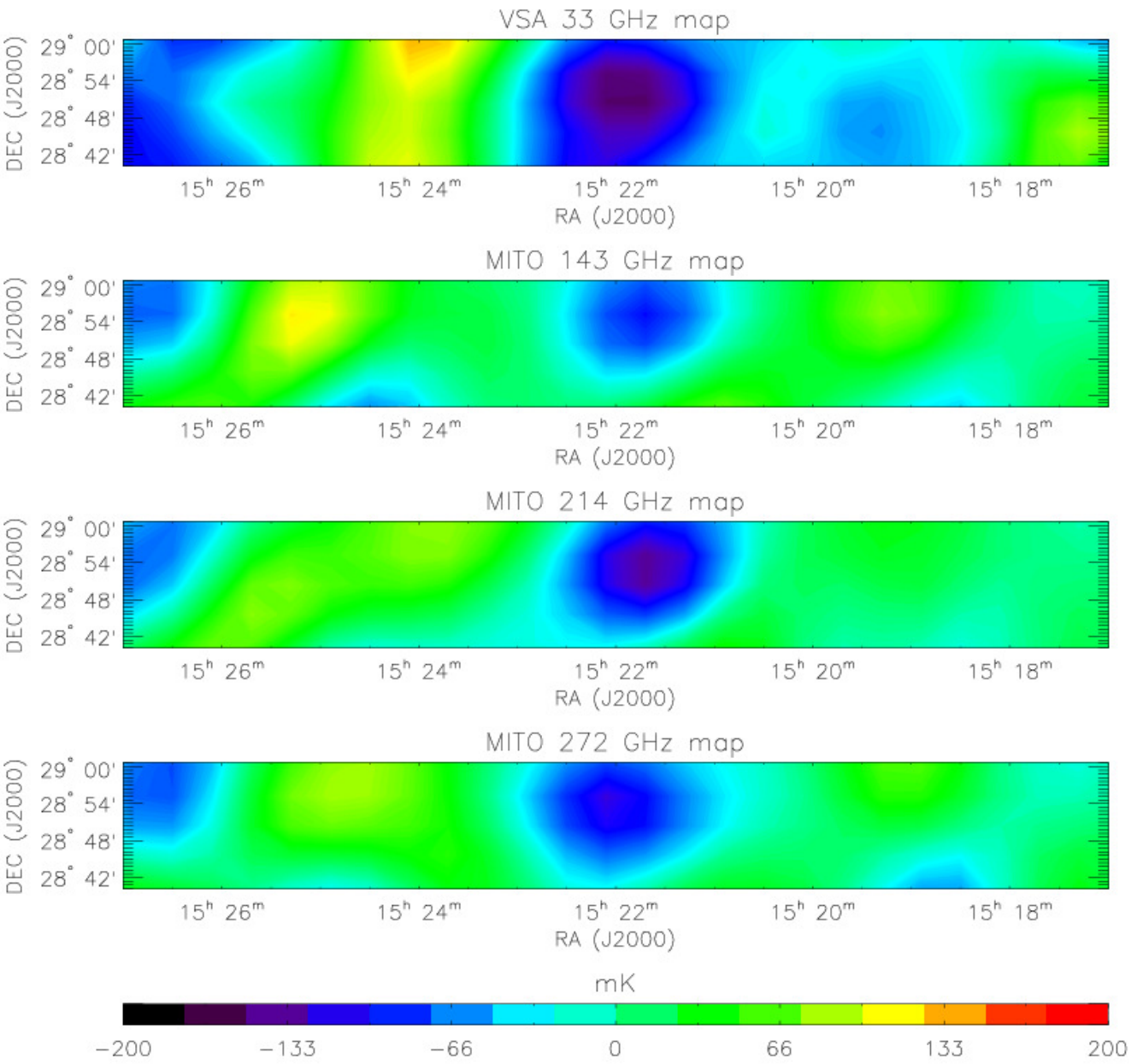

Fig. 2.— Strip of thermodynamic temperature maps derived from the MEM for VSA and the 3 MITO channels.

(Battistelli et al. 2006)

MITO observations:

- 105 scans across H spot.
- High frequency channel used for atmospheric decorrelation.
- Calibration using scans on Jupiter.
- Maximum Entropy method is used to reconstruct the signal of the three remaining channels plus the VSA data.
- Multi-pixel Maximum Likelihood code is used to look for common (CMB) and frequency dependent (SZ) signals.

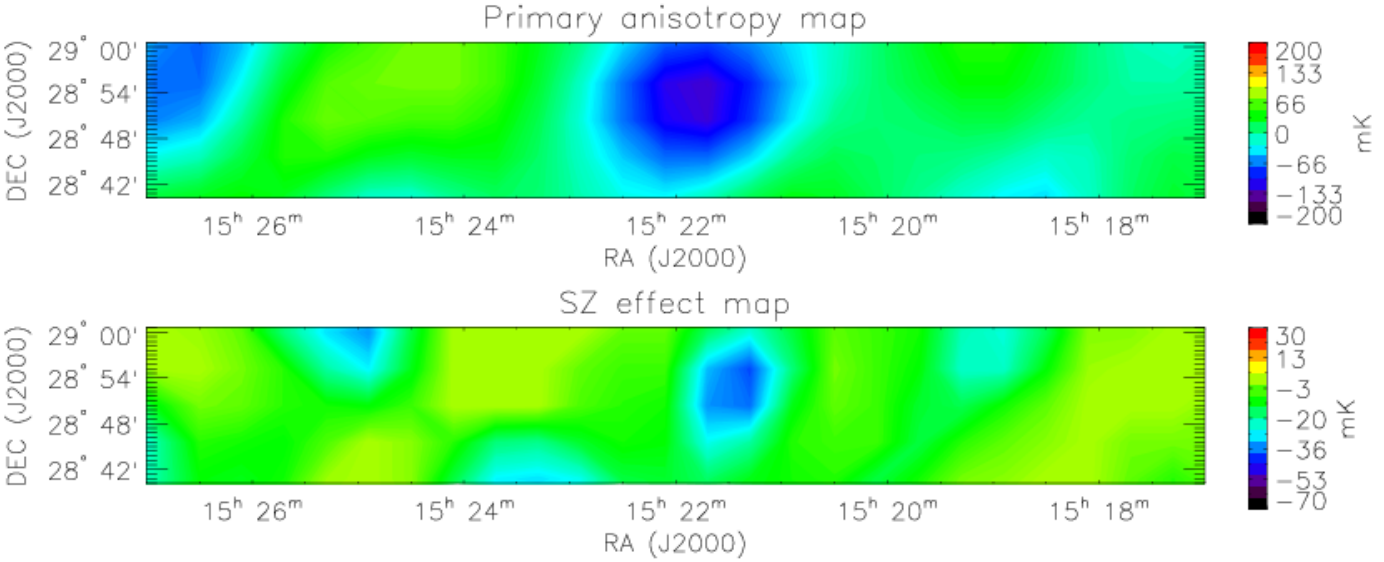

Fig. 3.— Primary anisotropy and SZE maps derived by maximum likelihood. It is evident a spot in the SZ map. This seems to be not resolved by MITO *f.o.v.* even if the low S/N doesn't allow a complete description of it.

MITO results

- A Maximum-Likelihood derived maps for the primary and SZ-like (in RJ units) components.
- There is a detection of a SZ component with amplitude:

$$y=(7.8\pm 4.9)\cdot 10^{-6}$$

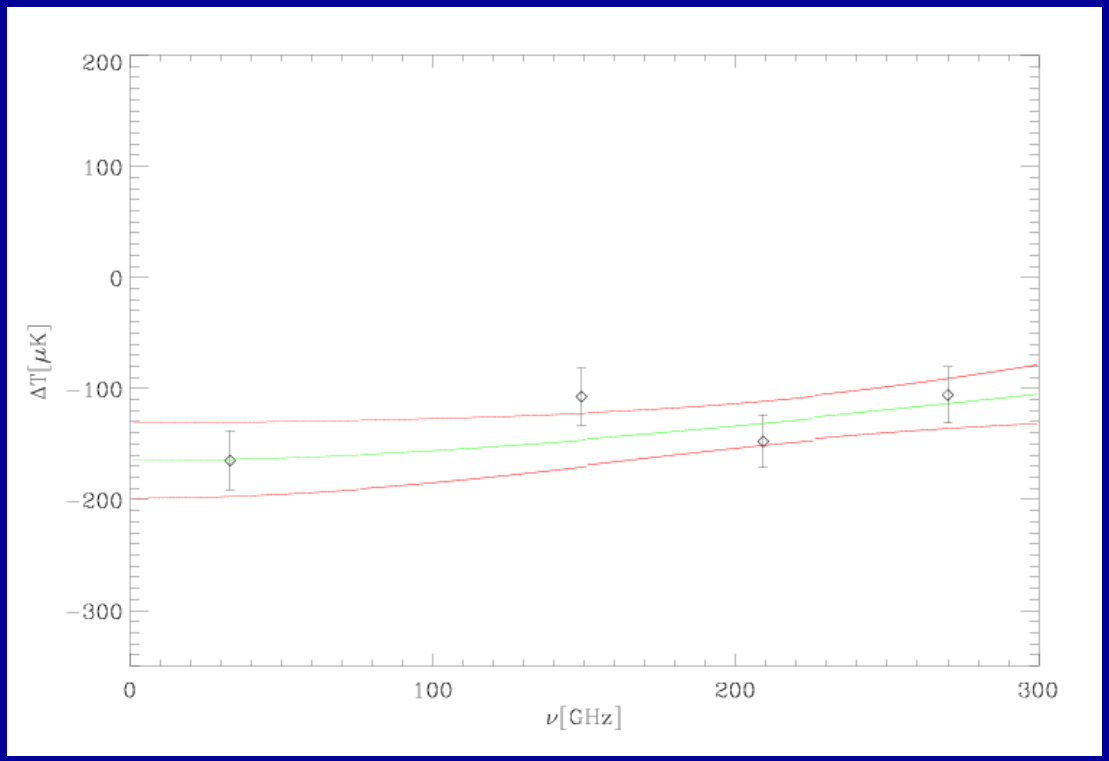

- This implies that 25% of the VSA detection is due to SZ.
- If we assume temperatures of 0.5-0.8 keV, then δ~400-600 to be consistent with X-ray constraints.

Conclusions

- We report the detection with the VSA of a negative extended feature inside the Cr-B supercluster, which is not associated to known clusters of galaxies, and is not detected in ROSAT SXRB maps.
- A multifrequency analysis with the MITO telescope confirms that the signal is a combination of primordial CMB and a SZ component.
- If produced by extended gas, it would contribute with a signicant fraction of the missing baryonic mass.
- This is the first detection of a SZ signature in a “blind observation”. In the coming years, many SZ experiments (ACT, SPT, AMI, APEX) will be doing these kind of studies.

The COSMOSOMAS Experiment

(Aimed to measure COSMOlogical Structures On Medium Angular Scales)

*Consists of two circular scanning instruments (**COSMO11** and **COSMO15**) operating at four different frequencies in the range 10-17 GHz.*

IAC team:

Carlos Gutiérrez
Sergi Hildebrandt
Roger Hoyland
Rafael Rebolo (P.I.)
J. Alberto Rubiño-Martín
Bob Watson
Roger Oliva

Former collaborators:

Silvia Fernández Cerezo
Juan Macías (Grenoble)
Julio Gallegos
Elia Battistelli

(http://www.iac.es/project/cmb/cosmosomas/)

COSMOSOMAS receivers layout

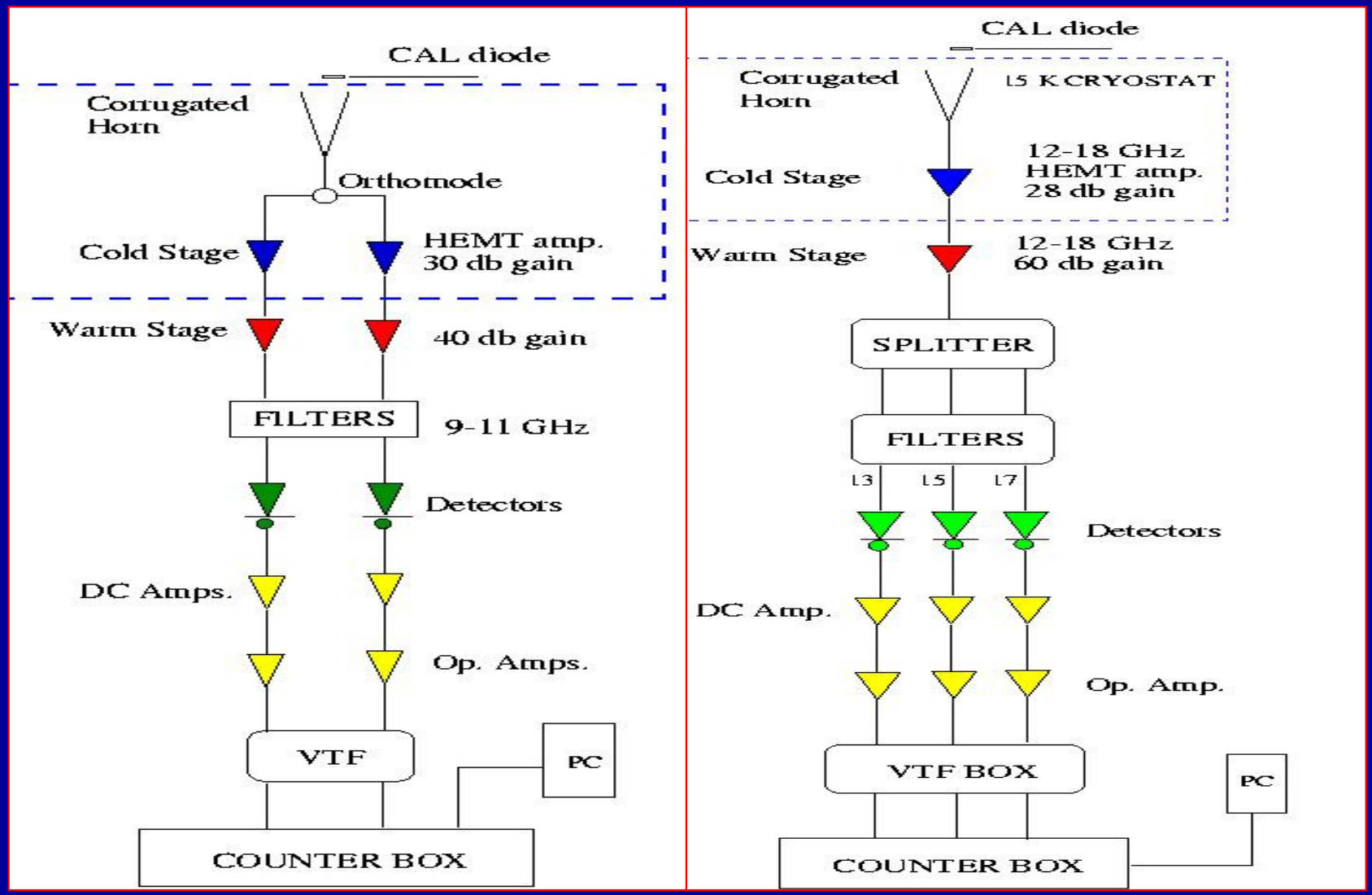

COSMO11

(one channel @ 10.8 GHz)

COSMO15

(3 channels @ 13, 15, 17 GHz)

Relative spectral response of the three COSMO15 channels

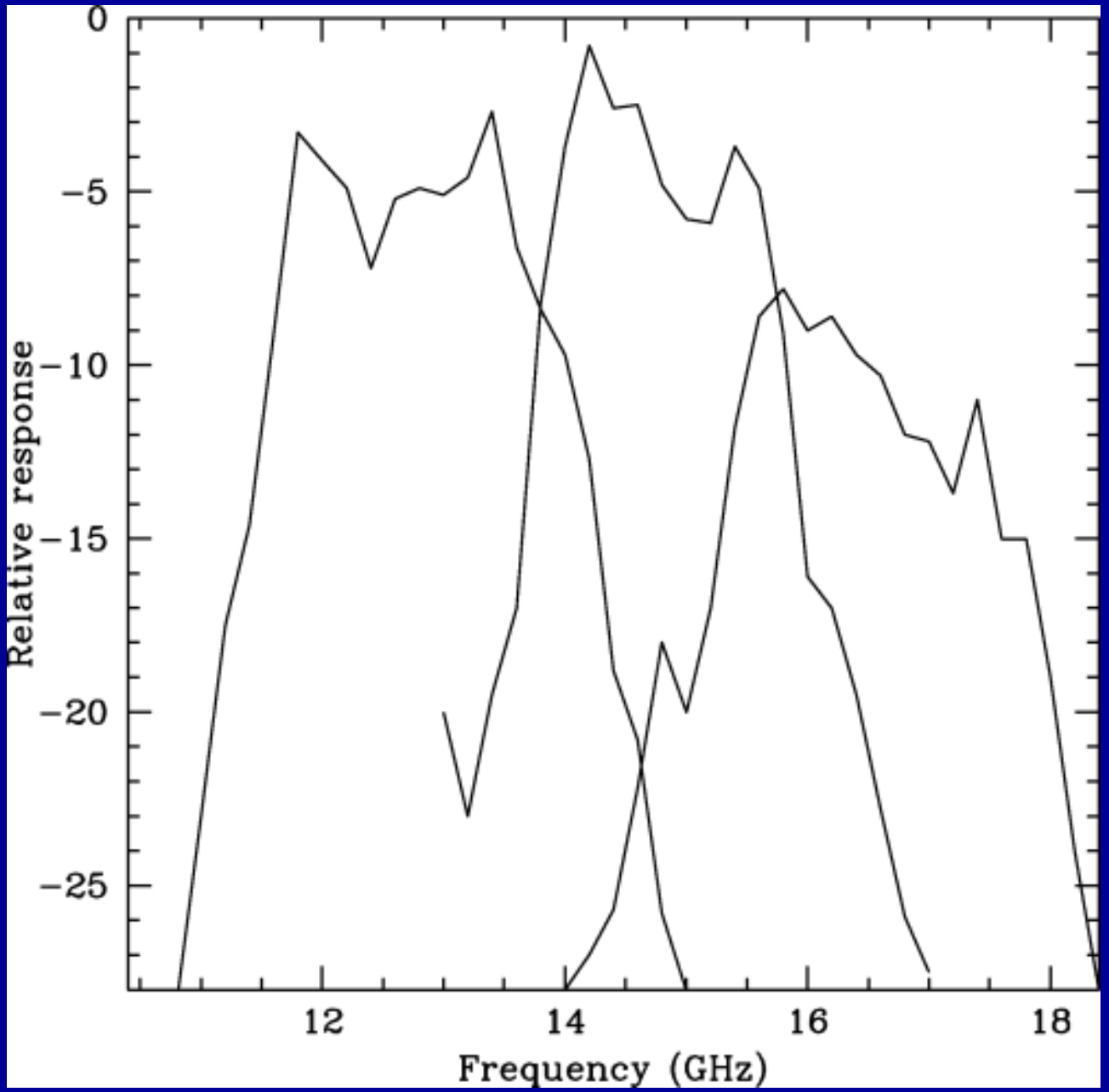

COSMO15 at Teide Observatory.
Instrumental setup, showing the 2.5 m flat primary mirror, the 2.4 m parabolic, and the HEMT-based receiver cooled at 20 K.

COSMO15 at Teide Observatory.

Optical system. The tilted flat primary rotates at 1 Hz allowing to scan 20 deg circles in the sky in each revolution.

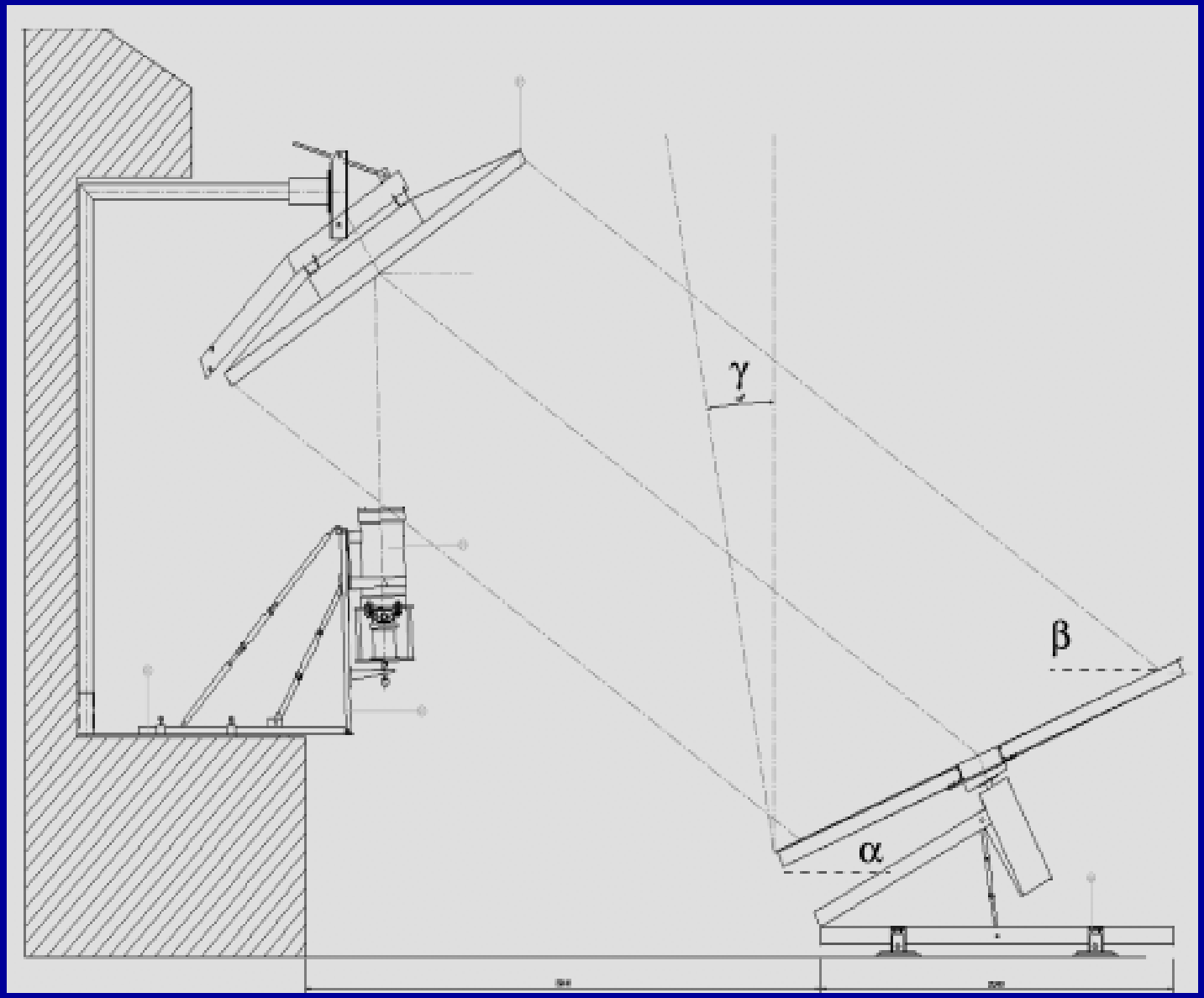

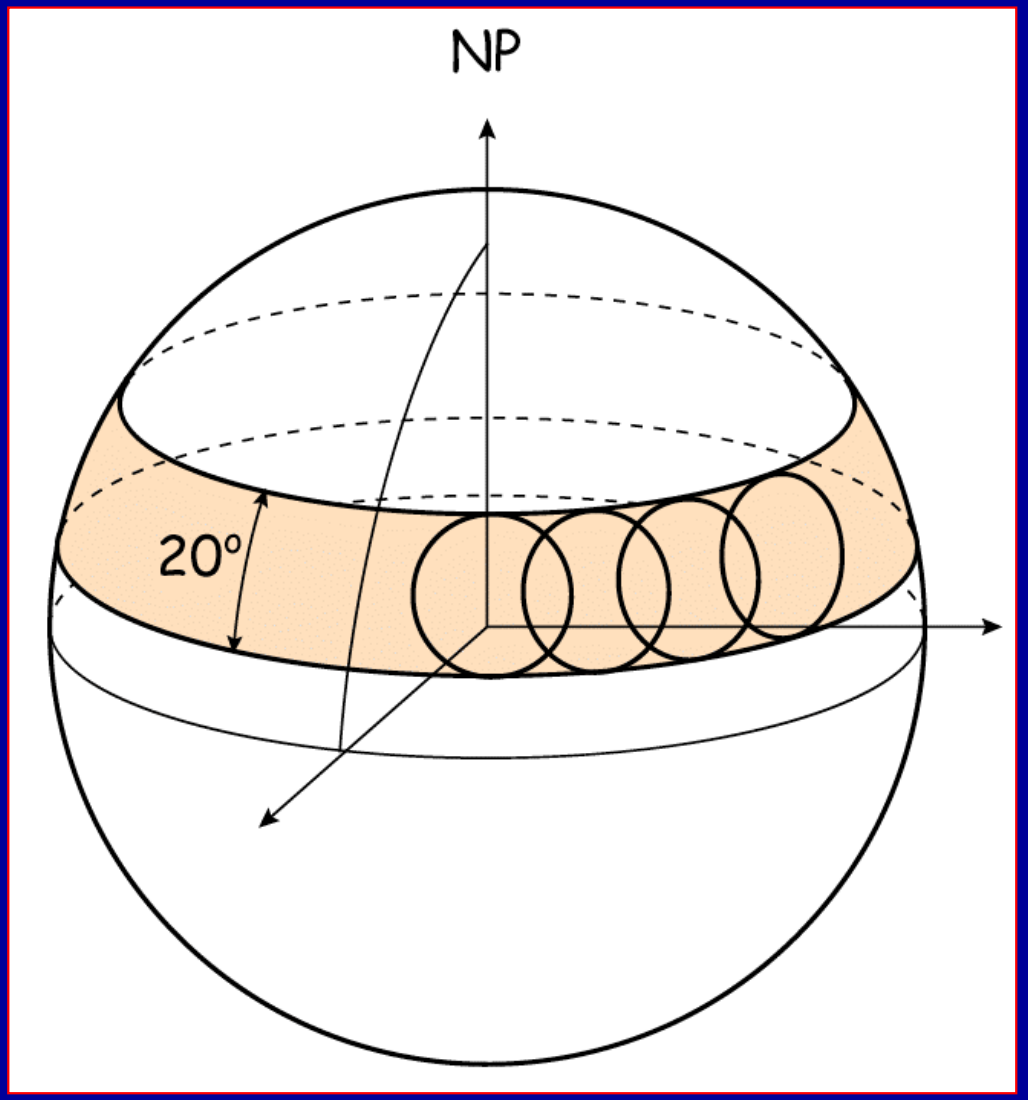

Scanning strategy

COSMOSOMAS provides 4 daily maps of microwave emission at 11, 13, 15 and 17 GHz with spatial resolution ~1 degree in a sky region of ~7000 sq.degrees. Each map with sensitivity of ~ 900 μK/beam.

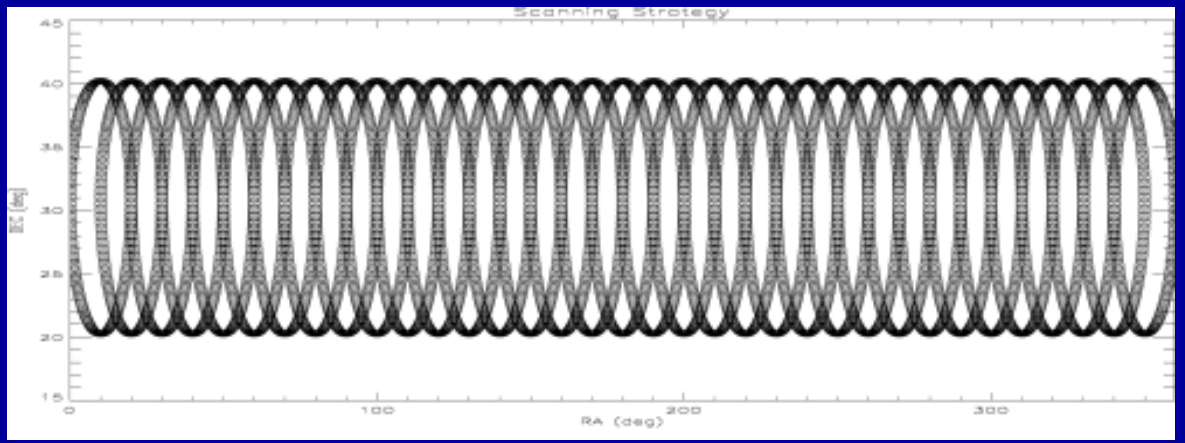

Signal recorded during one spin of COSMOSOMAS and atmospheric demodulation

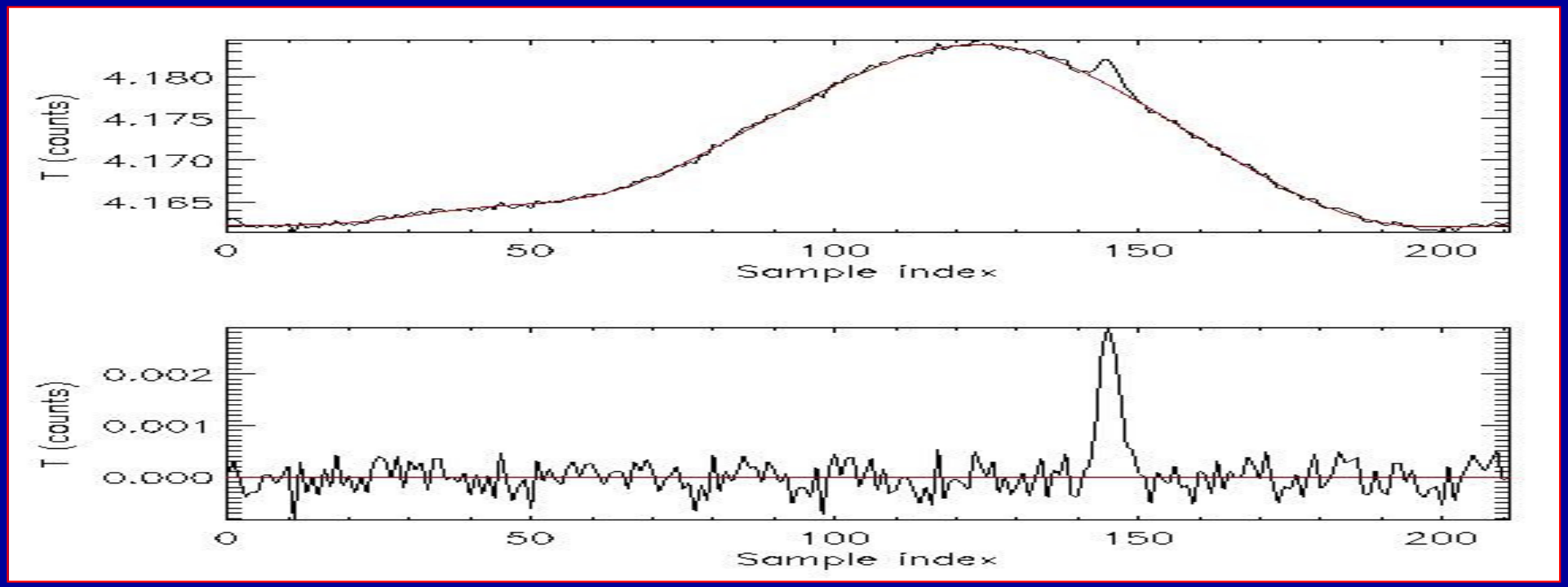

•Details of the experiment and data processing in the Fourier space: Gallegos et al. (2001) MNRAS, 327, 1178

Dominant component in each scan is a spin-synchronous signal introducing large scale modulations. It is removed using a combination of low order sinusoidal functions

Beam pattern: Response to a point source

Daily calibration: Cygnus A and/or Tau A (Crab)
uncertainty ~10 % (Baars et al. model corrected
at high frequency with WMAP fluxes)

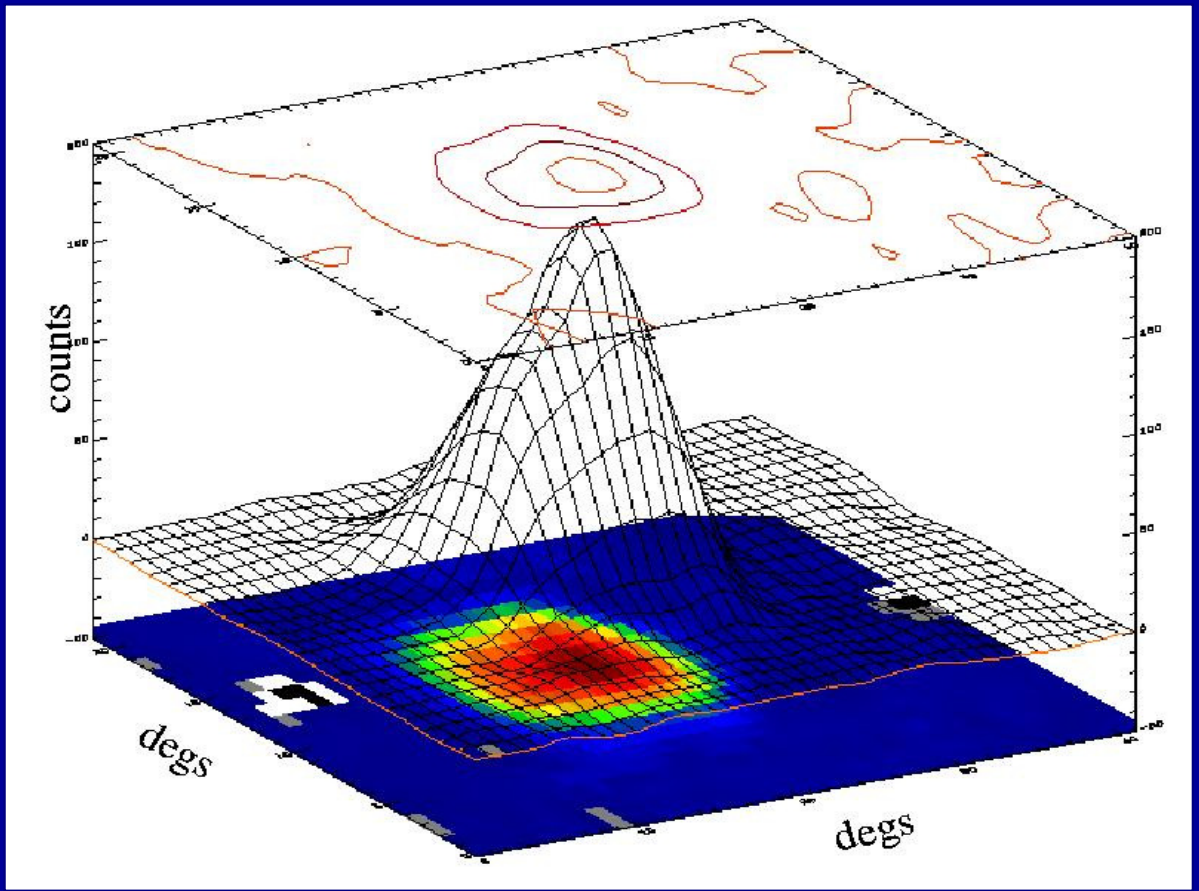

COSMOSOMAS window function

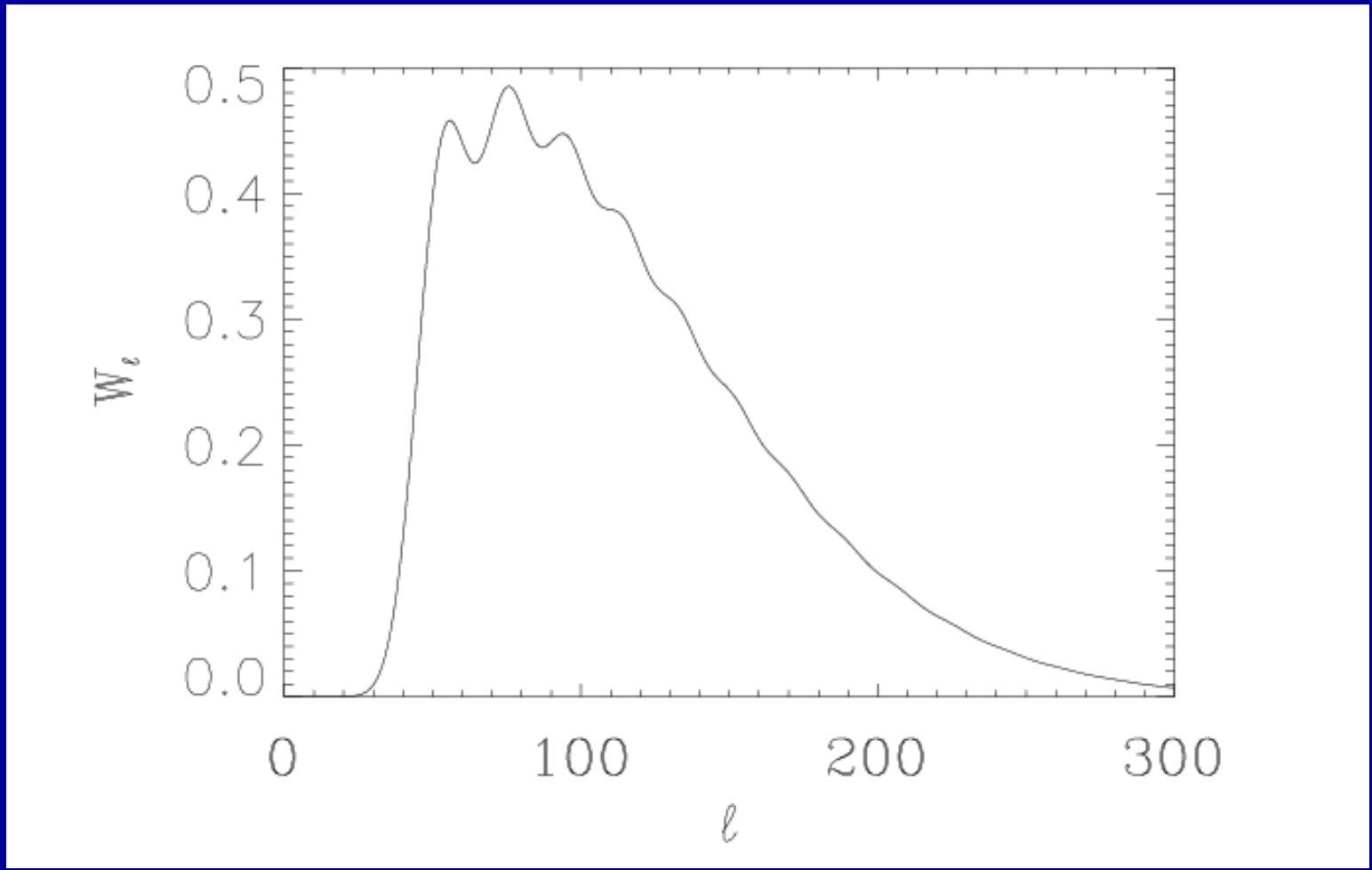

COSMOSOMAS
First 18 months of data

About 100 useful maps stacked at each frequency.
25% of the whole sky observed
100,000 observed data points (0.3º x 0.3º pixelization)

Achieved sensitivity at high Galactic latitude:

~ 40,50, 60, and 115 *μK/beam*

at

11, 13, 15 and 17 GHz, respectively.

Fernández-Cerezo et al. 2006, MNRAS in press
Hildebrandt et al. in prep.

COSMO15: 13GHz band

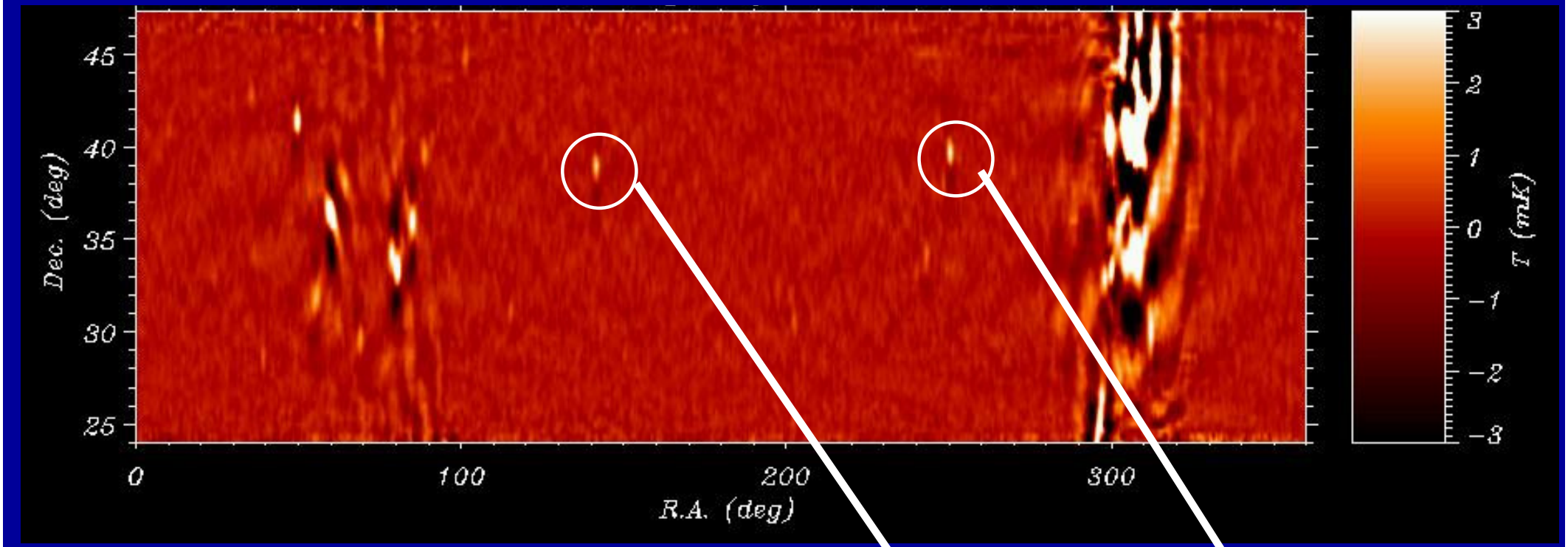

Beam FWHM= 54’ x 66’
Pixelization 20’ x 20’
25% of the whole sky

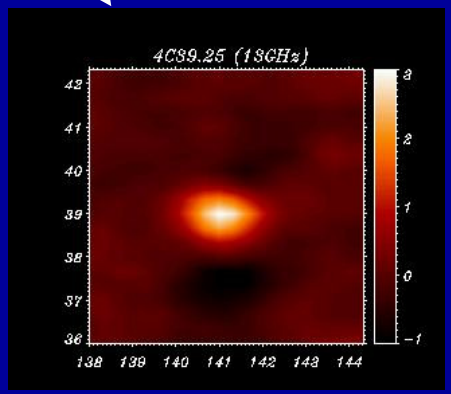

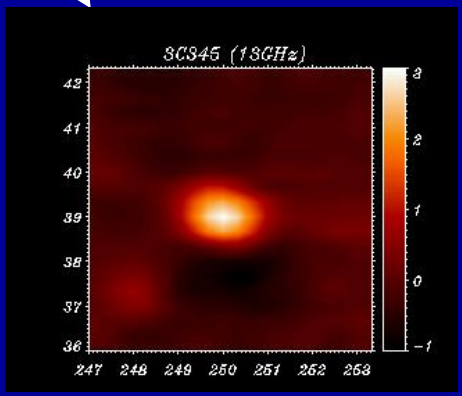

COSMO15: 15GHz band

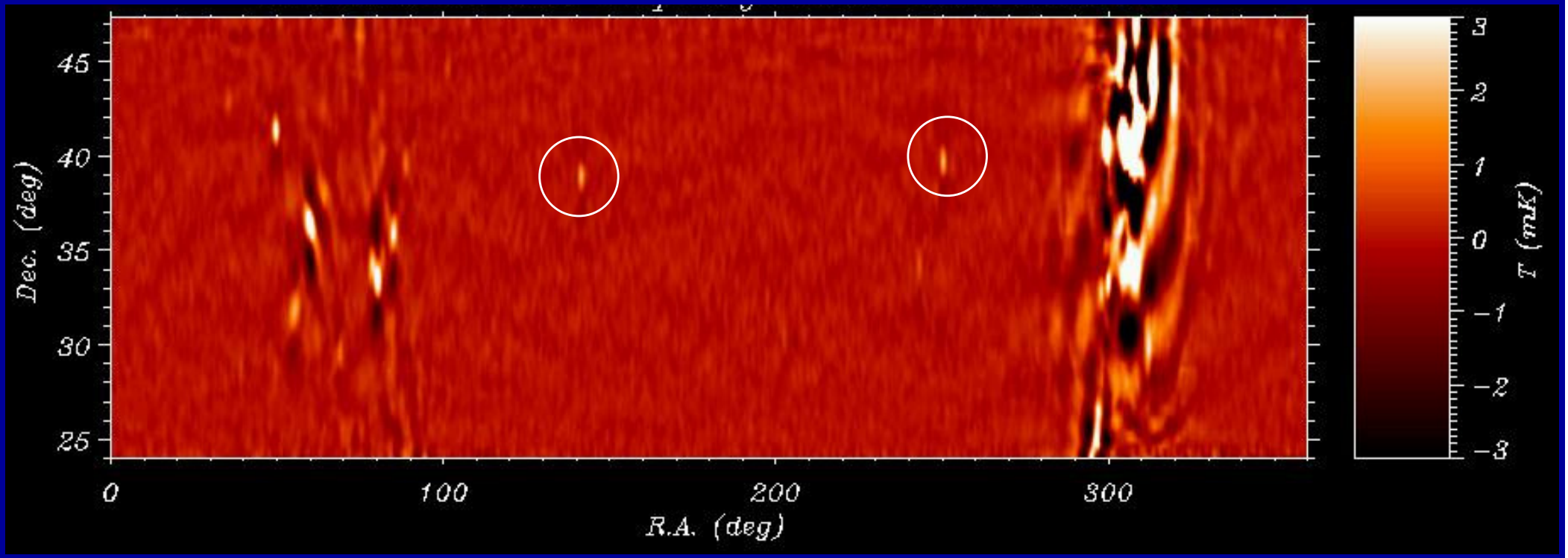

Beam FWHM= 49’ x 60’
Pixelization 20’ x 20’
25% of the whole sky

COSMO15: 17GHz band

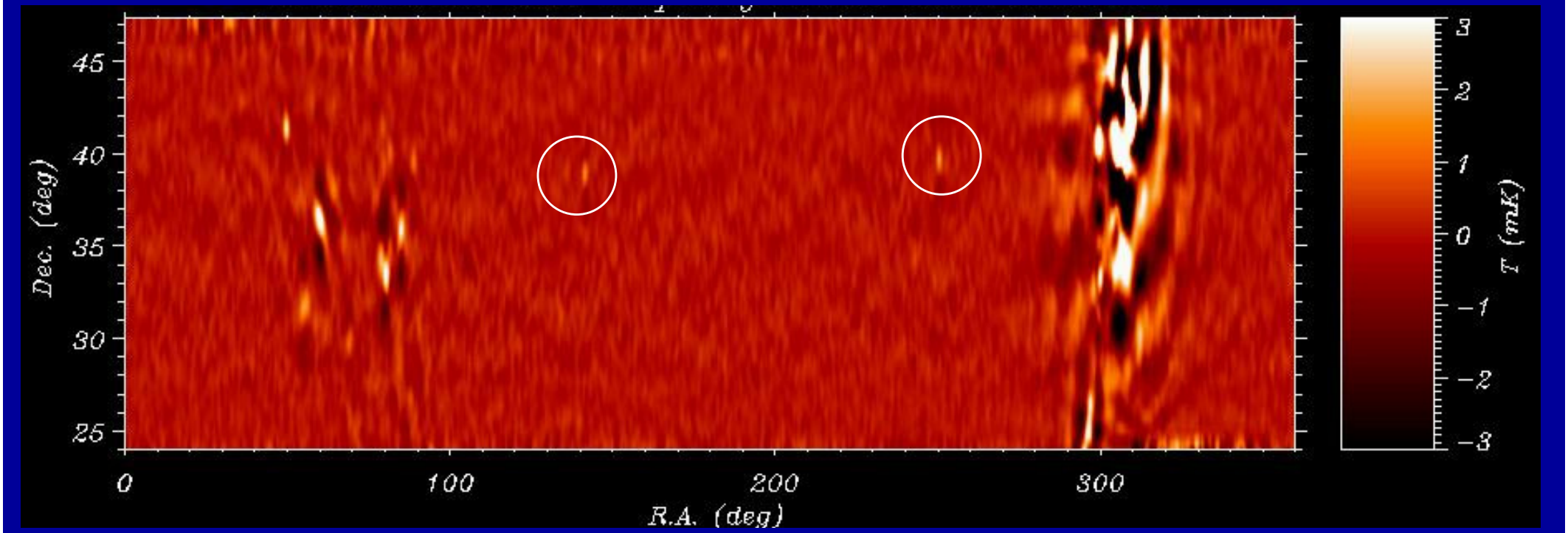

Beam FWHM= 46’ x 51’
Pixelization 20’ x 20’
25% of the whole sky

Fluxes for radiosources

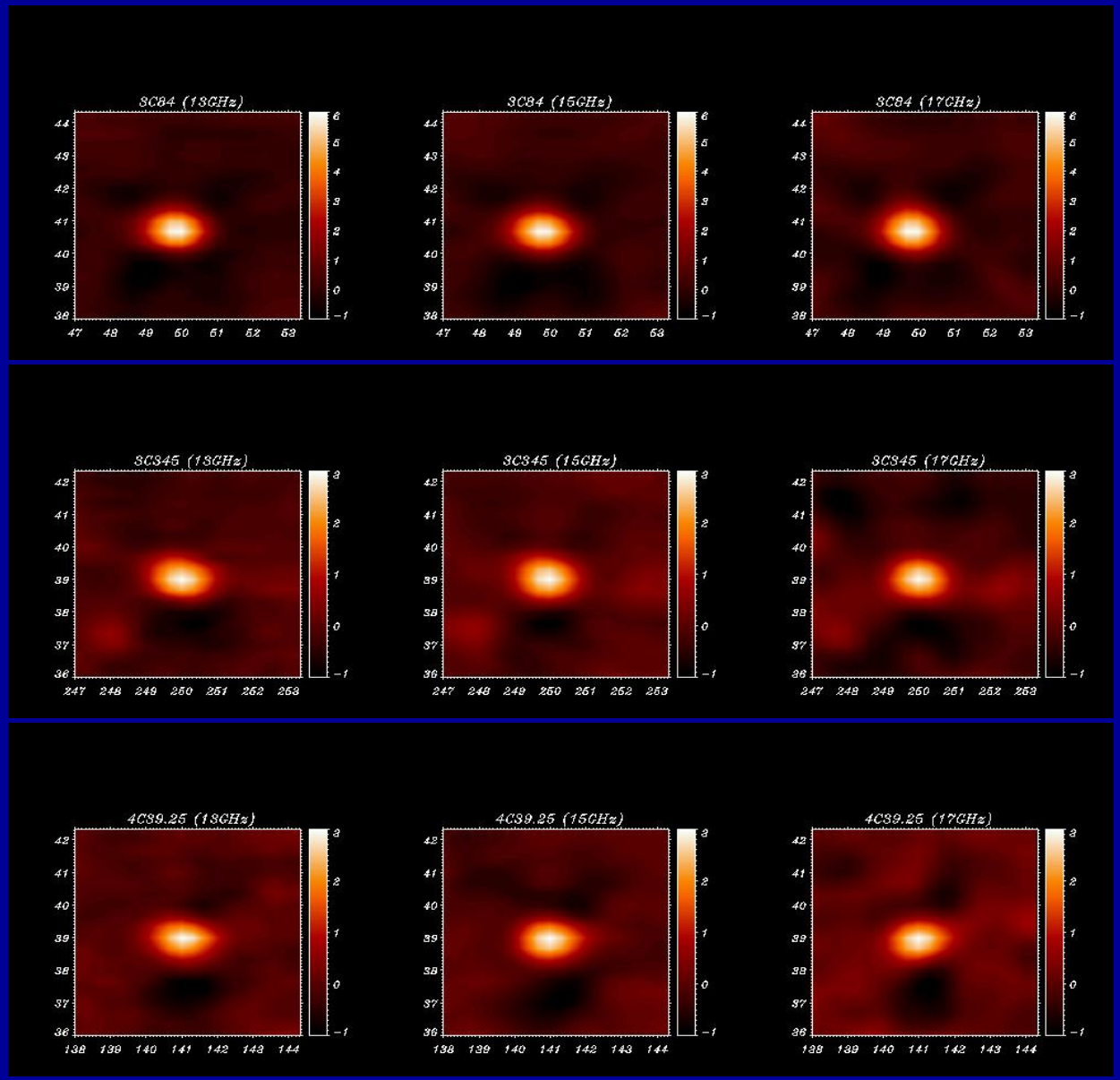

	13GHz	15GHz	17GHz
3C84	18.4 Jy	18.6 Jy	18.4 Jy
3C345	11.5 Jy	10.9 Jy	12.0 Jy
4C39.25	9.8 Jy	10.1 Jy	10.2 Jy

Consistent with values from Univ. Michigan (UMRAO data) at 4, 8 & 14.5GHz, and extrapolations of Obs. Metsahovi values (22 & 37 GHz).

COSMOSOMAS: comparison with WMAP at the galactic plane crossing

13 GHz 15 GHz 17 GHz

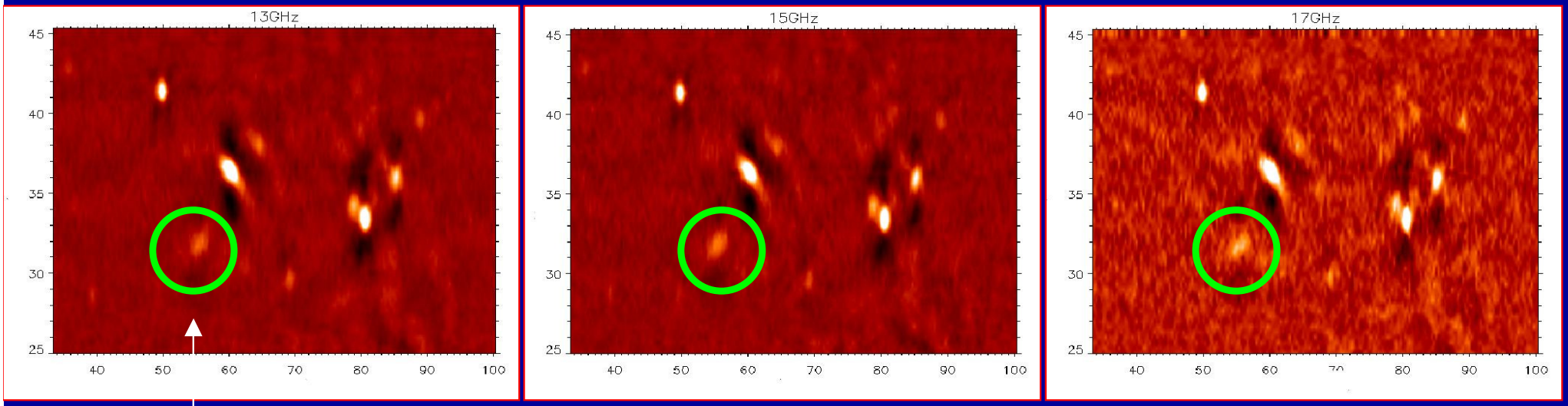

23 GHz WMAP K (FILTERED)

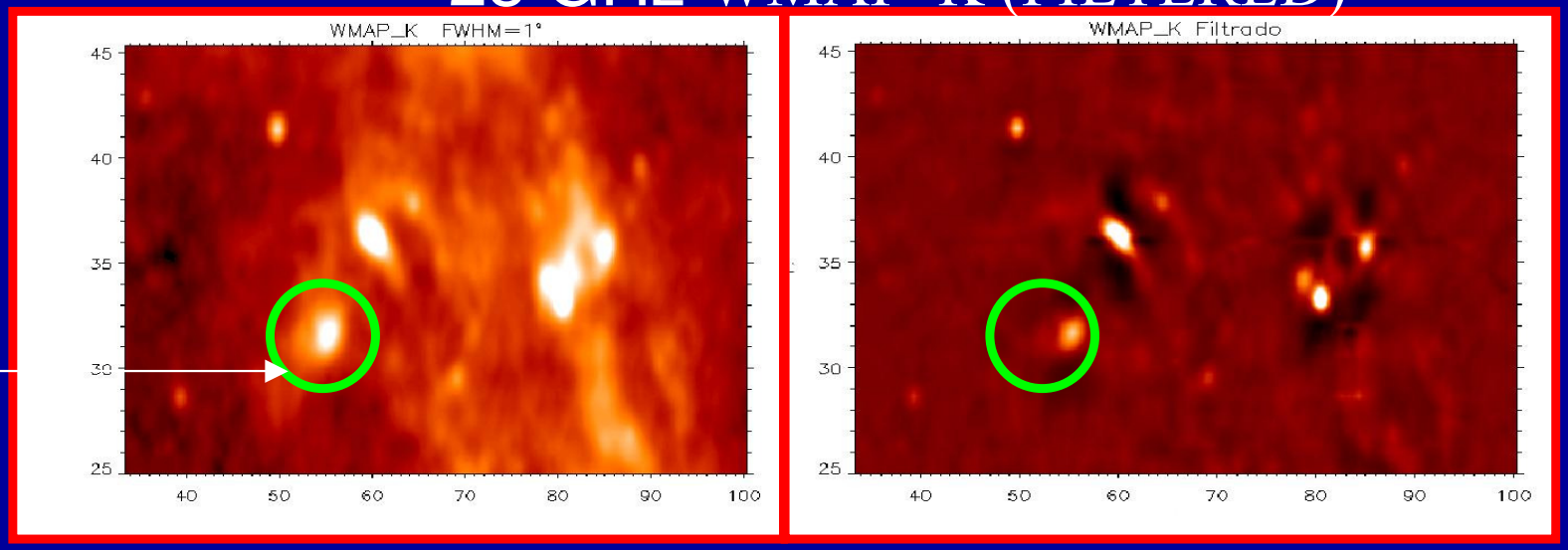

Perseus molecular complex

Watson, Rebolo, Rubiño et al. 2005, ApJ 624 L89

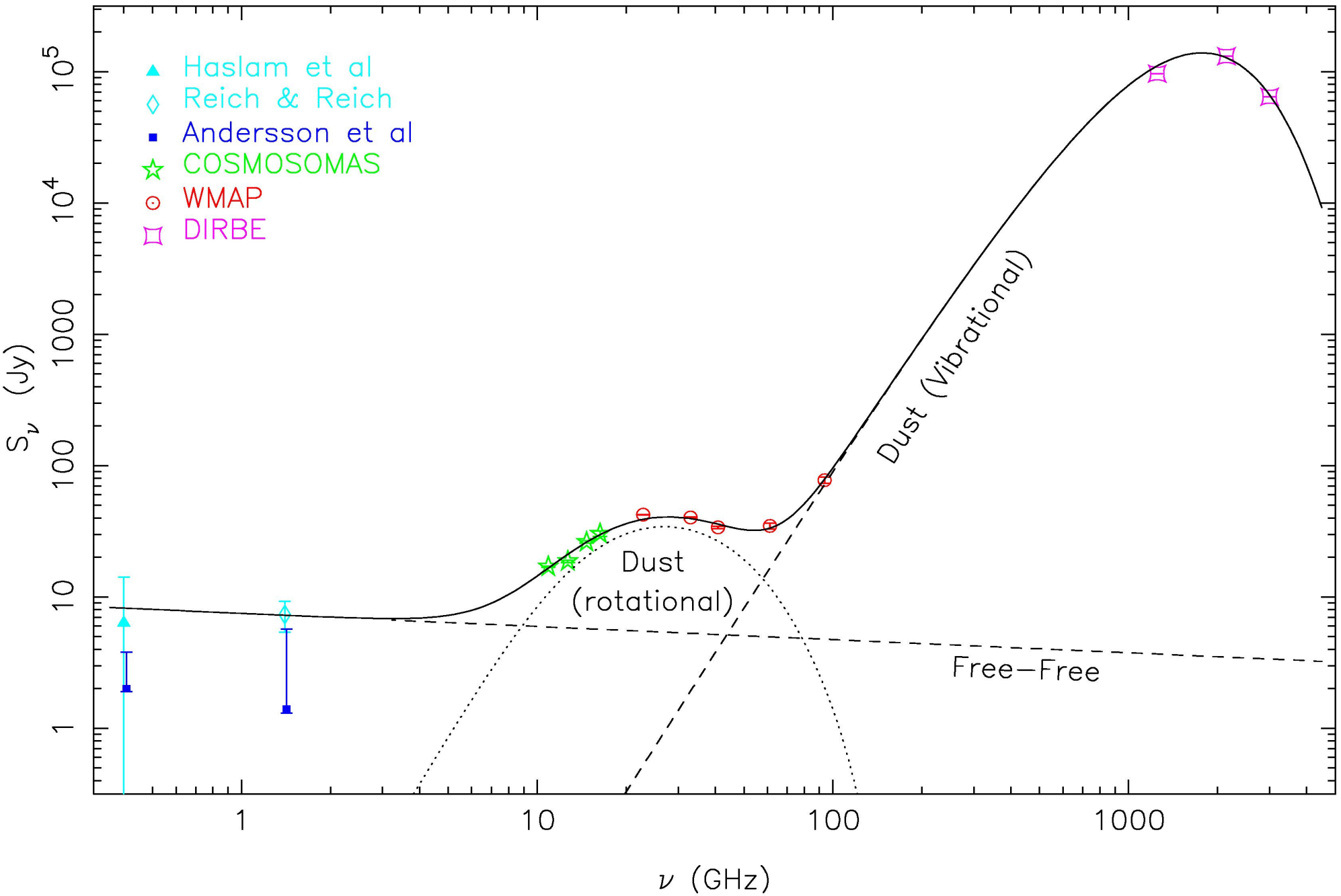

Electric dipole emission by hydrogenated fullerenes (C_NH_p) can explain the anomalous emission in Perseus

Iglesias-Groth 2005, ApJ 632 L25

Key point: fullerane dipole emission proportional to degree of hydrogenation

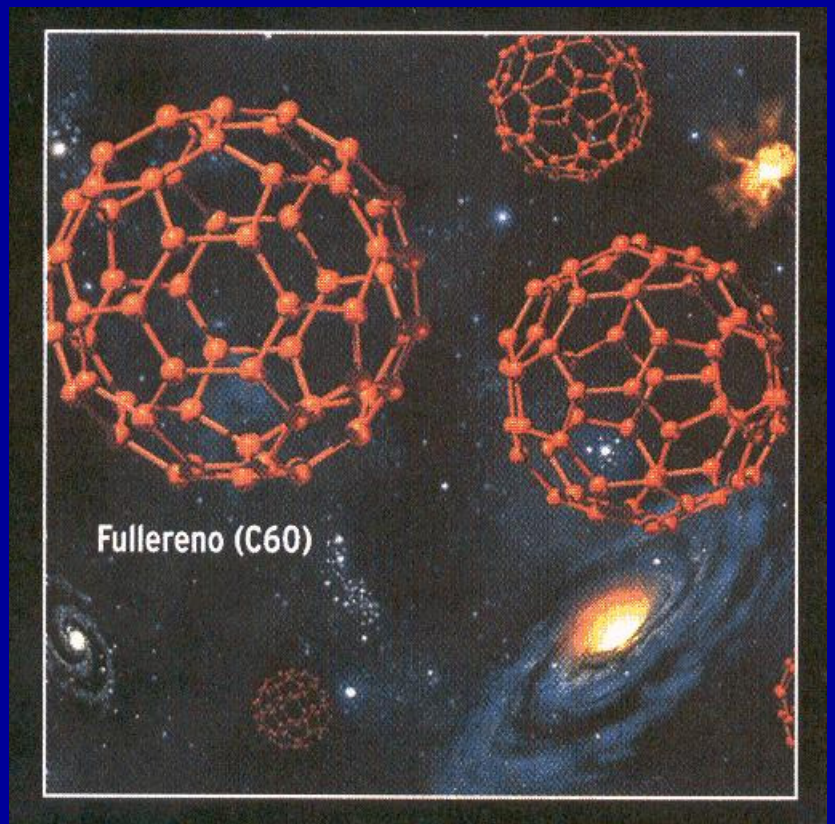

Emissivity (Jy cm^2 sr^{-1}) per H atom

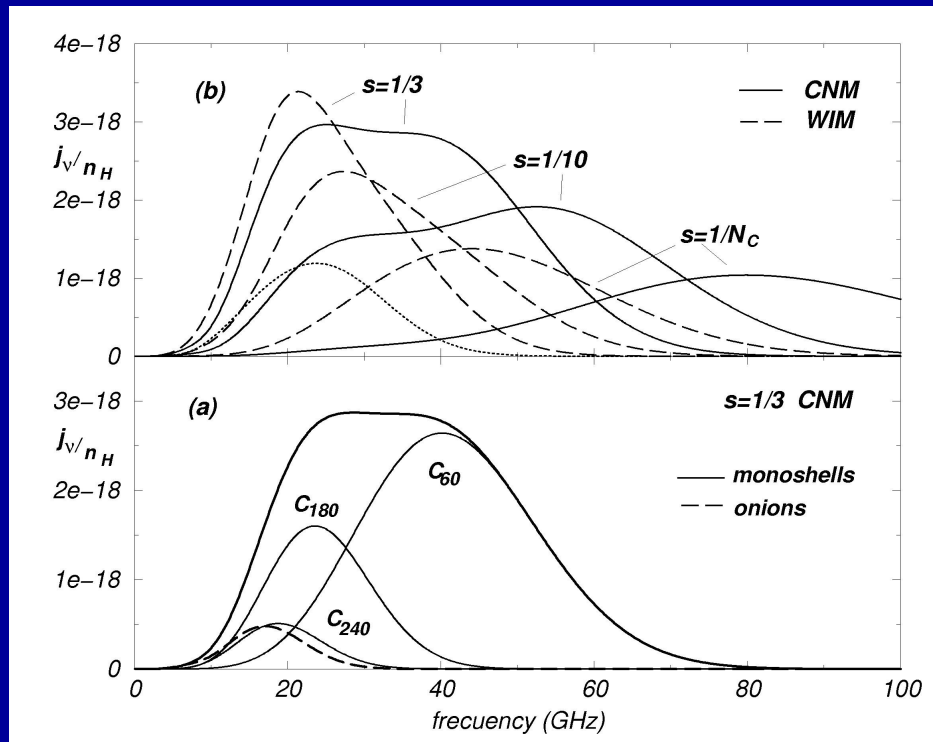

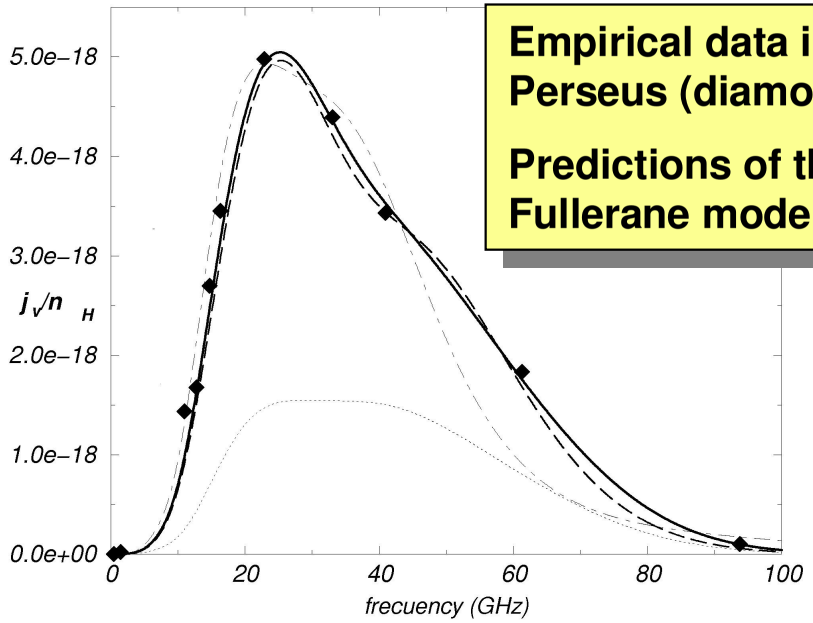

Polarization observations of anomalous microwave emission at 11 GHz in the Perseus molecular complex

Battistelli, Rebolo, Rubiño et al. 2006 ApJ Lett.

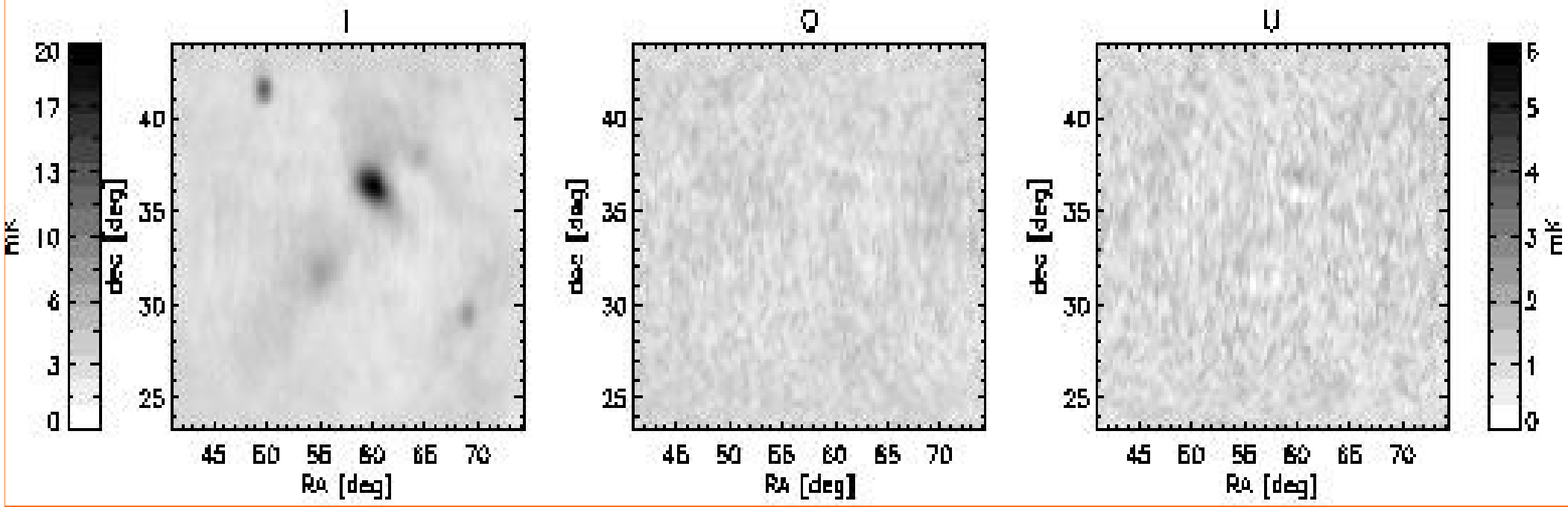

Q: difference between the radiation intensity collected by COSMOSOMAS in the 0º plane (North-South) and the 90º one. **Q= - 0.2 ±1.0 % (95% c.l.)**

U : difference between the orientation –45º and +45º. **U=-3.4±2% (95% c.l.)**

Overall polarization parameter Π=3.4 ± 2%.

The maps are calibrated to the nearby California Nebula (free-free dominated) which is assumed unpolarized (systematic error of less than 1%).

Polarization of rotational electric dipole radiation

Lazarian and Draine 2000 ApJ

Are the molecules aligned and their emission polarized?

The energy level splitting arising from grain rotation ensures maximum efficiency of paramagnetic dissipation : time dependent magnetization, energy dissipation and torque causing the molecule to rotate with the axis parallel to the magnetic field

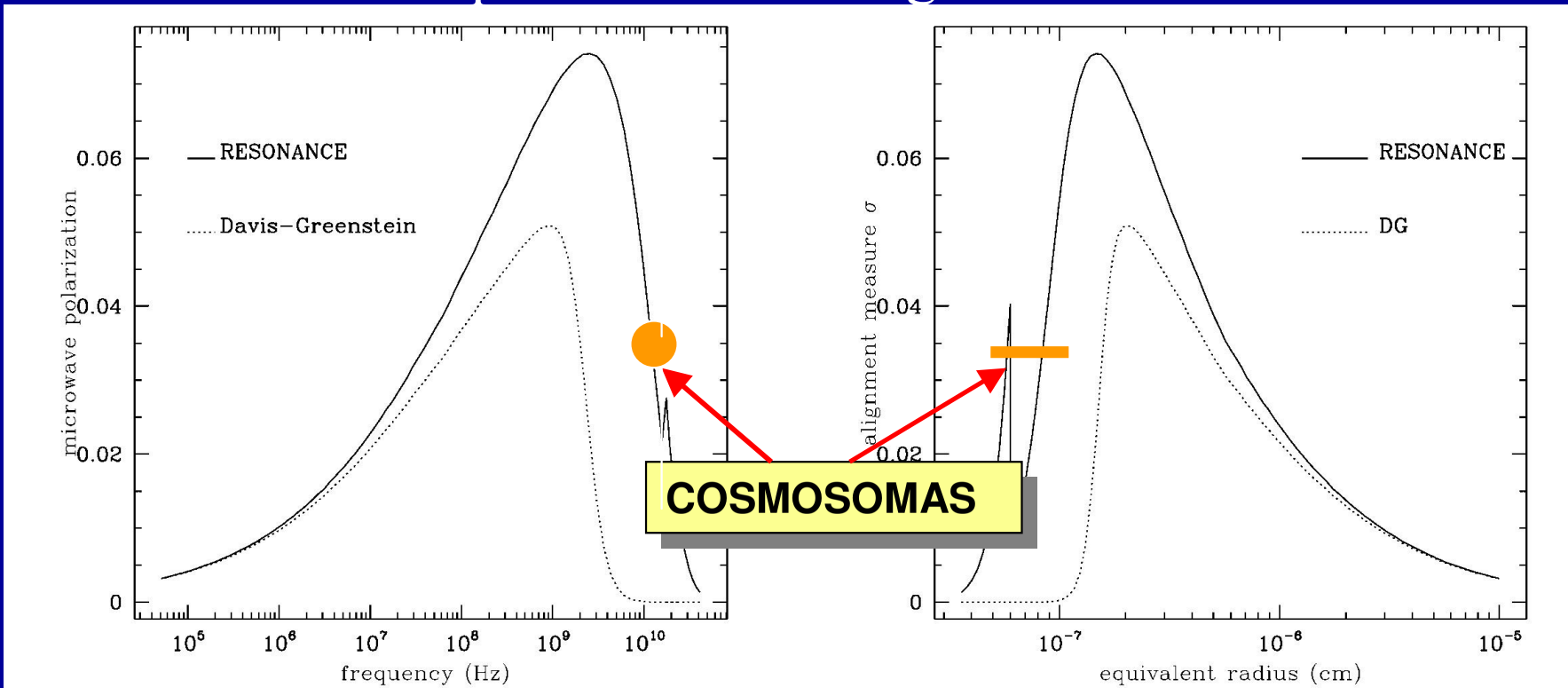

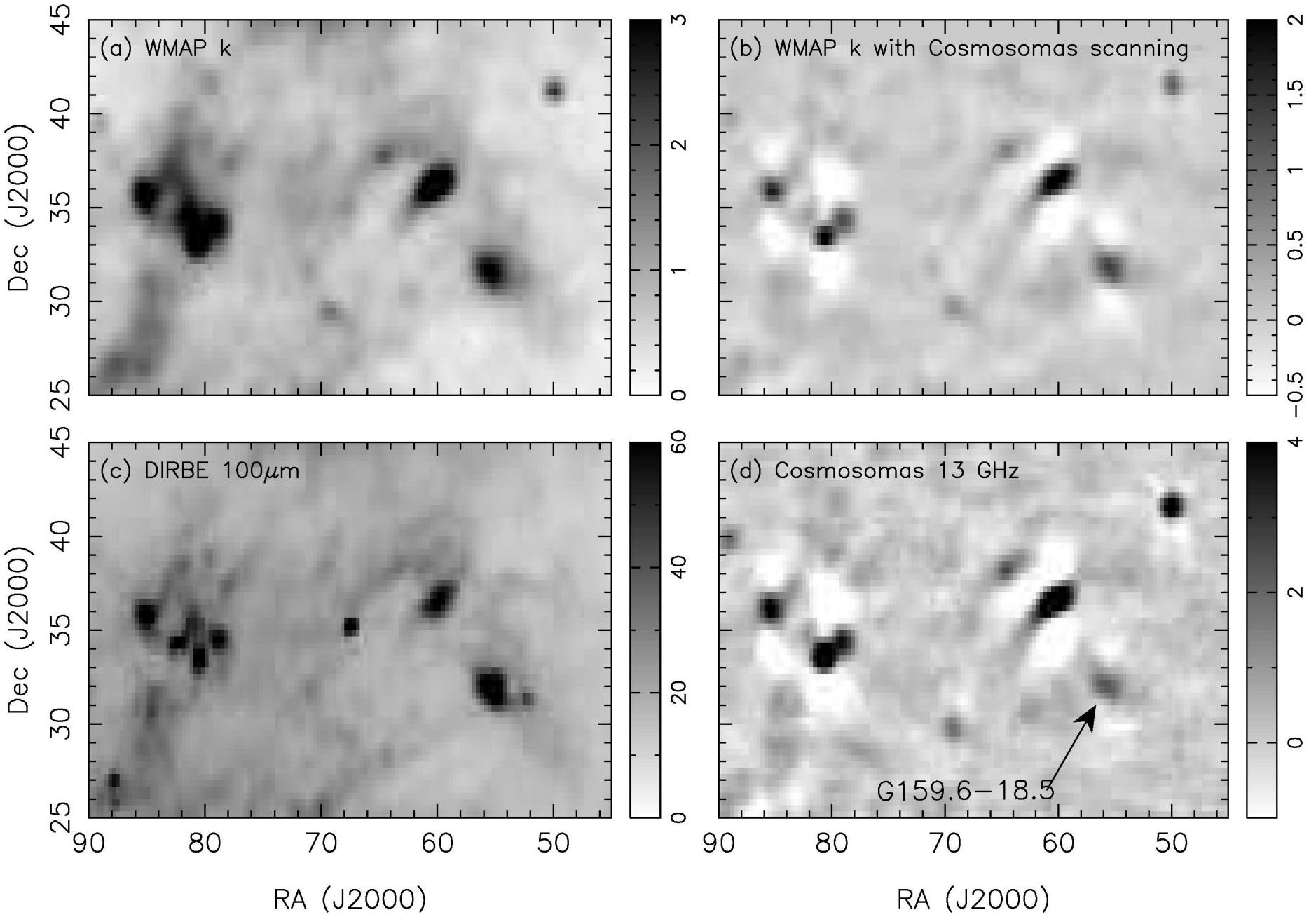
(a) WMAP k
(b) WMAP k with Cosmosomas scanning
(c) DIRBE 100μm
(d) Cosmosomas 13 GHz
G159.6−18.5
Dec (J2000)
RA (J2000)
90
80
70
60
50
25
30
35
40
45
0
1
2
3
20
40
60
−0.5
0.5
1.5
4

Results at High Galactic Latitudes

Fernández-Cerezo, Gutiérrez, Rebolo, Rubiño et al. 2005, MNRAS

astro-ph/0601203

Cross correlation method

$$\vec{y} = \vec{n} + \vec{x}_{cmb} + \alpha\ \vec{x}_{gal} + \vec{y}_{gal},$$

- x_{CMB}: contribution of the fluctuating component of the CMB;
- x_{gal} : brightness fluctuations of the Galactic template map. α converts units of the Galactic template into antenna temperature;
- y_{gal} : represents any residual Galactic contribution which is uncorrelated with x_{gal}

Covariance matrix is sum of covariances of CMB and noise:

$$C \equiv \langle \boldsymbol{y}\boldsymbol{y}^T \rangle - \langle \boldsymbol{y} \rangle \langle \boldsymbol{y}^T \rangle = \langle \boldsymbol{x}_{\rm CMB}\boldsymbol{x}_{\rm CMB}^T \rangle + \langle \boldsymbol{n}\boldsymbol{n}^T \rangle$$

Cross correlation method (II)

Minimizing $\chi^2 = (\vec{y} - \alpha\ \vec{x}_{gal})^T C^{-1} (\vec{y} - \alpha\ \vec{x}_{gal})$ we obtain

the minimum varianze estimator for α,

$$\alpha = \frac{\vec{x}_{gal}^T C^{-1} \vec{y}}{\vec{x}_{gal} C^{-1} \vec{x}_{gal}}$$

with a varianze

$$\delta\alpha^2 = \frac{1}{\vec{x}_{gal} C^{-1} \vec{x}_{gal}}$$

The contribution of the galactic template map (x_{gal}) to the observed sky map is given by $\alpha\,\sigma_{gal}$ (so this scaled quantity is in the units of the observed sky map).

Cross correlation method (III)

In the case of white noise and noise dominating over astronomical signals we have

$$C_{ij} \approx < n_i \, n_j > \approx \sigma_i^2 \, \delta_{ij}.$$

Cosmosomas noise is correlated and dominates over CMB signal.

We proceed in two ways:

i. Diagonal covariance matrix (CMB in diagonal only);

ii. Non-diagonal covariance matrix (full covariance for CMB and noise). Analysis is carried out in different patches.

Estimates from both methods are consistent

Masks

We adopt the Kp0 mask for the Galaxy.
We mask point sources.

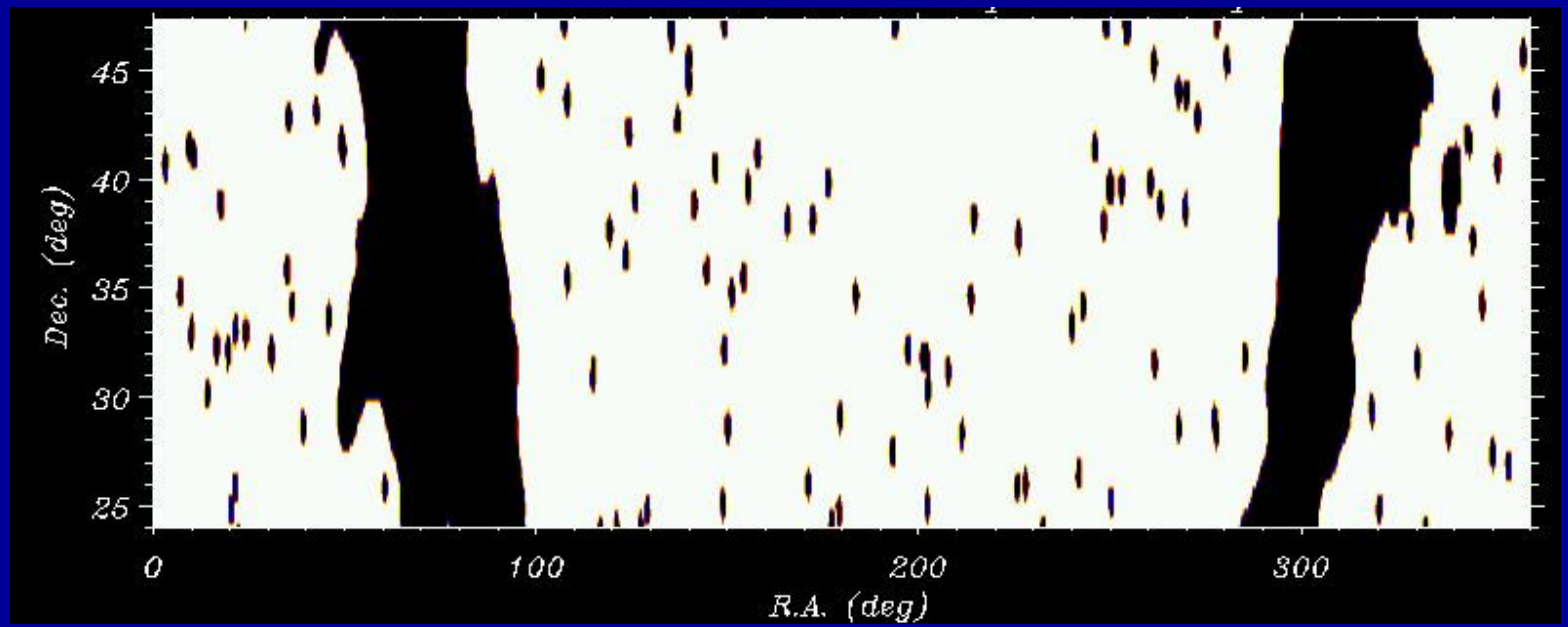

Cross-correlation results

Cross-correlation of COSMOSOMAS and WMAP

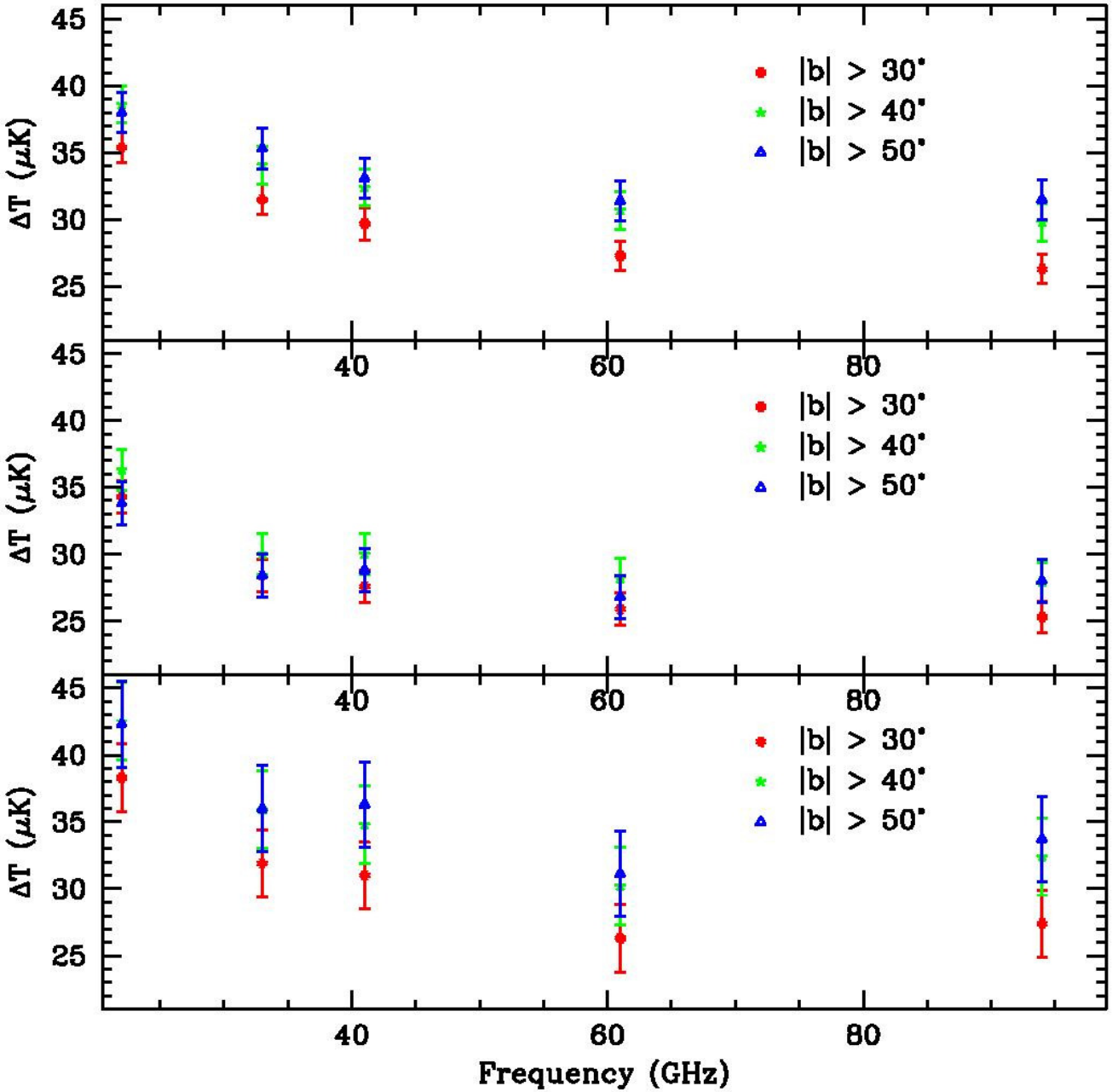

Figure 8. Common signal between COSMOSOMAS (*top* : 12.7, *middle* : 14.7, *bottom* : 16.3 GHz) and WMAP for three Galactic cuts.

CMB fluctuations in antenna temperature in the combined COSMOSOMAS map

$b > 40°$

$\Delta T_{CMB} = 29.7 \pm 0.7\ \mu K$ (V band)

$\Delta T_{CMB} = 30.0 \pm 0.7\ \mu K$ (W band)

Monte Carlo simulations: pixels of template maps are re-arranged in random order.

We find the distribution of the α´s consistent with zero mean and with standard deviations about a factor 1.2 larger than the formal errors.

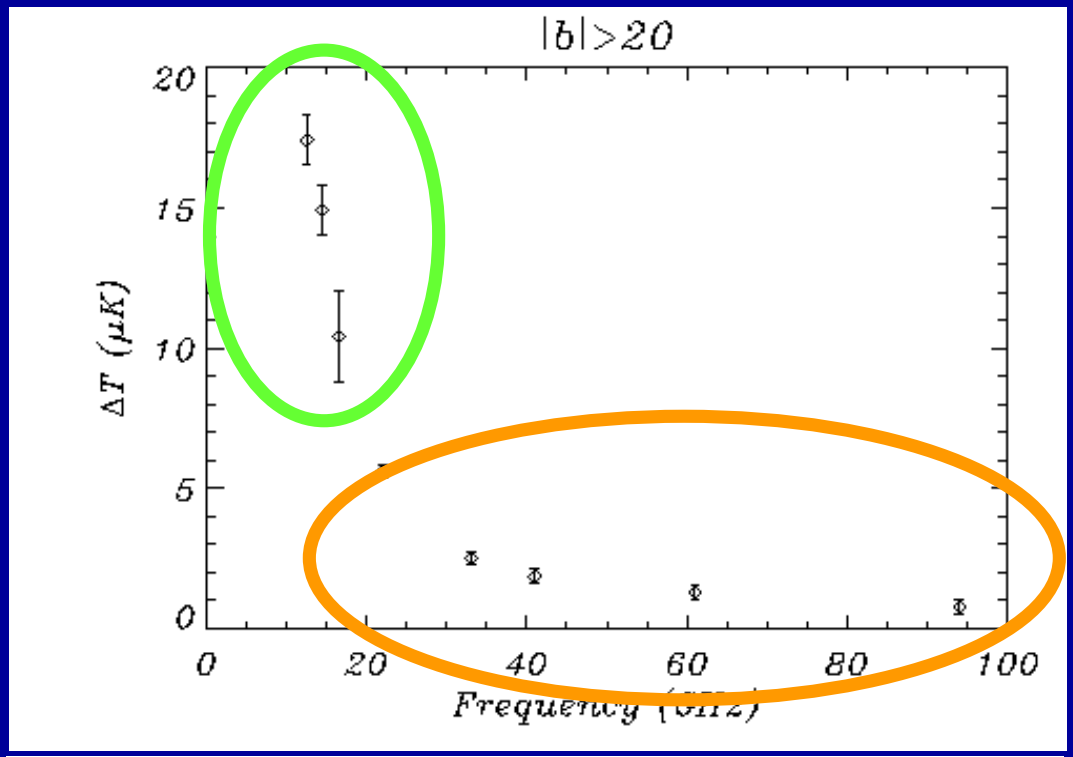

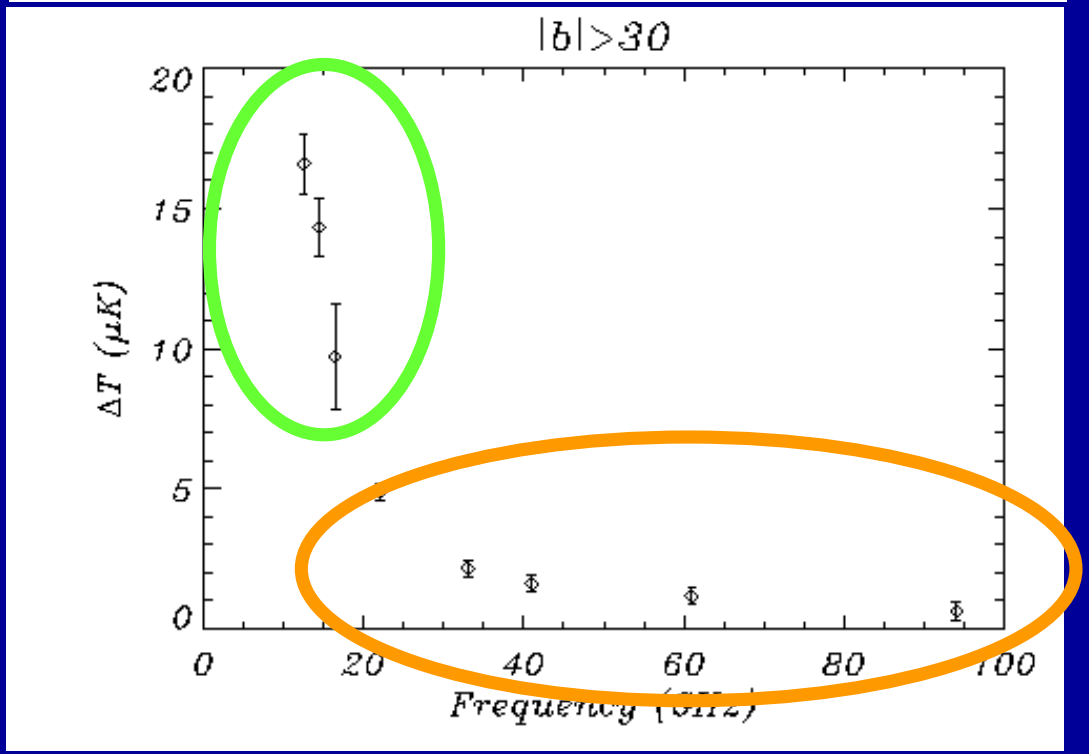

Correlation with Haslam (408 MHz)

- Cosmosomas
- WMAP

Derived spectral index between 408MHz and Cosmosomas frequencies:

Gal.cut	13GHz	15GHz	17GHz
|b|>30	-3.16	-3.05	-3.01
|b|>40	-3.20	-3.03	-2.94

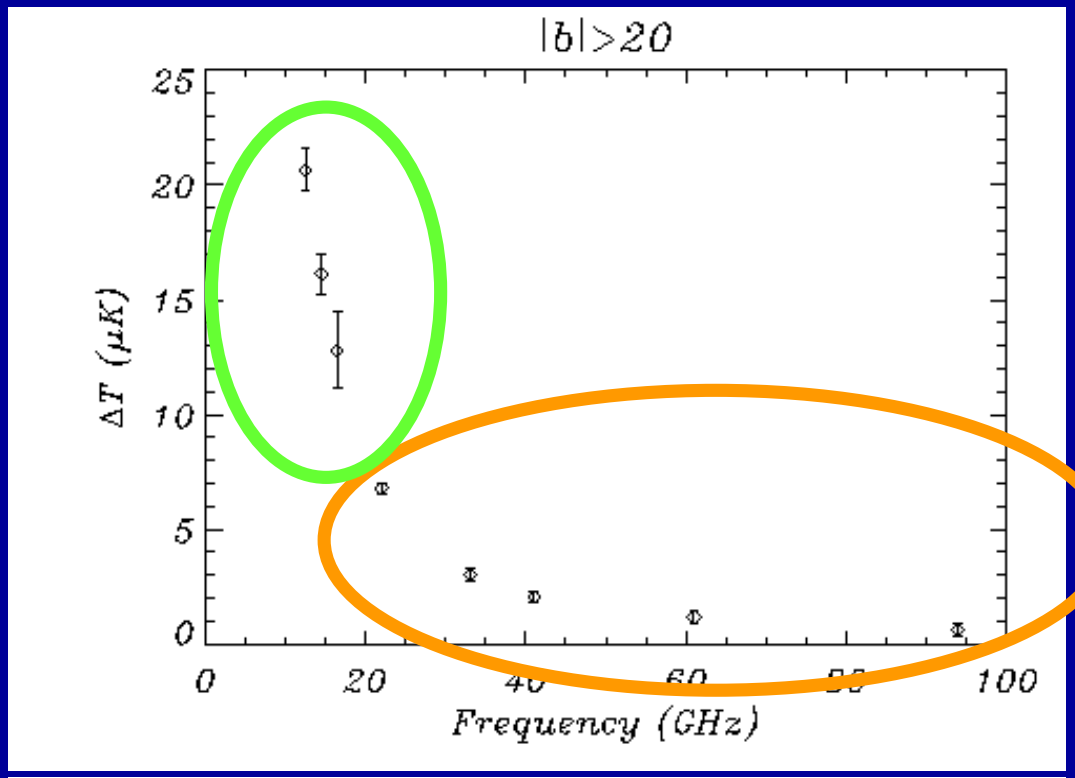

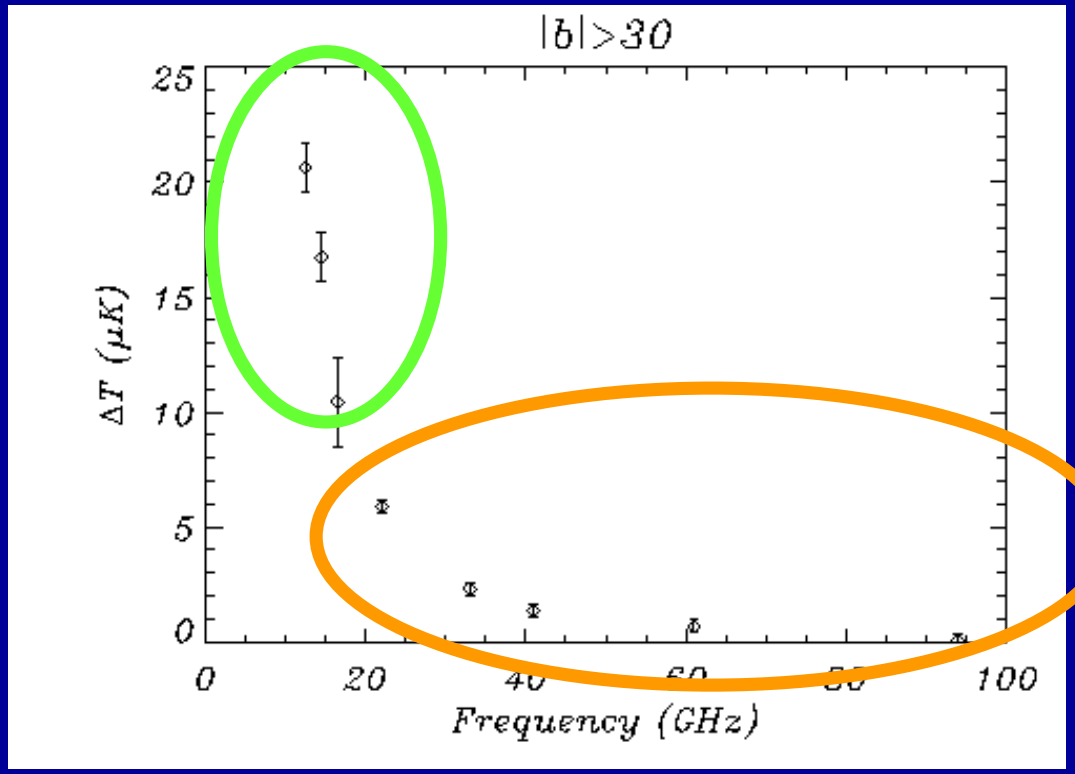

Correlation with Reich & Reich (1420MHz)

- Cosmosomas
- WMAP

Checking results

Rotation of templates.
We checked our results against template maps rotated around the Galactic poles. The Galaxy was rotated in 10 different angles. We found a zero average correlation. The rms of the correlations appears to be a factor 2 larger than the formal statistical error bar of our cross-correlation method.

Correlations with DIRBE 100 μm

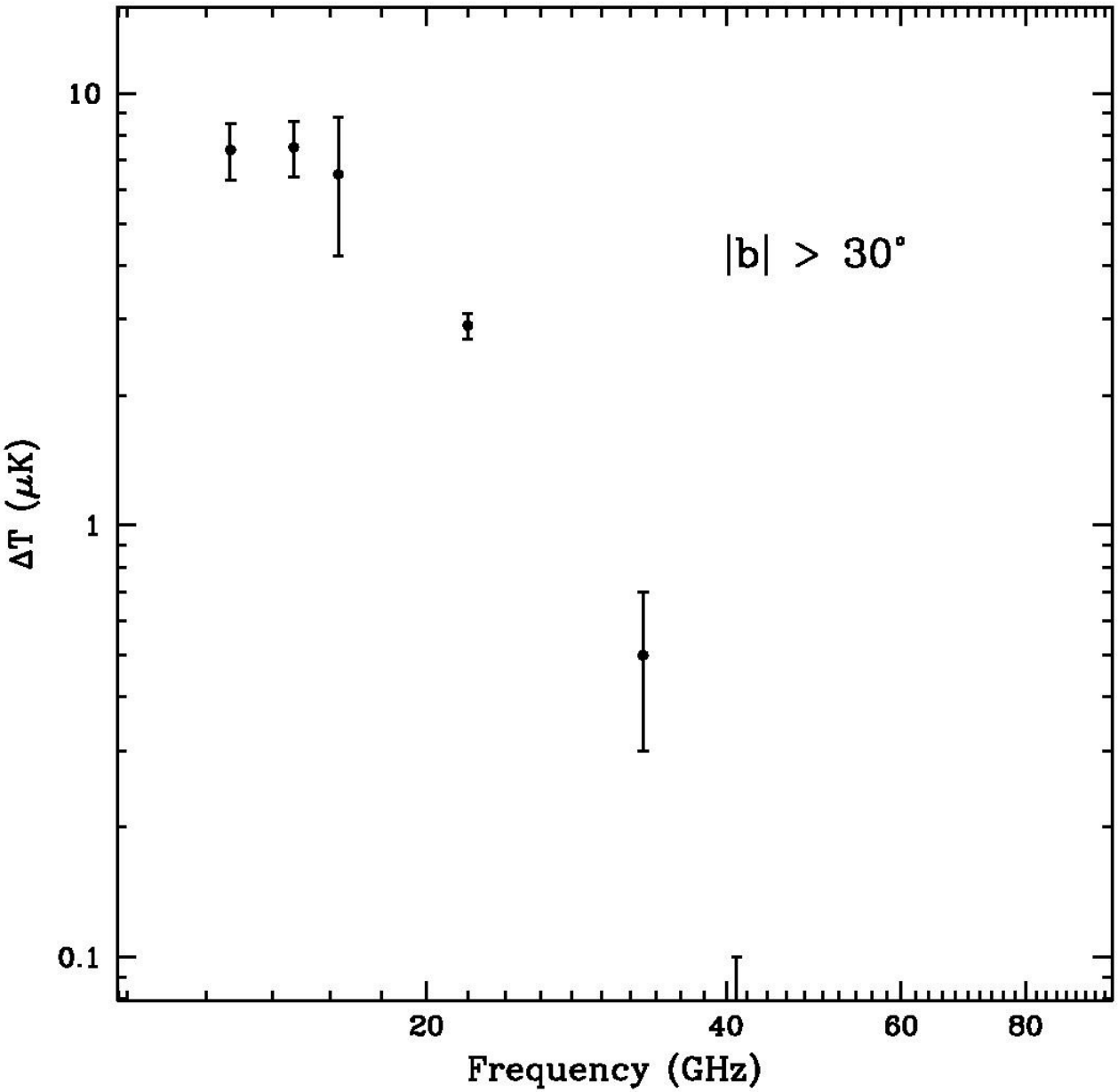

Figure 10. Amplitude of the correlated signal between COSMOSOMAS and WMAP with the DIRBE map at 100 μm for a Galactic cut of $|b| > 30°$.

Cross-correlations with Hα map (Finkbeiner 2003)

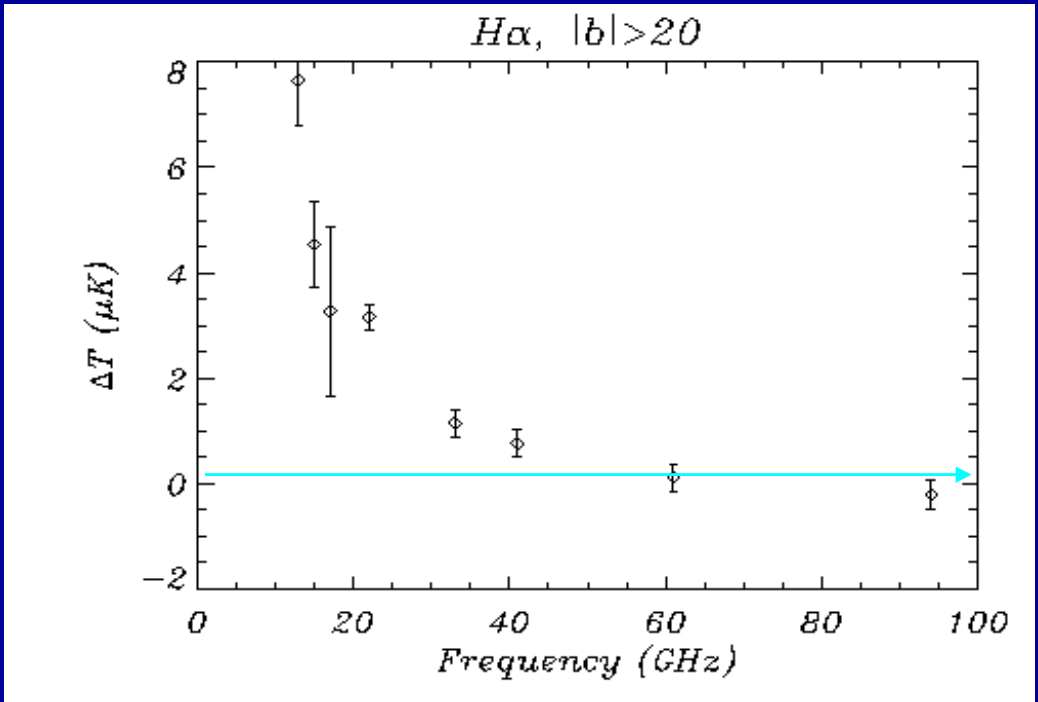

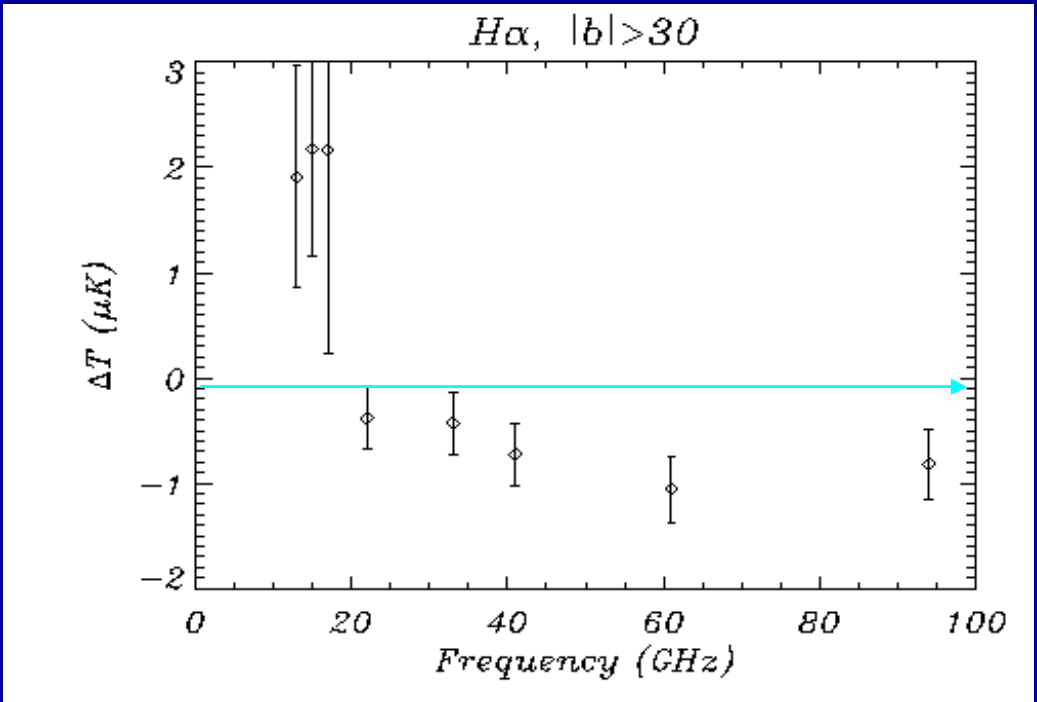

- Traces free-free emission. Values comparable to those from Banday et al. (2003)
- Not enough to explain the dust correlated signal.

Correlations with DIRBE 100 μm

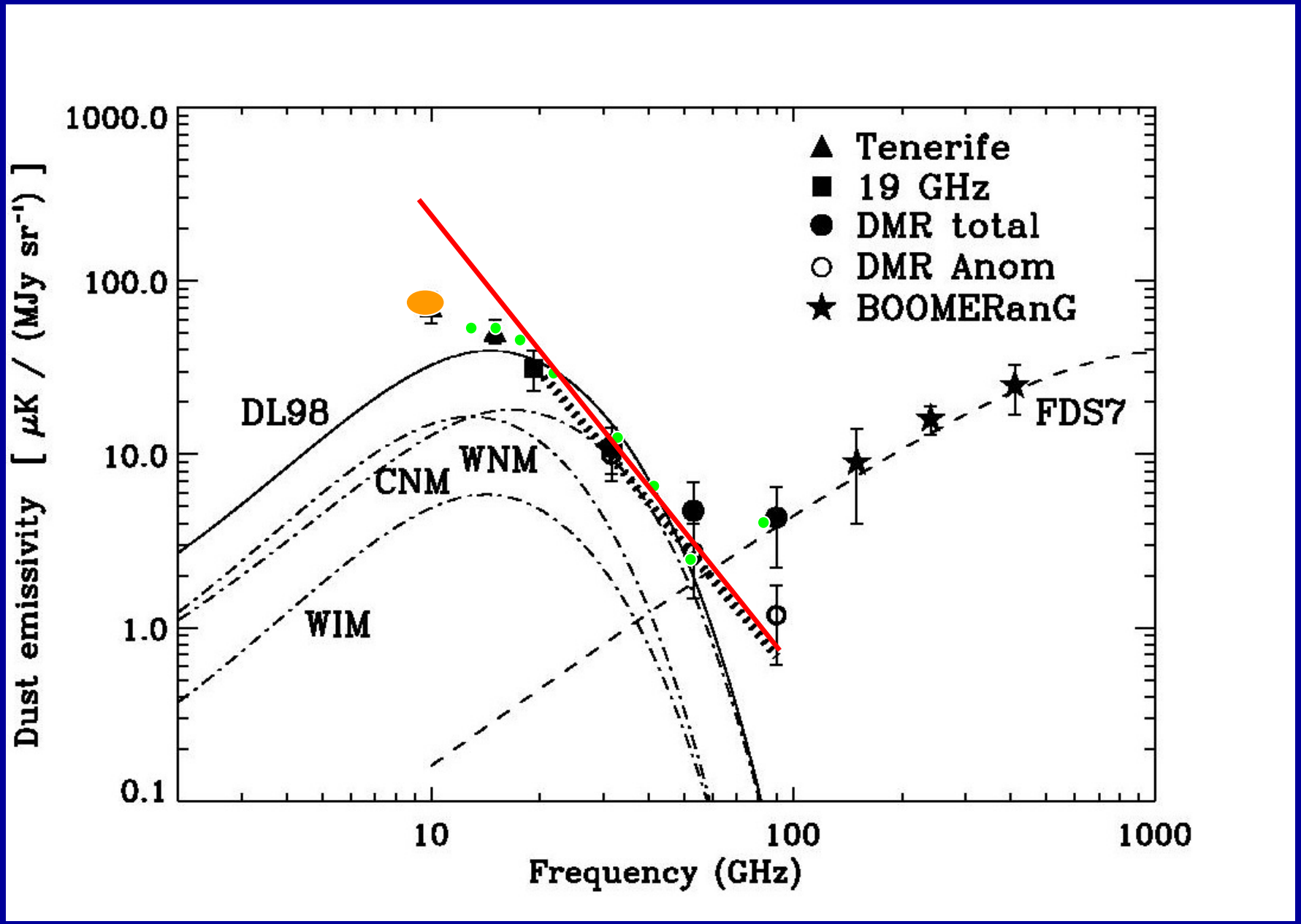

(Banday et al. 2003)

CONCLUSIONS

- The COSMOSOMAS CMB data agree well with WMAP, detecting the WMAP **CMB signal** (~30 μK) at about 15σ.
- **Synchrotron**: The COSMOSOMAS data are correlated with 408 MHz and 1420 MHz maps. The antenna temperature - frequency dependence of the Haslam-correlated signal is described with a power-law with index $|\beta| \approx 3$, as expected for synchrotron.
  - However, COSMOSOMAS does not correlate with the K-band synchrotron map proposed by WMAP as it would be expected for a synchrotron dominated signal.

CONCLUSIONS

- The **DIRBE-correlated signal** may turn out to be the dominant Galactic foreground seen by COSMOSOMAS.
  - It decreases significantly as we go to higher Galactic latitudes and higher frequencies. Most of the signal is detected between $20< |b| <40$.
  - The largest correlations are found with the 100 μm map.There are significant detections (>2 σ) at 140 and 240 μm.
  - The DIRBE-correlated signal is also detected in all the frequencies of WMAP. At $|b|>20$ it contributes about 4% to the antenna temperature fluctuations in WMAP_Q and progressively less as we increase the frequency
  - We find a remarkable agreement with predictions from spinning dust models.

CONCLUSIONS

- **Free-free emission** is detected from correlations with Hα maps. Amplitude of the signal is not high enough to explain the dust-correlated signal at high Galactic latitudes.
- The anomalous microwave emission is the dominant continuum emission process at 10-40 GHz in the Perseus molecular complex.
- The polarization level of this anomalous emission is less than 5% at 11 GHz. Our best estimate is 3.4±2 % which would argue strongly in favour of rotational electric dipole radiation of fast spinning small molecules.

Thanks for your attention !